

A SELF-CLEANING, LOW-TEMPERATURE MOLECULAR
LUMINESCENCE SPECTROMETER AS A DETECTOR FOR
GAS CHROMATOGRAPHY

By

JOHN F. CLOS

A DISSERTATION PRESENTED TO THE GRADUATE SCHOOL
OF THE UNIVERSITY OF FLORIDA IN PARTIAL FULFILLMENT
OF THE REQUIREMENTS FOR THE DEGREE OF
DOCTOR OF PHILOSOPHY

UNIVERSITY OF FLORIDA

1991

ACKNOWLEDGEMENTS

First, I would like to thank Dr. Jim Winefordner for allowing me to be a part of this group. It was a difficult decision to stay here and work for Jim instead of transferring to Cincinnati with Dr. Dorsey; however, I feel very lucky to have had the opportunity to be a part of the Winefordner research group. I will always be grateful to Jim for all I have learned while being a member of this group.

I would also like to thank all the friends I have made during my graduate school years. Their help and friendship have been invaluable in my graduate studies. I would especially like to thank Nancy Mullins for all of her help while working on this project.

Finally, I would like to thank my parents, Frank and Betty. I am very lucky to have had parents who guided me in the right direction as they did.

TABLE OF CONTENTS

ACKNOWLEDGEMENTS.	ii
LIST OF TABLES	v
LIST OF FIGURES	vi
ABSTRACT	xi
CHAPTER 1	
INTRODUCTION	1
Polycyclic Aromatic Hydrocarbons	1
Molecular Effects of PAH	3
Physical Effects of PAH	7
Methods for Determining PAHs	7
Room-Temperature Techniques	7
Matrix Isolation Spectrometry	11
Shpol'skii Spectroscopy	14
CHAPTER 2	
THEORY	23
Luminescence Spectroscopy	23
Band Broadening	25
Cooling Effect	30
Shpol'skii Effect.	36
CHAPTER 3	
EXPERIMENTAL	41
Instrumentation	41
Reagents	51
Procedure	51
CHAPTER 4	
RESULTS AND DISCUSSION	54
Phosphorescence Background	54
Chromatography	64
Chromatograms	64
Retention Times, Peak Widths, and Limits of Detection	97
CHAPTER 5	
CONCLUSIONS AND FUTURE WORK	129

REFERENCE LIST	132
BIOGRAPHICAL SKETCH	136

LIST OF TABLES

Table 2-1	Data showing the dimensions for several PAHs and their best Shpol'skii solvent. Taken from reference [50].	38
Table 4-1	List of experimental procedures to delineate and to minimize the phosphorescence background problem	57
Table 4-2	Retention times and dead volumes measured using the FID and the LTMLS system	108
Table 4-3	Peak widths measured using the FID and the LTMLS system	110
Table 4-4	Estimated limits of detection.	118

LIST OF FIGURES

Figure 1-1	Some examples of polynuclear aromatic hydrocarbons along with their carcinogenicity. Redrawn from reference [2].	2
Figure 1-2	Possible mechanism for the formation of benzo(a)pyrene by pyrolysis. Redrawn from reference [3].	4
Figure 1-3	Reaction mechanism for the metabolism of benzo(a)pyrene. Redrawn from reference [10]	5
Figure 1-4	Structure of benz(a)anthracene showing the K, L, and bay regions. Redrawn from reference [11]	6
Figure 1-5	Diagram of a supersonic expansion showing the pressure outside the chamber (P_o), the pressure inside the chamber (P_i), the start of free molecular flow (X_f), and the Mach disc (X_M)	10
Figure 1-6	Diagrams of a) optical system (top view) and b) cryostat head (side view) used by Conrad et al. for GC/matrix isolation. Taken from reference [24].	13
Figure 1-7	Diagram of experimental system used by Reedy et al. for GC/matrix isolation/FTIR Taken from reference [25].	15
Figure 1-8	Diagram of self-cleaning belt.	21
Figure 2-1	Energy level diagram showing absorption (A), fluorescence (F), phosphorescence (P), and radiationless processes (dashed arrows). S_o is the ground state, S_1 is the excited singlet state, and T_1 is the excited triplet state.	24

Figure 2-2	Graphs showing a) Lorentzian and b) Gaussian profiles. Taken from reference [43]	28
Figure 2-3	Diagram showing a) an energy level diagram and b) well resolved and c) poorly resolved spectra	29
Figure 2-4	Spectra of perylene (700 ng/mL) in n-hexane at three different temperatures. Taken from reference [46].	31
Figure 2-5	Schematic showing inhomogeneous broadening: a) a transition for a single molecule, b) transitions for many molecules, and c) how the band actually appears. Redrawn from reference [47]. . .	33
Figure 2-6	Fluorescence spectra of various compounds in different organic matrices at 4.2 K by ordinary excitation (dotted lines) and laser excitation (solid lines): a) perylene in ethanol, b) protonated form of 9-aminoacridine in ethanol, c) tetraphenylporphyrin in polystyrene, and d) protochlorophyll in ether. Taken from reference [47]	35
Figure 2-7	PAHs along with their optimum Shpol'skii solvent showing how they relate: a) naphthalene and pentane, b) anthracene and heptane, and c) naphthacene and nonane. Redrawn from reference [51].	39
Figure 2-8	Orientation of coronene and heptane molecules with respect to the crystallographic axis. Taken from reference [54]	40
Figure 3-1	GC/vacuum chamber interface used in these experiments. Based on the work by Brown and Wilkins [54]	43
Figure 3-2	Vacuum chamber used in these experiments: a) top and b) side views. Belt and spools are shown as dashed lines.	45
Figure 3-3	Schematic showing how the belt was tightened: a) the belt loose and b) the belt tightened. Belt and spool are shown as dashed lines.	47

Figure 3-4	Schematic diagram of the spectroscopic portion of the system. Dashed lines indicate light rays.	50
Figure 4-1	Phosphorescence spectrum of the background when hexane was injected	56
Figure 4-2	Spectra of 126 $\mu\text{g/mL}$ phenanthrene in hexane, hexane, and an empty tube (blank). Spectra were taken at 77 K using the SPEX fluorimeter. Excitation wavelength was 250 nm	60
Figure 4-3	Spectra of hexane and pump oil diluted in hexane. Spectra taken at 77 K using the SPEX fluorimeter. Excitation wavelength was 317 nm	62
Figure 4-4	3-D chromatogram of 78 $\mu\text{g/mL}$ phenanthrene; impurity peak (I): 8.39 min; phenanthrene peak (Ph): 8.59 min; phenanthrene aggregation: Ph(A); time scale is from 7.80 to 8.93 min	66
Figure 4-5	3-D chromatogram of 10 $\mu\text{g/mL}$ phenanthrene; conditions are the same as in Figure 4-4 .	69
Figure 4-6	Spectrum of manual injection of 131 $\mu\text{g/mL}$ phenanthrene (Ph); impurity: I; where aggregation peaks appear in Figure 4-4: Ph(A).	71
Figure 4-7	Spectrum of 78 $\mu\text{g/mL}$ of phenanthrene at its chromatographic peak maximum	73
Figure 4-8	3-D chromatogram of 94 $\mu\text{g/mL}$ pyrene; impurity peak (I): 10.76 min; pyrene peak (Py): 10.95 min; pyrene aggregation: Py(A); time scale is from 10.42 to 11.22 min.	75
Figure 4-9	Spectrum of 94 $\mu\text{g/mL}$ of pyrene at its chromatographic peak maximum	77
Figure 4-10	Spectrum of manual injection of 123 $\mu\text{g/mL}$ pyrene (Py); impurity: I; where aggregation peak appears in Figure 4-7: Py(A).	79
Figure 4-11	Spectrum of pyrene impurity at its chromatographic peak maximum	82

Figure 4-12	3-D chromatogram of 87 $\mu\text{g/mL}$ fluorene; impurity peak (I): 7.09 min; fluorene peak (Fl): 7.51 min; time scale from 6.97 to 8.09 min	84
Figure 4-13	Spectrum of 87 $\mu\text{g/mL}$ of fluorene at its chromatographic peak maximum	86
Figure 4-14	3-D chromatogram of 82 $\mu\text{g/mL}$ chrysene; time scale is from 13.72 to 15.01 min. . .	88
Figure 4-15	Spectrum of 82 $\mu\text{g/mL}$ of chrysene at its chromatographic peak maximum	90
Figure 4-16	3-D chromatogram of 82 $\mu\text{g/mL}$ triphenylene; time scale is from 15.17 to 17.93 min. . .	92
Figure 4-17	Spectrum of 82 $\mu\text{g/mL}$ of triphenylene at its chromatographic peak maximum	94
Figure 4-18	3-D chromatogram of approximately 100 $\mu\text{g/mL}$ mix of pyrene (Py), 1,2- and 2,3-benzofluorene (B), chrysene (Ch), and triphenylene (Tri); impurity: I; pyrene aggregation: Py(A); benzofluorene aggregation: B(A); time scale is from 10.42 to 17.93 min	96
Figure 4-19	2-D chromatogram of approximately 100 $\mu\text{g/mL}$ mix of fluorene (Fl), phenanthrene (Ph), pyrene (Py), benzofluorene isomers (B), chrysene (Ch), and triphenylene (Tri). Wavelength monitored: 421 nm. Time scale is from 6.00 min to 17.67 min.	99
Figure 4-20	2-D chromatogram of approximately 100 $\mu\text{g/mL}$ mix of fluorene (Fl), phenanthrene (Ph), pyrene (Py), benzofluorene isomers (B), chrysene (Ch), and triphenylene (Tri). Wavelength monitored: 495 nm. Time scale is from 6.00 min to 17.67 min.	101
Figure 4-21	2-D chromatogram of approximately 100 $\mu\text{g/mL}$ mix of fluorene (Fl), phenanthrene (Ph), pyrene (Py), benzofluorene isomers (B), chrysene (Ch), and triphenylene (Tri). Wavelength monitored: 587 nm. Time scale is from 6.00 min to 17.67 min.	103

Figure 4-22	2-D chromatogram of mix of approximately 100 $\mu\text{g/mL}$ mix of fluorene (Fl), phenanthrene (Ph), pyrene (Py), benzofluorene isomers (B), chrysene (Ch), and triphenylene (Tri). Wavelength monitored: 513 nm. Time scale is from 6.00 min to 17.67 min.	105
Figure 4-23	2-D chromatogram of mix of approximately 100 $\mu\text{g/mL}$ mix of fluorene (Fl), phenanthrene (Ph), pyrene (Py), benzofluorene isomers (B), chrysene (Ch), and triphenylene (Tri). Wavelength monitored: 459 nm. Time scale is from 6.00 min to 17.67 min.	107
Figure 4-24	Calibration curve for phenanthrene	113
Figure 4-25	Calibration curve for chrysene	115
Figure 4-26	Calibration curve for triphenylene	117
Figure 4-27	3-D chromatogram of 1.16 $\mu\text{g/mL}$ of fluorene	120
Figure 4-28	3-D chromatogram of 1.04 $\mu\text{g/mL}$ of phenanthrene	122
Figure 4-29	3-D chromatogram of 12.6 $\mu\text{g/mL}$ of pyrene	124
Figure 4-30	3-D chromatogram of 10.9 $\mu\text{g/mL}$ of chrysene	126
Figure 4-31	3-D chromatogram of 1.09 $\mu\text{g/mL}$ of triphenylene	128

Abstract of Dissertation Presented to the Graduate School
of the University of Florida in Partial Fulfillment of the
Requirements for the Degree of Doctor of Philosophy

A SELF-CLEANING, LOW-TEMPERATURE MOLECULAR
LUMINESCENCE SPECTROMETER AS A DETECTOR FOR
GAS CHROMATOGRAPHY

By

John F. Clos

August 1991

Chairperson: James D. Winefordner
Major Department: Chemistry

In recent years, there has been much interest in the presence of polycyclic aromatic hydrocarbons (PAHs). PAHs are found in many places, including crude oil, foods, and water. They are formed either by the decay or the pyrolysis of organic matter. Also, it has been shown that many of them are highly carcinogenic.

In the early nineteen fifties, it was noticed that many PAHs show very sharp spectral lines ("quasi-linear") when frozen in certain n-alkanes. This phenomena was named the Shpol'skii effect after the person who discovered it. Since then, much research has been carried out in this area since it greatly improves the selectivity for the compounds which show this effect.

Although this technique has many desirable qualities, it does have some drawbacks. One of the major problems is

the sample throughput, since samples must be cooled to near absolute zero temperatures before a spectrum can be taken. Once the spectrum has been obtained, the cell must be warmed to remove the sample so the next sample can be applied. This entire cycle can take several hours. To overcome this problem, a low-temperature molecular luminescence spectrometer (LTMLS), with a self-cleaning belt rotating around a cooled spool and an ambient spool was previously developed in our laboratory. However, this spectrometer had its problems, including reproducibility and freezing of the belt to the spool.

In the present research, the LTMLS was interfaced to a gas chromatograph (GC). Phosphorescence background and chromatographic broadening severely degraded the limits of detection. Even though the background degraded the limits of detection, chromatograms were collected which show the potential of this technique. The effect of the hexane-to-PAH ratio was also investigated. The retention times and peak widths obtained using the GC/LTMLS system were compared with those found using GC with flame ionization detection. The peak widths were found to be approximately 5 to 10 times worse using the LTMLS system. Finally, the estimated limits of detection were compared to those found previously using the LTMLS system and other low-temperature work. The limits of detection were found to be approximately two orders of

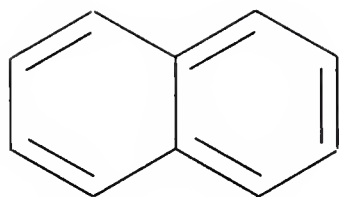
magnitude worse than those obtained previously using the LTMLS sytem alone.

CHAPTER 1 INTRODUCTION

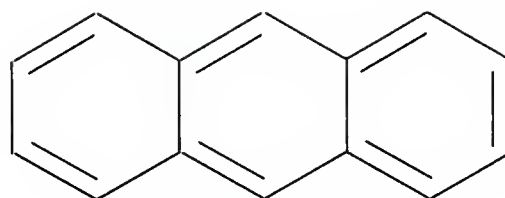
Low-temperature luminescence spectroscopy has become increasingly popular because it provides greater selectivity than room-temperature luminescence spectroscopy. This is predominantly due to the reduction in vibrational, rotational, and environmental broadening. In the early nineteen fifties, Shpol'skii and coworkers noted that certain compounds when frozen in n-alkanes would give "quasi-linear" spectra [1]. Polycyclic aromatic hydrocarbons (PAHs) are especially suited for low-temperature Shpol'skii studies because these molecules fit into the frozen n-alkane matrices and they have strong fluorescent and phosphorescent properties. They are also of great concern because of their significant mutagenic and carcinogenic effects.

Polycyclic Aromatic Hydrocarbons

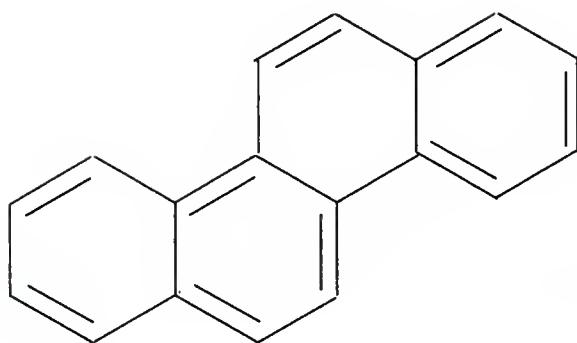
Some examples of PAHs along with their carcinogenicity are shown in Figure 1-1 [2]. PAHs are predominantly formed either by the long-term degradation of biological material or by the pyrolysis of organic matter. A possible reaction scheme for the formation of benzo(a)pyrene (BaP) by



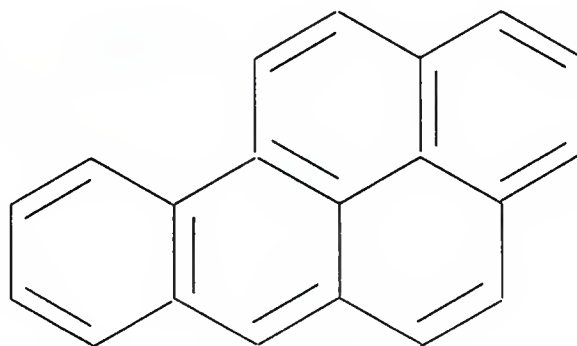
NAPTHALENE
(Inactive)



ANTHRACENE
(Inactive)



CHRYSENE
(Disputed)



BENZO(A)PYRENE
(Highly Active)

Figure 1-1. Some examples of polynuclear aromatic hydrocarbons along with their carcinogenicity. Redrawn from reference [2].

pyrolysis is shown in Figure 1-2 [3]. PAHs are found in marine sediments [4], coal and shale oil [5], airborne particulates [6], and vegetable oils [7]. Of particular importance is the presence of PAHs in tobacco smoke, since they are inhaled directly into the lungs and have been shown to be carcinogenic [8].

Molecular Effects of PAHs

Of the many causes of cancer, environmental factors are by far the largest cause, and of these, PAHs are the most significant group [9]. It is apparent from most research that the PAHs themselves are not the cause of cancer, but rather their metabolites [10].

As shown in Figure 1-3, BaP is eventually converted into two diol-epoxide isomers by Cytochrome P-450 and epoxide hydase [10]. These two isomers are considered to be the ultimate causes of the adverse biological effects of BaP. They have been shown to bind to DNA, known as intercalation, resulting in mutations.

At first, it was believed that the carcinogenic effects of PAHs might be due to the presence of two structural regions, K and L regions, shown in Figure 1-4 [11]. However, this theory failed to correlate well with many carcinogens. Later, it was theorized that the presence of the so-called bay region might actually be a better test of

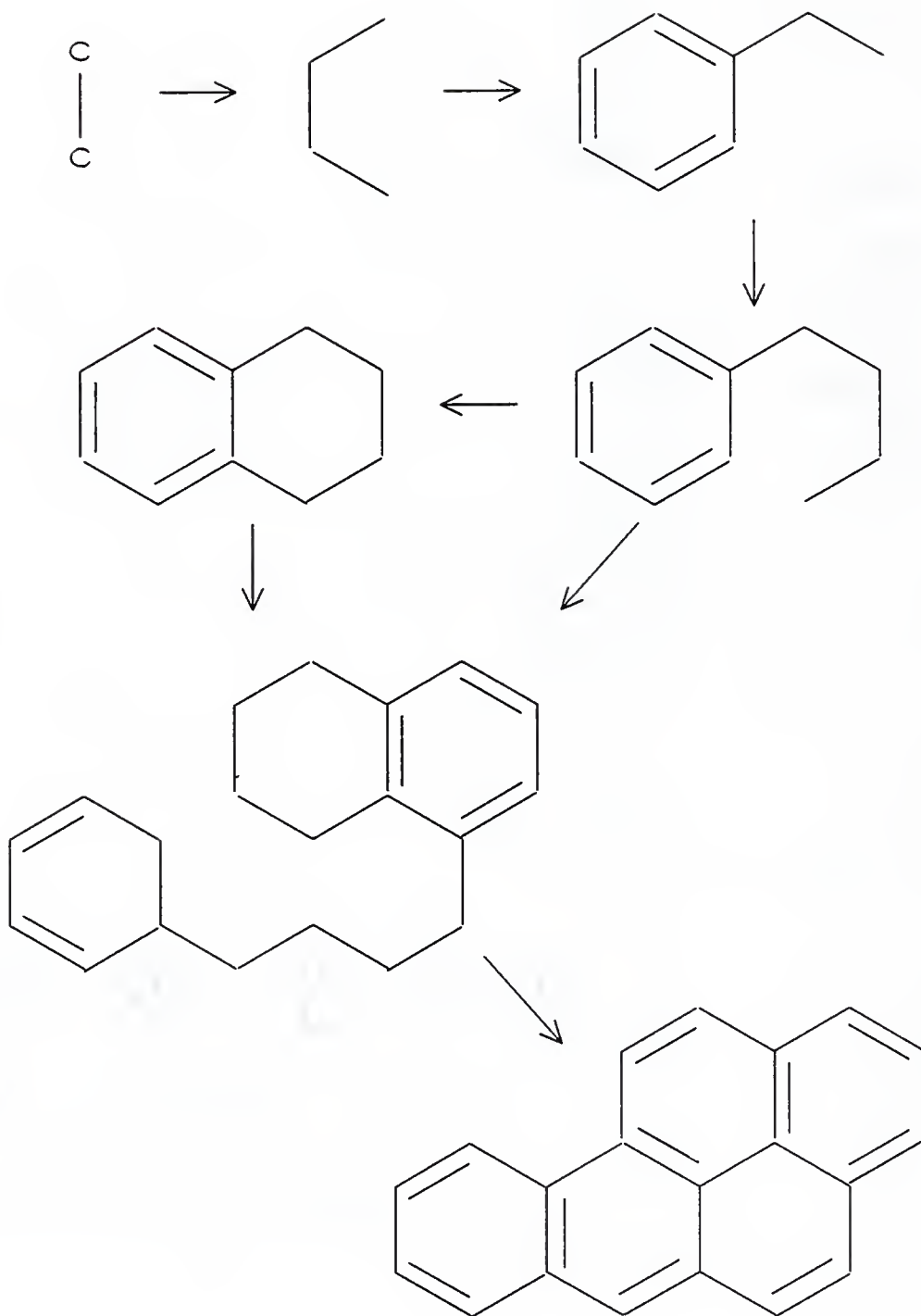


Figure 1-2. Possible mechanism for the formation of benzo(a)pyrene by pyrolysis. Redrawn from reference [3].

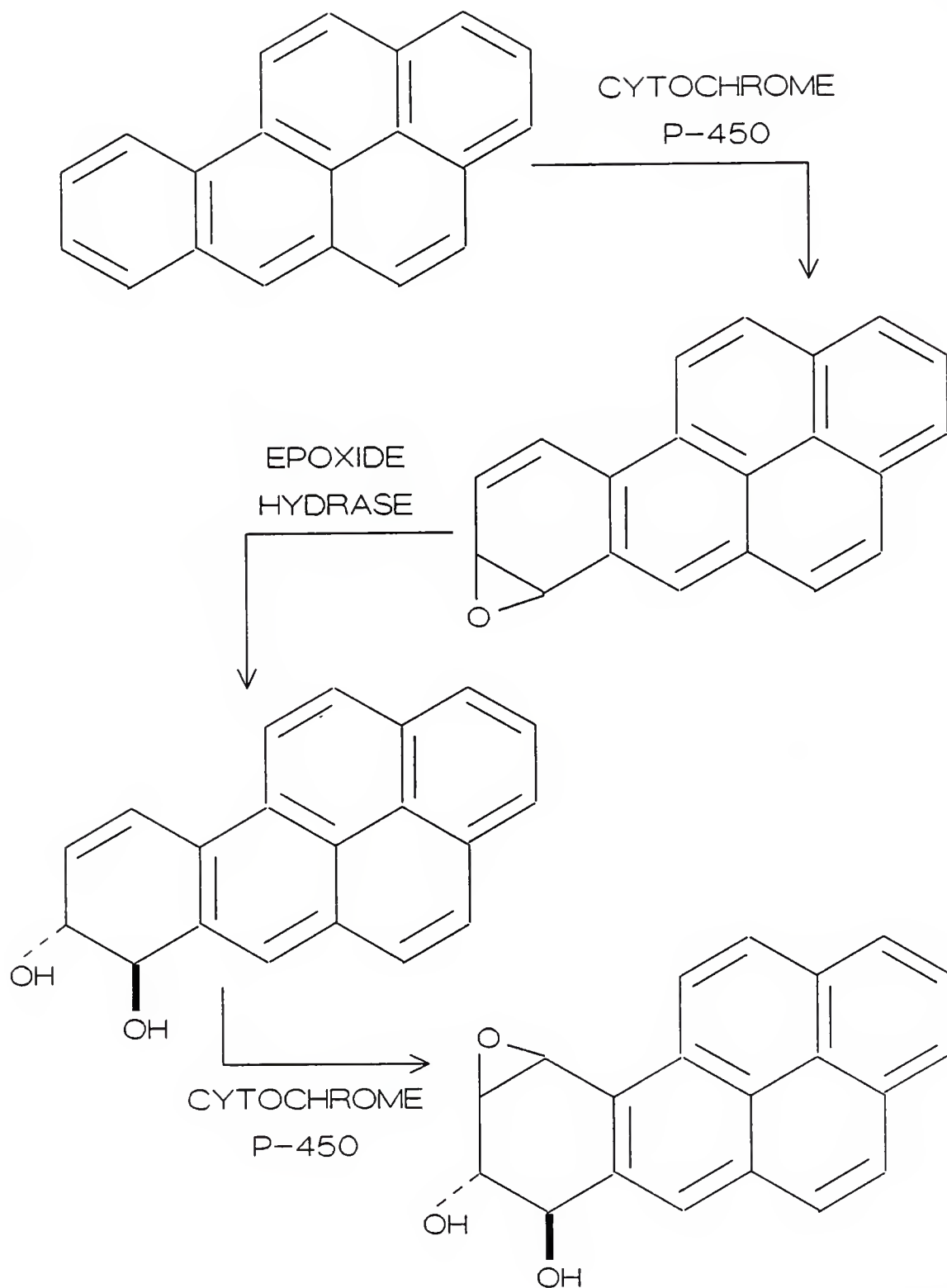


Figure 1-3. Reaction mechanism for the metabolism of benzo(a)pyrene. Redrawn from reference [10].

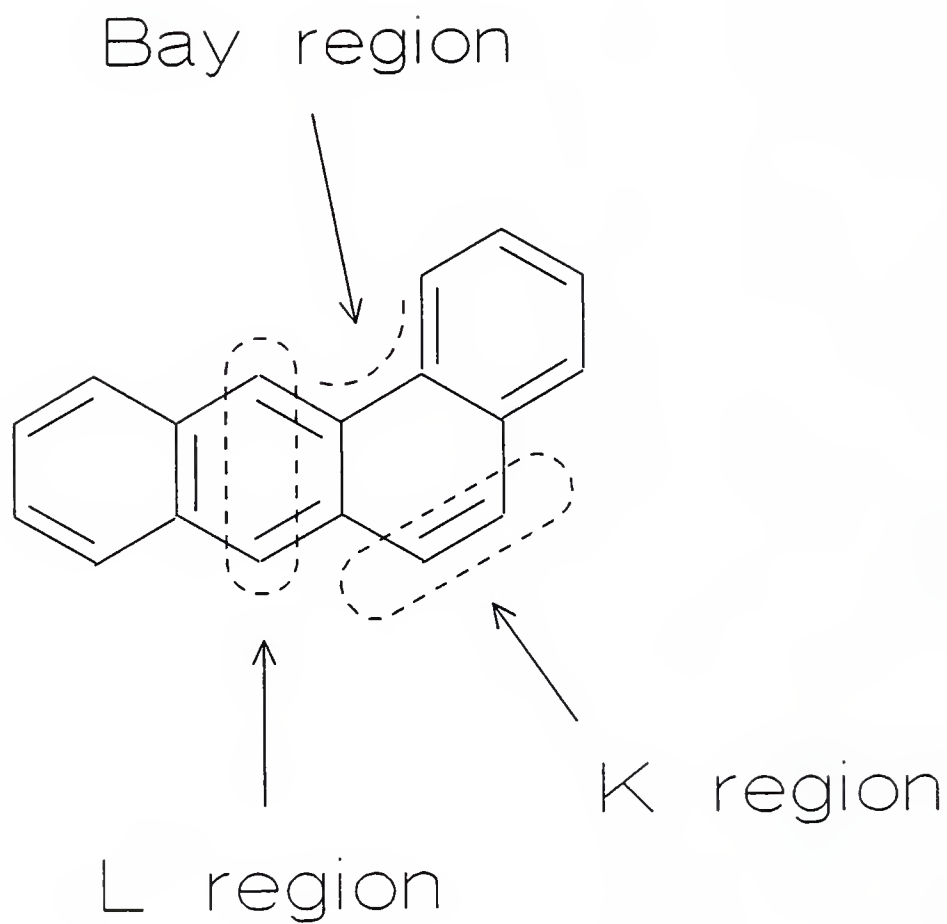


Figure 1-4. Structure of benz(a)anthracene showing the K, L, and bay regions. Redrawn from reference [11].

carcinogenicity of the PAHs [12]. In a recent study, it was shown that a bay region metabolite of BaP binds 2.7 times more tightly than a K region metabolite of BaP to DNA [13]. Some researchers have used computer modeling to predict the carcinogenicity of various PAHs [14]. Much more research is needed to discover the true pathway by which the PAHs produce their biological effects.

Physical Effects of PAHs

Regardless of how the PAHs cause their mutations, it has been well documented that they do result in serious physical abnormalities. It had previously been known that exposure to coal dust caused cancer; however, it was not recognized until the 1930s that exposure to BaP itself resulted in cancerous growths in humans [15]. It has also been shown to affect rats and mice [16], algae [17], and various higher plants [18], to name just a few examples. Due to the high toxicity of PAHs, an accurate method is needed to measure the various PAHs in widely differing complex mixtures.

Methods for Determining PAHs

Room-Temperature Techniques

One of the basic and more popular methods for determining PAHs is high performance liquid chromatography (HPLC) coupled with either ultraviolet (UV) or fluorescence

detection. This is because the sensitivity is adequate for most applications and the cost is low compared to other techniques. Joe et al. determined various PAHs in smoked foods by extraction with freon followed by column chromatography and HPLC analysis [19]. Although quite appealing for several reasons, there are also several drawbacks. The technique essentially relies on the separation for selectivity. Even when using fluorescence detection, there is little difference between the spectra of PAHs to provide selectivity. Also, since the spectra are essentially featureless, one has to rely on the retention time for identification of the analyte.

Along with HPLC, gas chromatography (GC) with flame ionization detection (FID) is also very popular for many of the same reasons stated for HPLC. Liberti et al. determined various PAHs in several different environmental samples by extraction with a benzene-methanol mixture followed by column chromatography, HPLC, and then finally GC separation [20]. The added sample preparation is needed due to the fact that the environmental samples analyzed, diesel exhaust and chimney smoke, are extremely rich in PAHs, both in concentration and variety. Although GC has much higher separation capacity than HPLC, it suffers from the non-selective response of FID to all organic compounds. Therefore, GC loses some of the advantage it has over HPLC in resolving power.

One way to overcome the loss in selectivity is by combining GC with mass spectrometry (MS). Liberti et al. also did GC/MS analysis of the same samples which he analyzed by GC/FID [20]. By monitoring certain ions, compounds which coelute can be differentiated by their mass spectrum. However, little is learned about the structure of the PAHs. Therefore, it can be difficult to discern between the PAHs, especially between isomers, unless GC/MS/MS is employed. However, this adds greatly to the cost, which is already considerable in doing GC/MS alone.

Some people have attempted to use spectroscopic methods other than UV detection to improve the selectivity. One technique which showed much promise initially as a detector for GC was supersonic expansion. At room temperatures, luminescence spectra consist of very broad and featureless peaks due to rotational and vibrational broadening. Supersonic expansion involves the flow of a gas from one region of a moderate pressure to another of a very low pressure through a small orifice (Figure 5). In Figure 5, the inner area of the expansion is the supersonic jet and the outer area is the shock wave. The shock wave prevents the hot molecules in the chamber from interacting with the rotationally and vibrationally cooled molecules in the expansion. Two important points in the supersonic expansion are the start of free molecular flow (X_f) and the Mach disc (X_M) [21]. Free molecular flow means that there are

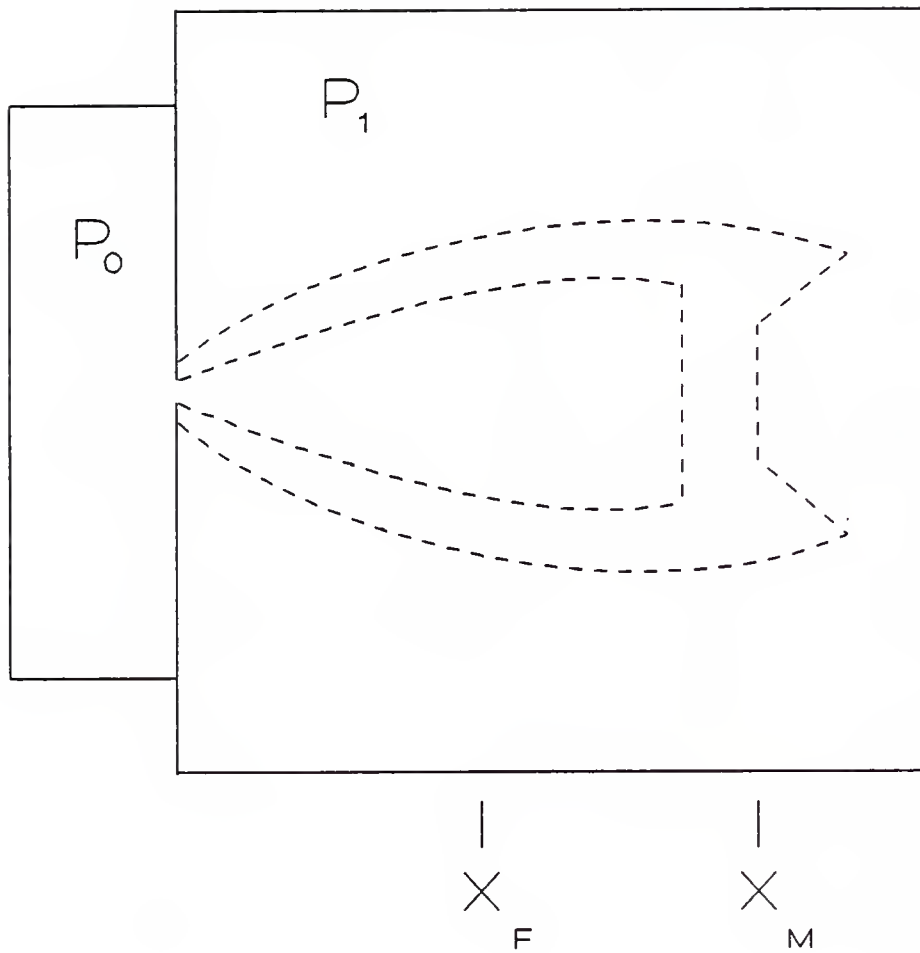


Figure 1-5. Diagram of a supersonic expansion showing the pressure outside the chamber (P_o), the pressure inside the chamber (P_1), the start of free molecular flow (X_f), and the Mach disc (X_M).

essentially no collisions, which in turn, produces cooled molecules free from environment effects. The Mach disc indicates the leading edge of the supersonic expansion. By allowing the gas to expand rapidly through the orifice into the area of lower pressure, the rotational and vibrational energy distributions are decreased. This results in a lowering of the temperature of the molecule and much sharper spectral peaks.

At first, one would think GC and supersonic expansions were well suited for each other. However, several problems arise when one attempts to interface the two. One problem is the limit of detection, which is rarely below 1 ppm. The problem is that the flow from the column is too low to give a good expansion, therefore the flow is pulsed [22]. This gives a good expansion, but it also creates dead volume which reduces the chromatographic performance. Another problem is that the best chromatographic performance is obtained with helium or hydrogen, while the most efficient rotational and vibrational cooling in supersonic expansions is obtained by using argon.

Matrix Isolation Spectrometry

Another technique which gives better selectivity than UV spectrometry and room temperature luminescence spectrometry is matrix isolation (MI) spectrometry. Matrix isolation involves the dilution of the compound of interest

(in the gas phase) with a "matrix" gas, usually nitrogen or argon, followed by deposition on a cryogenic surface. The principal characteristics of a matrix are [23]: (1) the molecules are sufficiently separated in the matrix such that they are unable to "communicate" with one another, (2) the solvent and the solutes mix in the gas phase and often poor solvents for the compounds are good matrix solvents, and (3) the solutes and the solvents should not react.

A significant amount of research has been done in the area of matrix isolation spectroscopy for detection in gas chromatography. Conrad et al. used a 12-sided block attached to the end of a cryostat for deposition of the GC eluents [24]. As shown in Figure 6a, the sample is deposited on one of the surfaces, using the carrier gas (either nitrogen or argon) as the matrix. The cryostat is then rotated until the sample comes into view of the excitation light. A spectrum is then taken using a polychromator to disperse a section of the emitted fluorescence onto the faceplate of a silicon intensified target vidicon. They used the GC/MI fluorescence spectrometer to determine 12 anthracene derivatives in a synthetic mixture. Since the eluent can not be interrogated continuously, it was necessary to collect the components in fractions. By doing this, they relied mainly on the spectral resolution to determine the original derivatives and were able to spectrally resolve 11 of the 12 components.

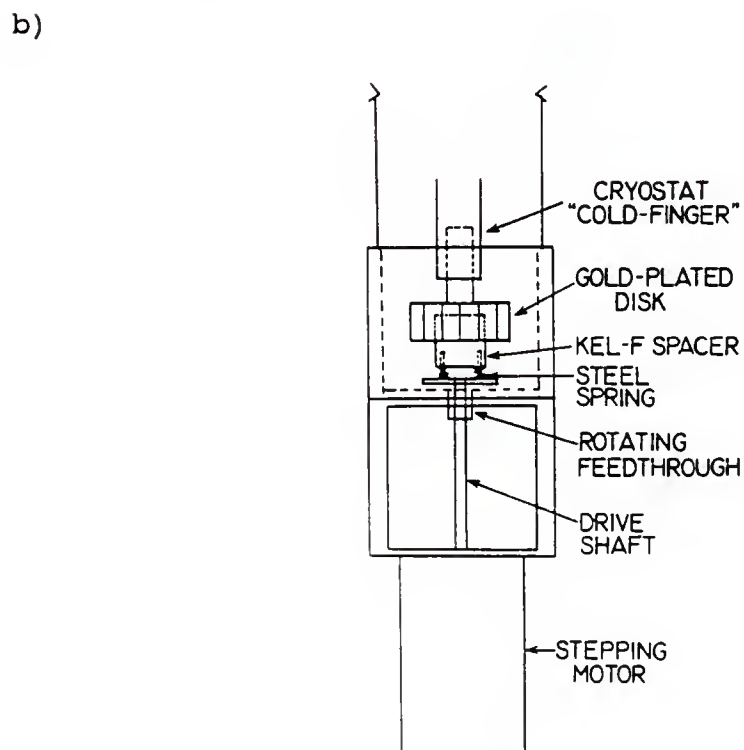
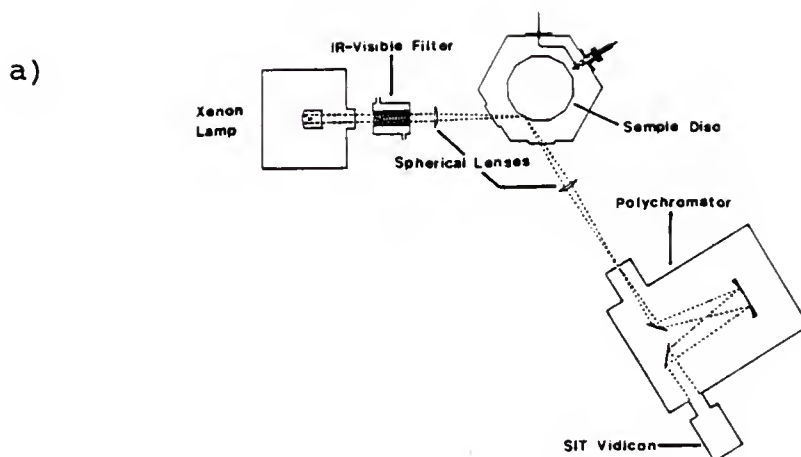


Figure 1-6. Diagrams of a) optical system (top view) and b) cryostat head (side view) used by Conrad et al. for GC/matrix isolation. Taken from reference [24].

Work has also been done on GC/MI infrared spectrometry. Reedy et al. built a spectrometer, shown in Figure 7, which was a disk connected to the cold stage of a cryostat for continuous sampling, although only for 110 min, unless the GC capillary was repositioned [25]. Instead of using argon as the carrier, they used helium with 2% argon since helium is cheaper and gives much better chromatographic efficiency. By using infrared spectrometry, they were not only able to measure pyrene and fluorene, but also several polychlorinated biphenyls and aliphatic hydrocarbons.

Organic glasses can also be used in matrix isolation. Brown et al. used hydroorganic mixtures as their matrix and a laser to produce what is called fluorescence line narrowing (FLN) [26]. FLN results from the narrow bandwidth of the laser beam and the weak electron-phonon coupling which causes broadening of the spectral peaks. They were able to distinguish between several isomers of anthracene and found detection limits to be in the parts-per-trillion range. One advantage of their procedure is that water samples can be analyzed directly without any extraction steps since water is a part of the matrix.

Shpol'skii Spectroscopy

As stated previously, a Russian scientist named Shpol'skii and his coworkers discovered that by freezing PAHs in n-alkanes, spectral peaks become unusually sharp -

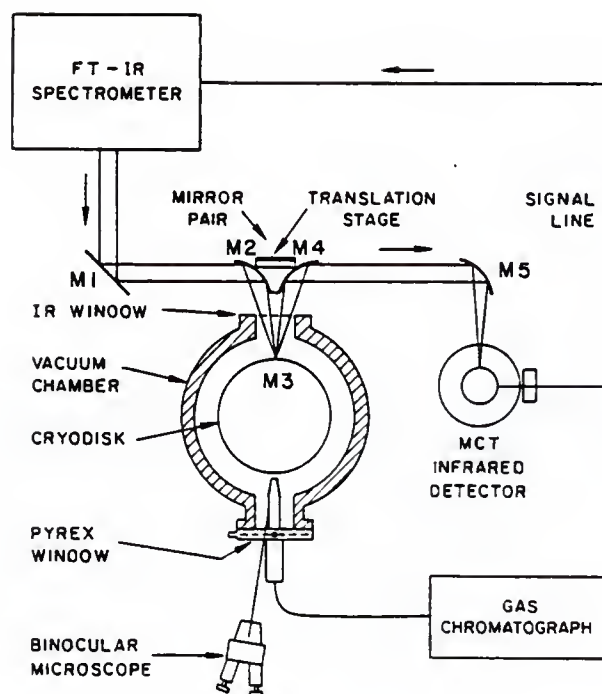


Figure 1-7. Diagram of experimental system used by Reedy et al. for GC/matrix isolation/FTIR. Taken from reference [25].

[1]. Since then, considerable research has been done in the area of Shpol'skii spectroscopy (SS). SS is essentially a matrix isolation technique, however, it is almost exclusively applicable to PAHs in n-alkanes.

Inman et al. studied the fluorescence of 41 compounds and the phosphorescence of 60 compounds at 77 K in Shpol'skii matrices [27]. Most of the compounds had detection limits in the low ppb range with some in the pptr range. One advantage of the system they used is that the instrumentation is commercially available.

One of the attractive features of SS is the ability to resolve compounds of rather similar structure. Colmsjo was able to show that 13 of the 16 PAHs of molecular weight 328 have distinct excitation and emission wavelengths [28]. He also did a similar study for PAHs of molecular weight 378 [29].

As previously stated, PAHs are of great concern because of their mutagenic and carcinogenic effects. Therefore, a significant amount of research has been done on the application of SS to environmental samples. Renkes et al. determined benzo(a)pyrene, benzo(k)fluoranthene, and benzo(ghi)perylene in particulate samples [30]. The PAHs were extracted from the samples by heating them in diphenylmethane or phenyl ether. These extracts were then diluted 10- to 100-fold with either n-heptane or n-octane.

The concentrations determined by this method were comparable to the certified values for the NBS standard studied.

The analysis of fossil fuels is another area in which SS has been applied. This is largely due to the high concentrations and wide variety of PAHs in fossil fuels and also the complicated matrix. Perry et al. were able to determine four PAHs in a coal reference standard and benzo(a)pyrene in a shale oil reference standard [31].

Although SS is a powerful tool for resolving PAHs, it can still be very difficult to determine them. This is especially true when analyzing complicated matrices or when many PAHs are present. Therefore, as with other matrix isolation techniques, many researchers have tried to combine SS with liquid or gas chromatography.

Colmsjo and Stenberg looked at six PAHs in automobile exhaust and air samples by HPLC fractionation followed by analysis using SS [32]. The samples were collected using a method which results in a particulate phase (on a glass fiber filter) and a condensed water phase. They were then prepared for separation by extraction using dimethylformamide, water and cyclohexane.

Two HPLC gradient separations were performed. The first was to separate the polar compounds from the three or more ring PAHs and the second fractionation was used to separate the PAHs for SS analysis at 63 K. By this method, they were able to identify six PAHs in automobile exhaust.

Petroleum samples are much more difficult to deal with due to their complexity if one wishes to analyze them for a wide variety of PAHs. Garrigues et al. used three chromatographic separations to analyze shale oil and coal for alkylphenanthrenes followed by SS [33]. The first separation used a semi-preparative alumina column to separate the aromatic compounds by ring class. The appropriate fraction was then separated on a reversed-phase column to resolve the PAHs based on their degree of alkylation followed by a second reversed-phase separation to further resolve the phenanthrene derivatives. These fractions were then analyzed by either SS or GC-MS. By combining these techniques, they were able to identify 17 of the possible 30 ethyl- and dimethylphenanthrene derivatives.

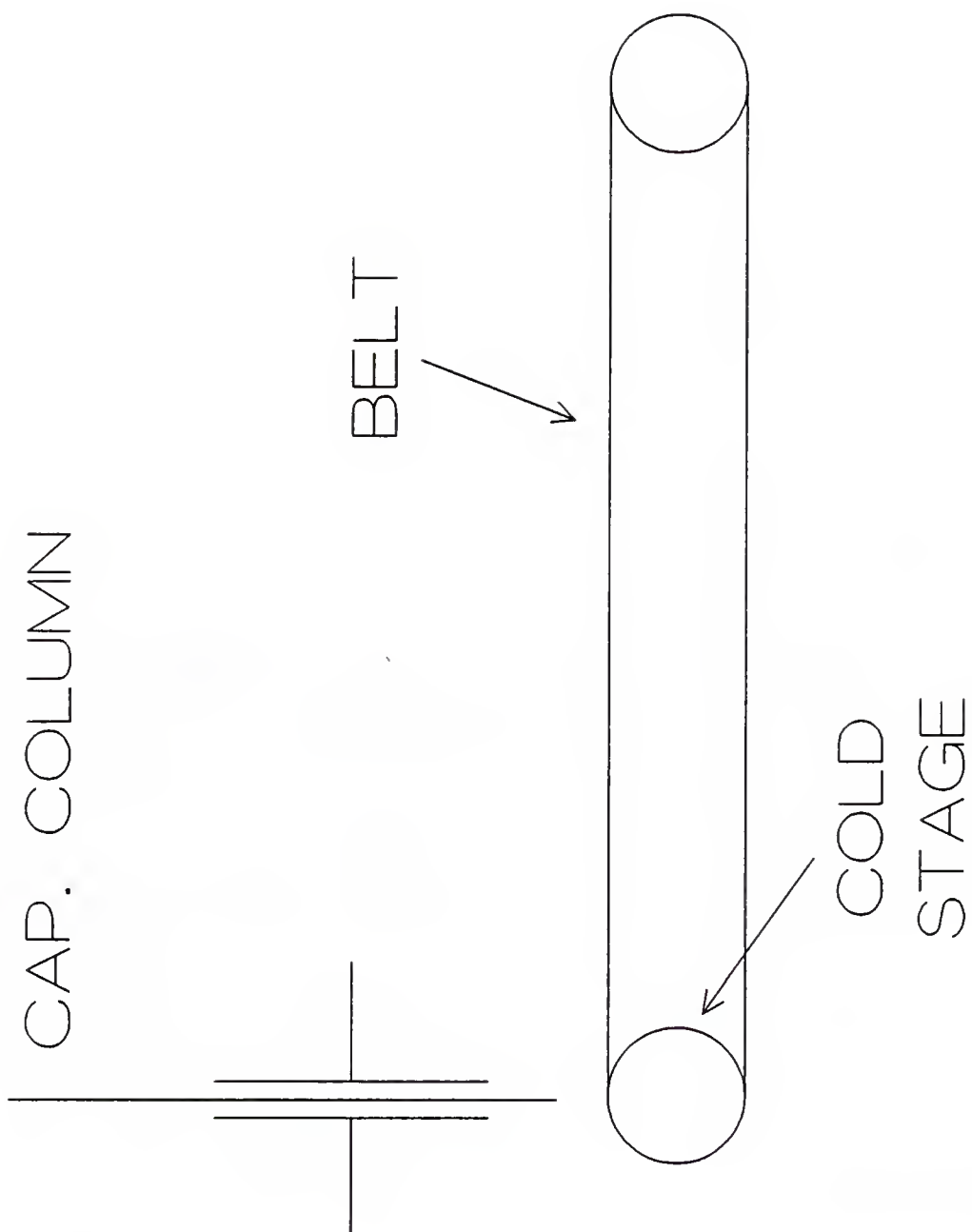
One problem with the combination of SS with chromatographic techniques is the necessity to collect fractions to analyze them. Up to now, fractions were collected, the eluent was switched to look at a few small sections of the chromatogram, or, at best, a few chromatograms could be analyzed continuously. This leads to errors introduced by the technician, lower effectiveness of the separation, hinderance of automation, and thus lower reproducibility. To overcome this, Jones and Winefordner described a luminescence spectrometric system with a self-cleaning continuously cooled belt [34].

As shown in Figure 8, the sample in n-hexane is introduced onto the belt where the belt is in contact with the cold stage of the closed-cycle helium refrigerator. Therefore, since the cold stage is at approximately 15 K, the sample is rapidly frozen to the belt. The sample is then rotated 90 degrees by means of a feedthrough connected to the rear spool so that it can be excited by the output from the xenon arc lamp. After a spectrum has been obtained, the belt is further rotated so that the part of the belt covered by the sample is no longer in contact with the cold stage. The sample then warms and the high vacuum (10^{-5} torr) removes it from the belt; therefore, the system is self-cleaning. They used this spectrometric system to analyze discrete extractions from cooked beef for PAHs [35].

Although it allowed continuous sampling without having to warm the chamber to remove the sample, low reproducibility of repeated injections of the same standard was a problem. This was partially due to the samples being injected manually with a syringe. Because of this, the spots on the belt were not reproducible in shape, which changed the amount of sample viewed, and therefore, the signal.

The current research involves the interfacing and evaluation of a gas chromatograph with the spectrometric system described by Jones and Winefordner. This should not only improve the reproducibility, but also greatly improve

Figure 1-8. Diagram of self-cleaning belt.



the selectivity due to the high resolving power of capillary gas chromatography. Phosphorescence background and chromatographic peak broadening were severe problems which degraded the limits of detection. However, chromatograms were collected which show the potential analytical usefulness of this technique. The effect of the hexane-to-PAH ratio was also investigated. The retention times and peak widths obtained using the LTMLS system as the detector for the gas chromatograph were compared with those found using flame ionization detection. Finally, the estimated limits of detection were compared to those found previously using LTMLS system alone and also other low-temperature work.

CHAPTER 2 THEORY

Luminescence Spectroscopy

Luminescence spectroscopy involves the absorption and subsequent emission of light. As shown in Figure 2-1, when an electron is excited to a higher energy level, it can return back to the ground state in several ways. First, it can release the energy by radiationless processes, such as heat or by collision. Second, it can emit light having the energy equal to the transition from the excited state to the ground state, which is termed fluorescence. Third, it can cross over to a triplet state by radiationless processes and then emit light to return to the ground state, called phosphorescence, or be quenched by interactions with the matrix.

There are several differences between fluorescence and phosphorescence [36]. First, the time scale for fluorescence is on the order of 10^{-8} to 10^{-5} s, while phosphorescence lasts 10^{-3} s or longer. This is because of the delay caused by the intersystem crossing from the singlet to the triplet state and the lifetime of the triplet state. Second, in fluorescence, the emission spectrum is the mirror image of the excitation spectrum, whereas in

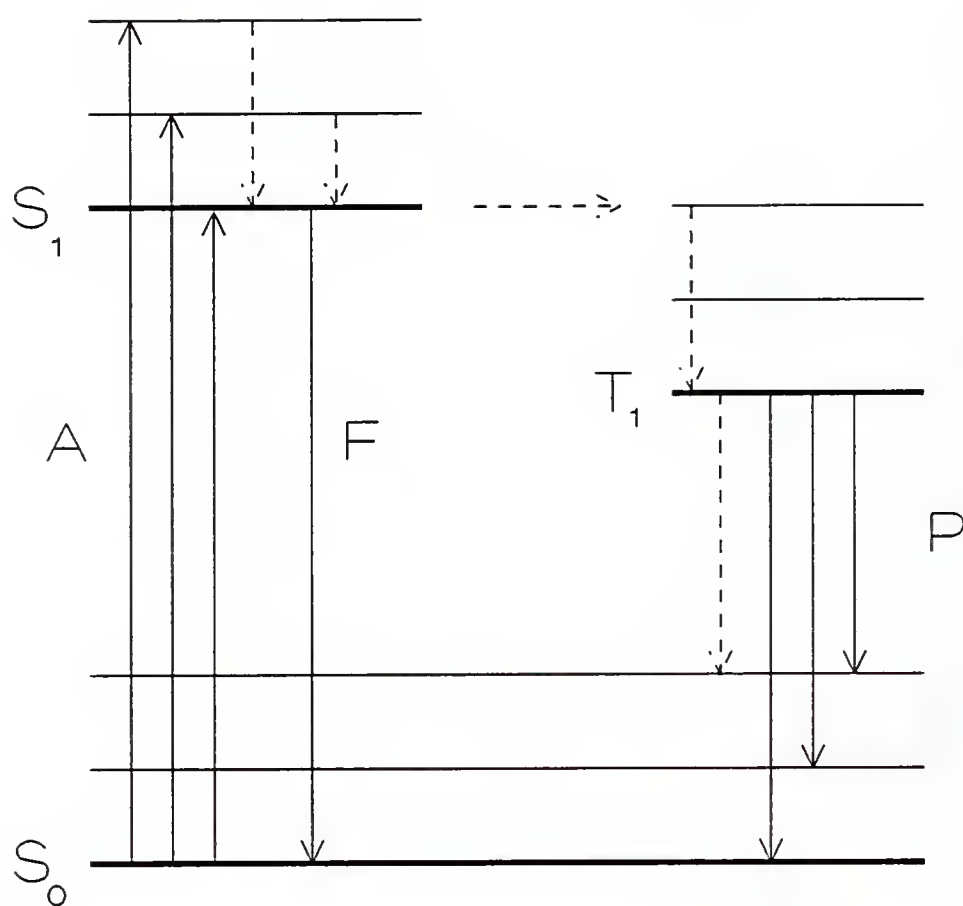


Figure 2-1. Energy level diagram showing absorption (A), fluorescence (F), phosphorescence (P), and radiationless processes (dashed arrows). S_0 is the ground state, S_1 is the excited singlet state, and T_1 is the excited triplet state.

phosphorescence, besides not being the mirror image, the emission spectrum is also shifted to longer wavelengths. Third, phosphorescence is rarely observed in gases and seldom at room temperature in solutions; however fluorescence is observed in both gases and room temperature solutions. This is because the time scale for molecular collisions is similar to that of fluorescence. Therefore, the absorbed energy is released by radiationless processes before the molecule has had time to phosphoresce.

Band Broadening

Although molecular luminescence techniques are more sensitive and selective than absorption spectroscopy, they still suffer from band broadening. There are several types of band broadening in molecular spectroscopy. First, an excited electron does not have a precisely defined energy, therefore it has an uncertainty in its amount of energy, depending on its lifetime [37]. Because of this inherent uncertainty, the spectral lines are broadened into bands; however, this natural broadening is only 10^{-3} to 10^{-4} cm^{-1} [38].

Molecular bands are also broadened by what is called the Doppler effect [36]. This is caused by movement of the molecule either away from or to the detector. If the molecule moves toward the detector, the apparent frequency

is increased, and if it moves away, then the apparent frequency is decreased.

Another cause of spectral band widening is collisional or pressure broadening [37]. Collisional broadening is probably the most significant cause of broadening of spectral bands. This is caused by the interaction of the molecule of interest with surrounding molecules. These interactions cause shifts in the excited state energy levels, changing the energy level for each individual molecule slightly.

Band broadening is also caused by what is known as the Stark effect [39]. In 1913, Stark discovered that an external electric field caused lines to split in atomic spectra. This is due to the influence of the electric field on the dipole moment of the atom. This has also been shown to apply to molecules as well as atoms.

Another cause of spectral band spreading is known as resonance broadening [40]. This results from the fact that like molecules will have the same natural frequency. This can cause a strong coupling between the two molecules, and therefore, results in a dispersion of the frequencies. These interactions also occur between unlike molecules, but the force between them is not as strong.

Most of these broadening effects fall under what is known as inhomogeneous broadening [41]. Essentially this is due to external effects acting on the molecule. These

effects are not consistent throughout the liquid or solid. This is usually due to the fact that each molecule is not surrounded by the same environment, so that each molecule is influenced differently. This, in turn, means that the excited energy state of each molecule is unique, and so when it returns to the ground state, it will emit at a slightly different wavelength. Finally, spectral bands can be broadened by the monochromator itself.

Broadening effects follow one of two equations, either the Lorentzian or the Gaussian profiles [42]. The Lorentzian profile is governed by the equation:

$$S_{\nu L} = \frac{2/(\pi \Delta \nu_L)}{1 + [2(\nu_m - \nu)/\Delta \nu_L]^2}$$

whereas, the Gaussian profile follows the equation:

$$S_{\nu G} = \frac{2(\ln 2/\pi)^{1/2}}{\Delta \nu_G} e^{-4(\ln 2)(\nu - \nu_m)^2/\Delta \nu_G^2}$$

where $S_{\nu L}$ is the normalized Lorentzian spectral profile in Hz^{-1} , $\Delta \nu_L$ is the half-intensity width of the Lorentzian profile, ν_m is the central frequency, $S_{\nu G}$ is the normalized Gaussian spectral profile in Hz^{-1} , and $\Delta \nu_G$ is the half-intensity width of the Gaussian profile. As can be seen in Figure 2-2, the Lorentzian profile has more extensive wings than the Gaussian profile [43].

An energy level diagram and two spectra are shown in Figure 2-3. The energy diagram shows not only the electronic levels, but also the rotational and vibrational

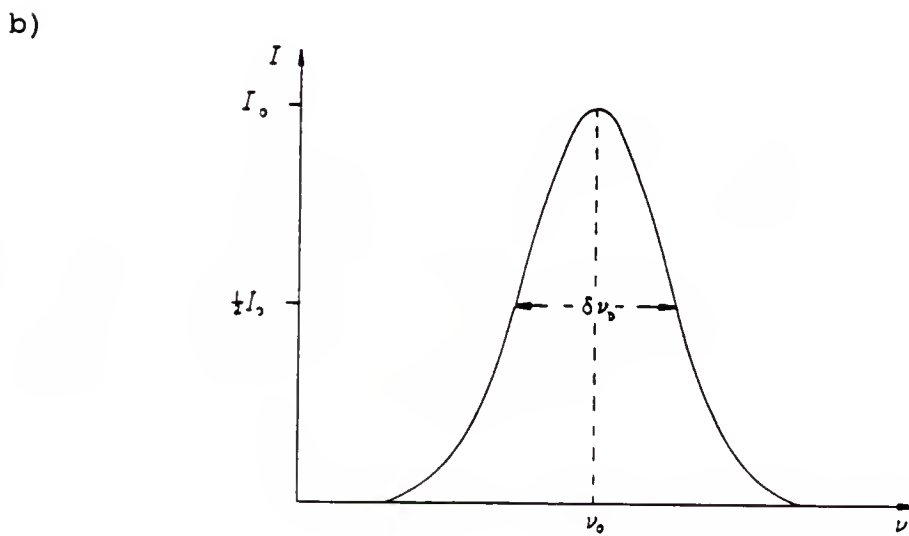
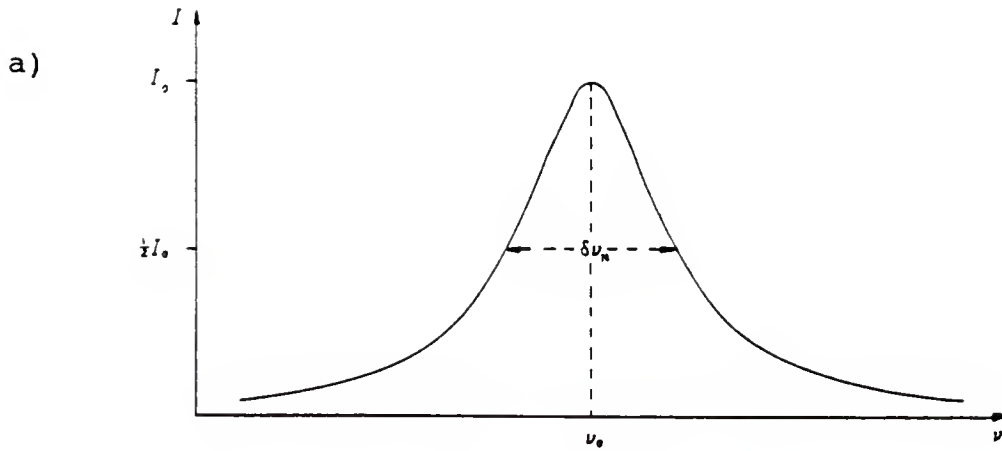


Figure 2-2. Graphs showing a) Lorentzian and b) Gaussian profiles. Taken from reference [43].

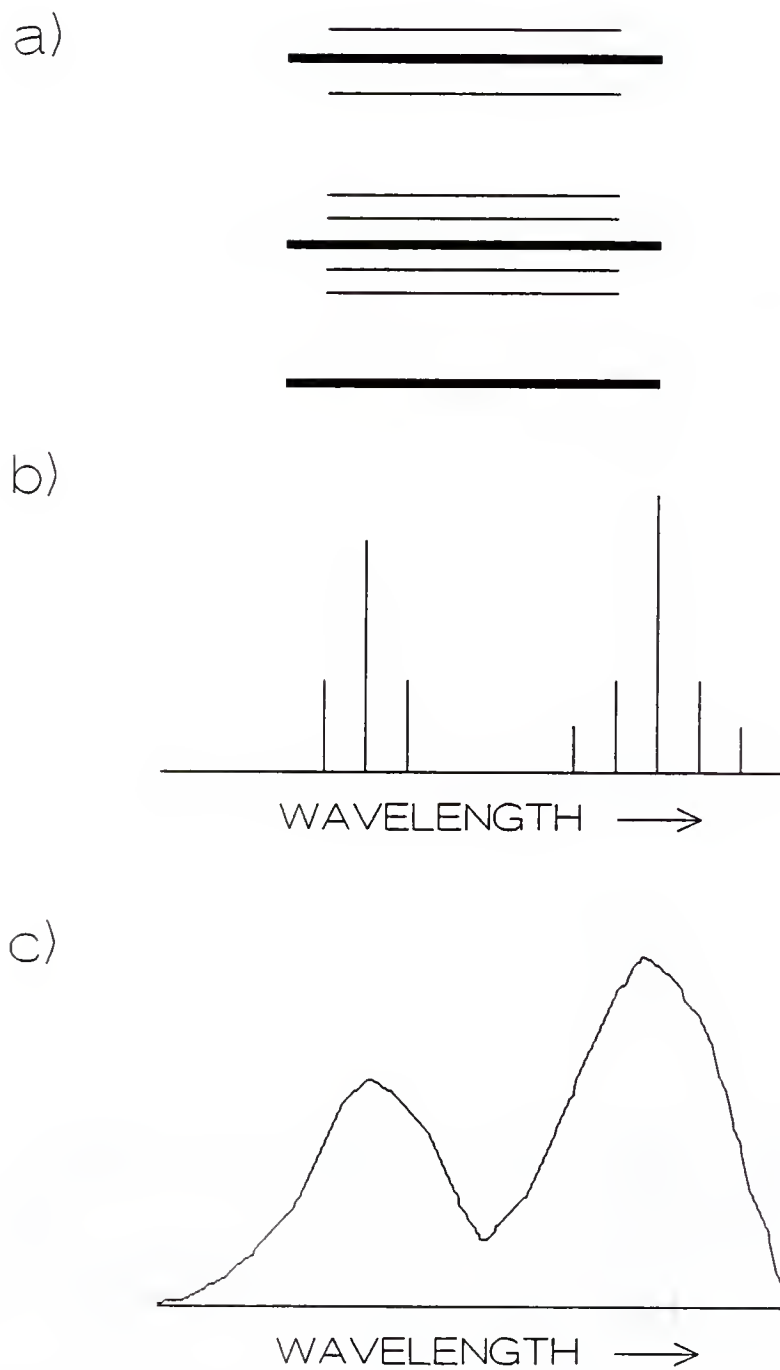


Figure 2-3. Diagram showing a) an energy level diagram and b) well resolved and c) poorly resolved spectra.

levels. One of the spectra has well resolved spectral bands, while the other has poorly resolved bands. Because of the broadening effects, electrons are spread into different vibrational and rotational levels [44]. Also because of the broadening effects, the fine structure of the spectrum is no longer resolved, but becomes smeared into much broader bands. This decreases the utility of luminescence spectroscopy for identifying the compound present and the selectivity when two or more luminescent compounds are present.

Cooling Effect

One way in which to reduce some of the broadening effects is by cooling the molecules, especially down to cryogenic temperatures (15 K) [45]. First, since the thermal motion is greatly reduced, the Doppler broadening is negligible. Also, because of the reduction in motion, collisional broadening is removed. Resonance broadening can also be eliminated by using mixed crystals. Finally, radiationless transitions to other vibrational and rotational levels are reduced because of the smaller available thermal energy.

As shown in Figure 2-4, there is a dramatic effect in the reduction of the temperature of the solution on the fluorescence spectra [46]. At room temperature, the spectrum is basically one broad band, offering no

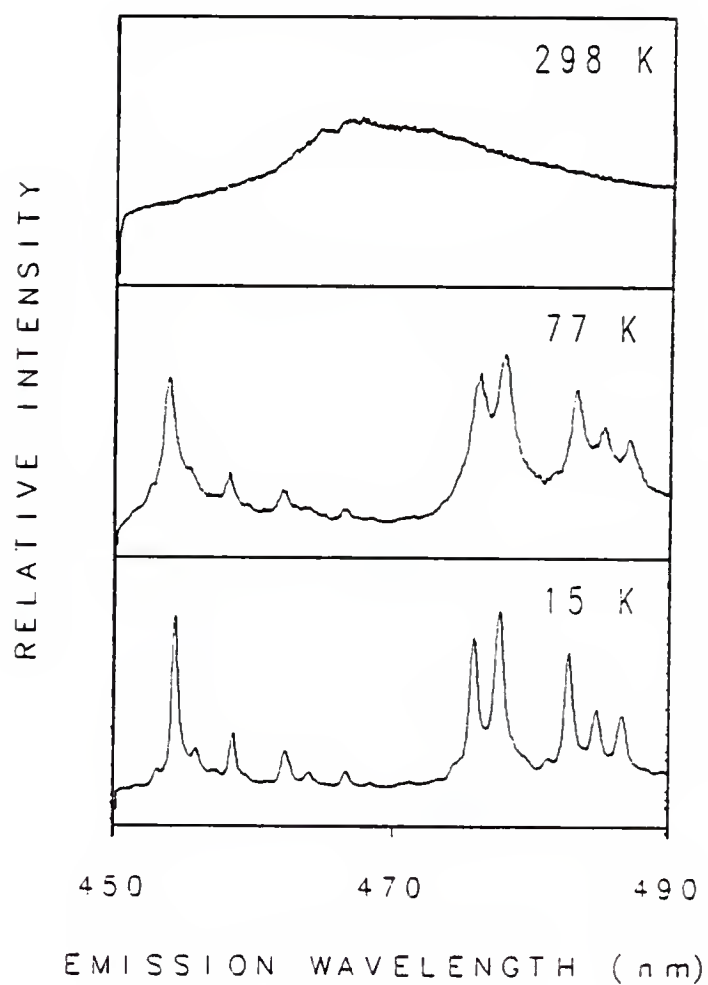


Figure 2-4. Spectra of perylene (700 ng/mL) in n-hexane at three different temperatures. Taken from reference [46].

information on the identity of the analyte. However, when the temperature is reduced to 77 K, individual bands begin to appear. At 15 K, there is an even greater improvement in resolution with some of the peaks becoming completely resolved. The reduction in band width is partially due to the Shpol'skii effect, but still demonstrates the usefulness in cooling the sample to increase the spectral information.

Although many of the broadening effects are removed by cooling, some of the remaining broadening effects still cause significant spreading of the spectral bands. This results from the fact that the matrix in which the compound is frozen still contains inhomogeneities [41]. As stated before, these different environments (called sites) cause the molecule to have different excited energy states, which in turn results in the slight variations in the emitted wavelengths. This is shown schematically in Figure 2-5. When molecules emit light, each produces a sharp peak, known as a zero phonon line (ZPL), and a broad phonon wing (Fig. 2-5a) [47]. Because of the environmental effects, the ZPLs occur at different wavelengths (Fig. 2-5b). The combination of the broad wings and the environmental effects results in the broad bands (Fig. 2-5c).

One method to reduce the spectral band broadening is by annealing the sample. When samples are cooled too rapidly, defects form in the crystalline lattice. These defects result in the analyte being exposed to different

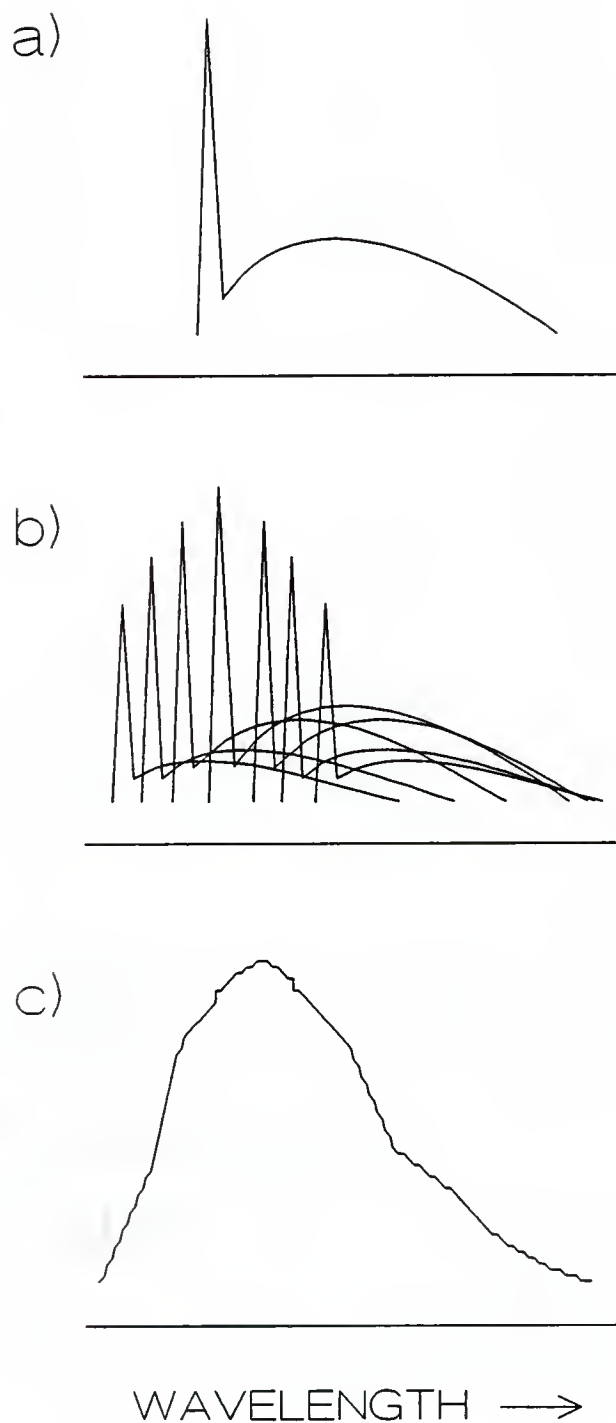


Figure 2-5. Schematic showing inhomogeneous broadening: a) a transition for a single molecule, b) transitions for many molecules, and c) how the band actually appears. Reproduced from reference [47].

environments, and therefore, giving slightly different spectral characteristics. Annealing involves heating the crystal to a temperature of about one-half the melting point of the solvent [45]. This allows the solvent structure to rearrange, and thus, eliminate the imperfections.

One must be careful, though, not to heat the sample too much, since the analyte molecules may aggregate together [45]. Because of this aggregation, coupling of the energy levels of the analyte may result. This would then lead to increased spectral broadening. Aggregation can also result if the solute to solvent ratio is too high or from cooling the sample too slowly.

Another technique for reducing spectral broadening is site selection spectroscopy [47]. By using a spectrally narrow excitation source, usually a dye laser, one is able to excite only those molecules which are in one or a small number of environments. This results in spectra with very sharp peaks, usually regardless of the matrix. Examples of this effect are shown in Figure 2-6 [47]. The dotted lines are spectra with ordinary excitation and the solid lines are with laser excitation. One can clearly see that by using selective excitation, the spectral peaks become much sharper. Also, in many cases, one can see the ZPLs along with their broad phonon wings.

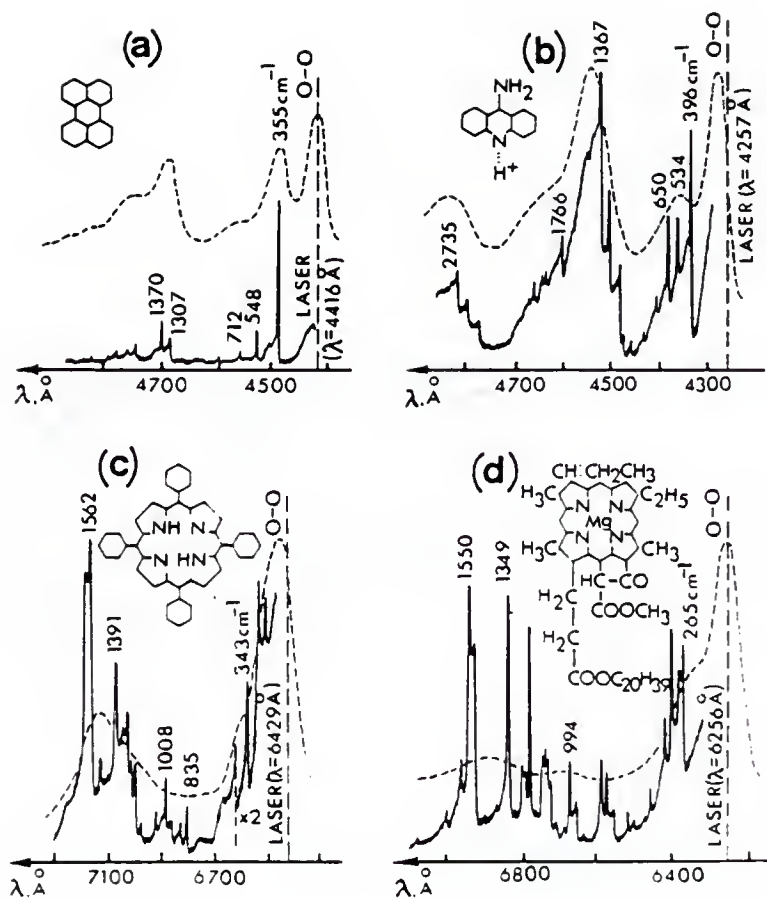


Figure 2-6. Fluorescence spectra of various compounds in different organic matrices at 4.2 K by ordinary excitation (dotted lines) and laser excitation (solid lines): a) perylene in ethanol, b) protonated form of 9-aminoacridine in ethanol, c) tetraphenylporphyrin in polystyrene, and d) protochlorophyll in ether. Taken from reference [47].

Shpol'skii Effect

Site selection spectroscopy can be very useful for reducing the amount of spectral broadening; however, there are two significant problems with the technique. First, it is only useful for those molecules in certain sites which can be excited at the specific wavelength of the laser. Secondly, phosphorescence, and in some cases fluorescence, spectral bands are not narrowed in site selection spectroscopy [48]. This results from the molecules being in similar sites, but not identical sites [49]. Therefore, the molecules may have the same S_1-S_0 (fluorescence) transition energies, but different T_1-S_0 (phosphorescence) transition energies. To overcome this, researchers have tried exciting the molecules directly to the triplet state [50]. However, since it is a forbidden transition, this excitation process has a low probability.

Shpol'skii spectroscopy, although not as universal as site selection spectroscopy, is applicable to nearly all PAHs. Therefore, an entire class of compounds can be determined, qualitatively and quantitatively, by the use of one technique. It is also useful for some compounds other than PAHs.

Even though Shpol'skii spectroscopy has been studied extensively, it is still not fully understood. However, it has been established that the Shpol'skii effect is related

to the shape and dimensions of the PAH in relation to the n-alkane used. This relationship is shown in Table 2-1 [51]. These data show that the optimum Shpol'skii solvent for each compound matches the linear dimension of that compound. As shown in Figure 2-7 [51], the alkanes have a zig-zag conformation which allows the PAHs to fit nicely into the frozen matrices. This was referred to as the "key and hole" rule by Pfister [52].

Although the principle works well for the linear PAHs, it becomes more difficult to see for other PAHs, such as coronene and 1,2-benzo(a)pyrene, which are not linear. The proper Shpol'skii solvents have to be determined experimentally for each individual PAH. Lai et al. determined the best solvent for 23 different PAHs [53].

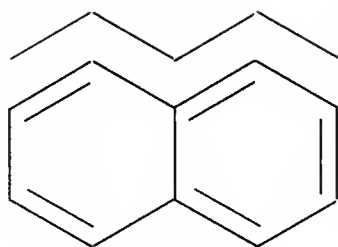
Work has also been performed using X-ray diffraction and ESR to study the Shpol'skii effect [54]. From the X-ray experiments, Merle et al. were able to determine the crystalline form of heptane and from the ESR experiments, the orientation of the coronene molecule with respect to the heptane lattice. The results of their studies are shown in Figure 2-8. The coronene molecule replaces three of the heptane molecules and lies in the plane of the other heptane molecules. Of course, the orientation and number of n-alkane molecules replaced will depend on the PAH and the n-alkane used for Shpol'skii spectroscopy.

Table 2-1. Data showing dimensions for several PAHs and their best Shpol'skii solvent. Taken from ref. [50].

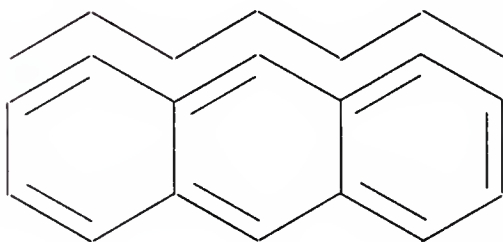
<u>PAH</u>	<u>length*</u>	<u>n-alkane</u>	<u>length*</u>
naphthalene	7.2	pentane	7.4
anthracene	10.0	heptane	10.0
naphthacene	12.8	nonane	12.8

*in angstroms

a)



b)



c)

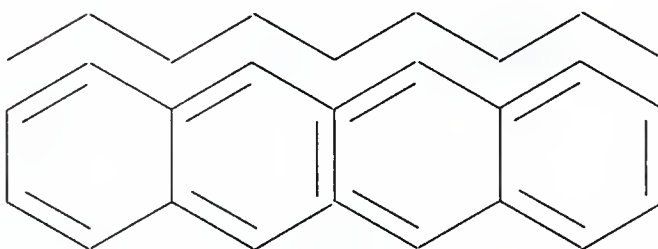


Figure 2-7. PAHs along with their optimum Shpol'skii solvent showing how they relate: a) naphthalene and pentane, b) anthracene and heptane, and c) naphthacene and nonane. Redrawn from reference [51].

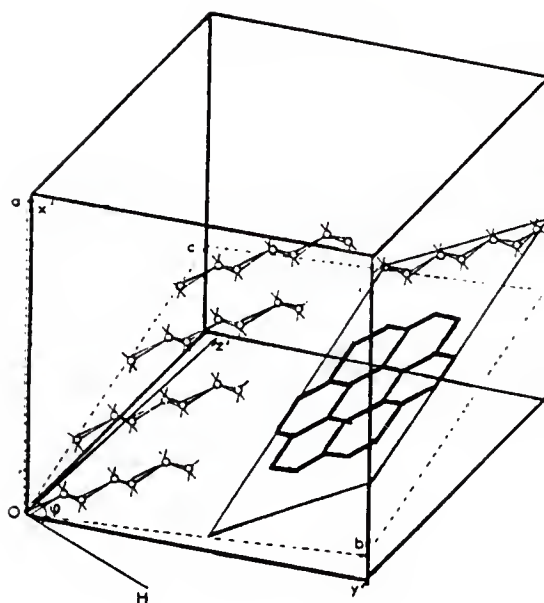


Figure 2-8. Orientation of coronene and heptane molecules with respect to the crystallographic axis. Taken from reference [54].

CHAPTER 3 EXPERIMENTAL

Instrumentation

A Perkin-Elmer (Norwalk, CT) Model 8500 gas chromatograph with a J & W Scientific (Folsom, CA) 30 m x 0.32 mm DB-5 capillary column was used for separating the PAHs. For the transfer line, part of the column itself was used. The heated transfer line was made from 0.030" x 1/16" 316 stainless steel tubing. A 1/16" stainless steel male union with an Alltech Associates, Inc. (Deerfield, IL) 1/16" to 0.4 mm graphite reducing ferrule was used to seal between the capillary column and the stainless steel tubing at the GC. A three way stainless steel tee was inserted into the transfer line for the introduction of hexane as a mixture of 781 ppm hexane in helium. The hexane/helium mixture was introduced with a Newport Corporation (Fountain Valley, CA) BV100 Molecular Beam Valve. The transfer line was heated using an SPC Technology universal step-down transformer distributed by Newark Electronics (Jacksonville, FL) and a Variac. The current was applied to the transfer line by silver soldering the wire to the union at the GC and silver soldering the other wire to the stainless steel tubing approximately 1.5 cm from the end of the tubing at the

vacuum chamber. Supelco, Inc. (Bellefonte, PA) Supeltex M-2A 1/16" ferrules were used for the three-way tee and the reducing union inside the chamber (see Figure 3-1) and at the GC.

The GC/vacuum chamber interface used in these experiments is shown in Figure 3-1. This design was based on the work by Brown and Wilkins [55]; the interface was built in our departmental machine shop. The 0.25" ID x 0.75" OD Teflon V-rings were obtained from Hyarco (Skokie, IL). The 1/8" ID x 1/4" OD ceramic tube was obtained from Omega Engineering, Inc. (Stamford, CT). High vacuum grease from Dow Corning Corp. (Midland, MI) was used to obtain a more efficient vacuum seal between the ceramic tube and the Teflon V-rings. Supeltex M-2A 1/16" and 1/4" ferrules were used for the reducing union. The interface formed a vacuum seal by tightening the lower nut which compressed the Teflon V-rings. The upper nut had retainer rings on each side of it, which stayed in place since the ceramic tube had been notched. When the upper nut was turned, it pushed on the retainer rings causing the ceramic tube, and therefore the tip of the capillary, to move. Thus, the tip of the capillary could be positioned precisely while still maintaining a high vacuum. When doing manual injections, the interface was replaced with a septum and a Cajon fitting welded to a face plate.

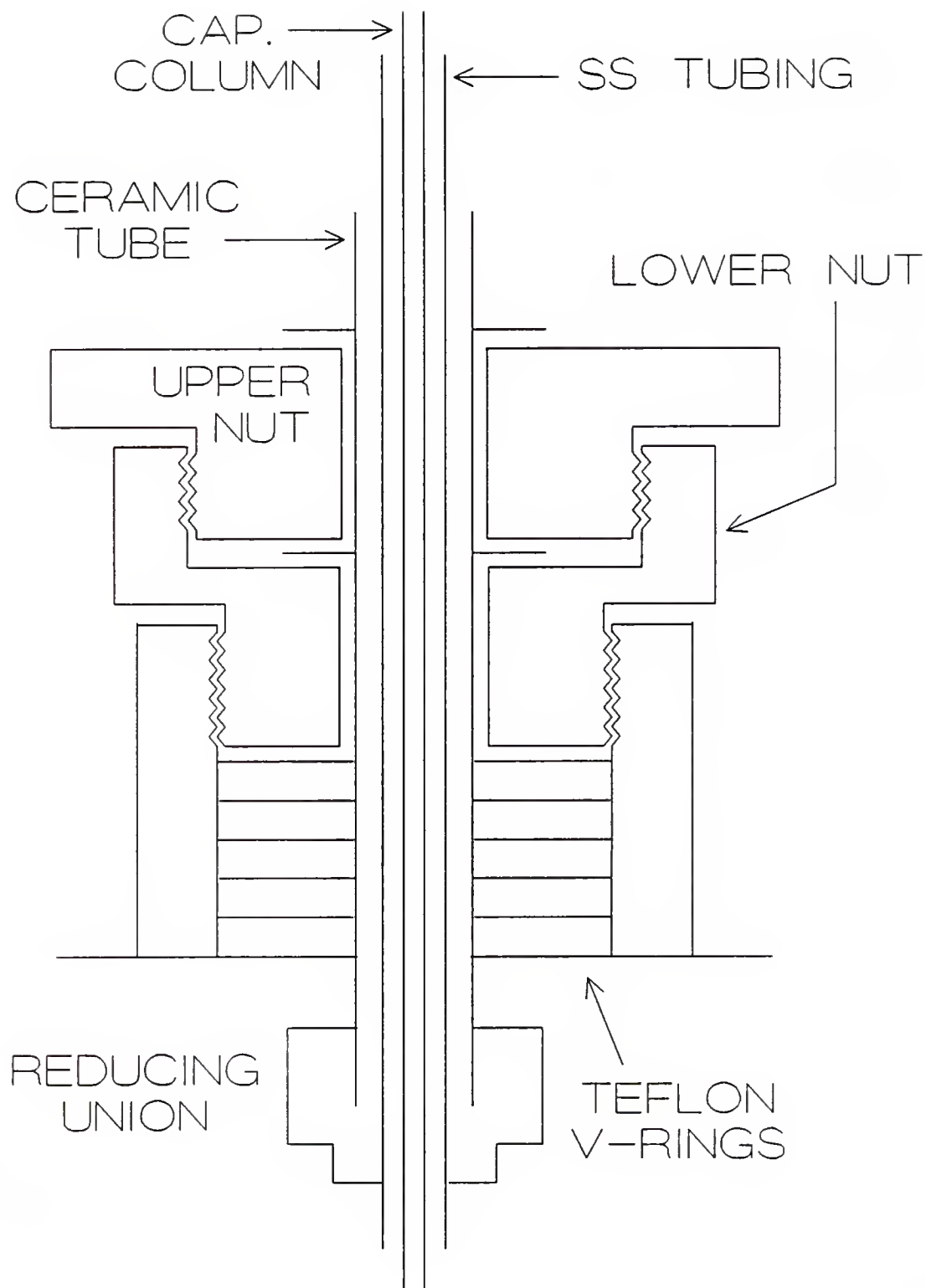


Figure 3-1. GC/vacuum chamber interface used in these experiments. Based on the work by Brown and Wilkins [55].

The vacuum chamber consisted of a Vac-U-Flat five-way cross and a Vac-U-Flat three-way cross, each with 6" flanges, a Vac-U-Flat three-way cross with 2" flanges, a 6" quartz viewport, and two direct-drive rotary motion feedthroughs which were all obtained from Huntington Mechanical Laboratories (Mountain View, CA). A Turbo-V80A turbomolecular pump, an SD-90 direct-drive mechanical pump, a Model 860A cold cathode ionization gauge, and a Model 801 thermocouple gauge were obtained from Varian Vacuum Products (Lexington, MA). The vacuum pressure was in the 10^{-5} torr range when the beam valve and the flow from the GC were off. When the beam valve was on, helium was flowing from the GC, and the system was cooled, the pressure was approximately 1 mtorr and the belt temperature was between 50 and 60 K. A laboratory built liquid nitrogen trap and a molecular sieve trap were placed between the turbo and mechanical pumps to reduce backstreaming. An APD Cryogenics, Inc. (Allentown, PA) displax Model CS-202 closed-cycle helium refrigeration system was used to maintain the cryogenic temperatures.

The vacuum chamber, which is similar to the one used by Jones et al. [56], is shown in Figure 3-2. The Cajon fitting, which had been welded directly onto the five-way cross, was removed and replaced with a plate which was welded on. In this way, either the GC interface or the Cajon fitting could be used for introducing the samples.

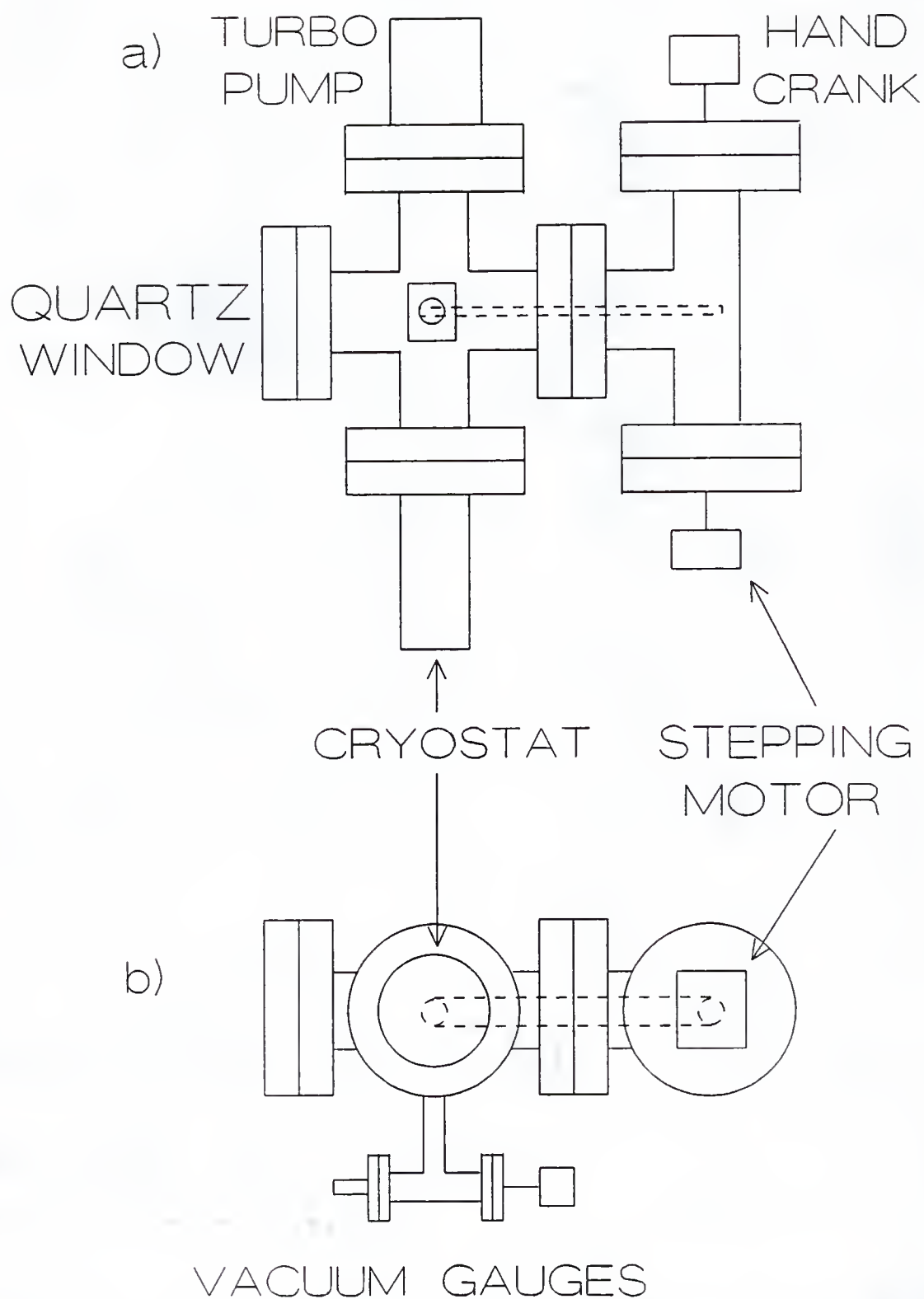


Figure 3-2. Vacuum chamber used in these experiments: a) top and b) side views. Belt and spools are shown as dashed lines.

Also, the Vac-U-Flat flexible coupling, which had been used to tighten the belt, was removed, since it was difficult to work with it and it was thought that the coupling was causing contaminants to remain in the chamber. The method which was then used for tightening the belt is shown in Figure 3-3. The two feedthroughs which had been used for rotating the rear spool to turn the belt were mounted on plates. These plates were held onto flanges with bolts and O-rings were placed between the plates and flanges to form the vacuum seal. The plates which held the feedthroughs onto the vacuum chamber had oval holes for the mounting bolts allowing the plates to be moved in the direction of the belt to tighten the belt.

To turn the belt continuously at a constant rate, a Hurst (Princeton, IN) Model ABS3008-003 stepping motor with 1800 steps per revolution and a Hurst Model EPC-015 stepping motor controller were employed. The stepping motor was mounted to a U-bracket which had one of the feedthrough plates as a part of the bracket. A knob was mounted on the other feedthrough for manually turning the belt, but the stepping motor had to be disconnected before using it.

As previously done by Jones et al., the front spool was bolted directly onto the end of the cold stage with an indium gasket between them and did not rotate. The spool was made of oxygen-free copper and was $3/4$ " in diameter and $7/8$ " wide. It had a groove cut in it $1/64$ " deep and $11/16$ "

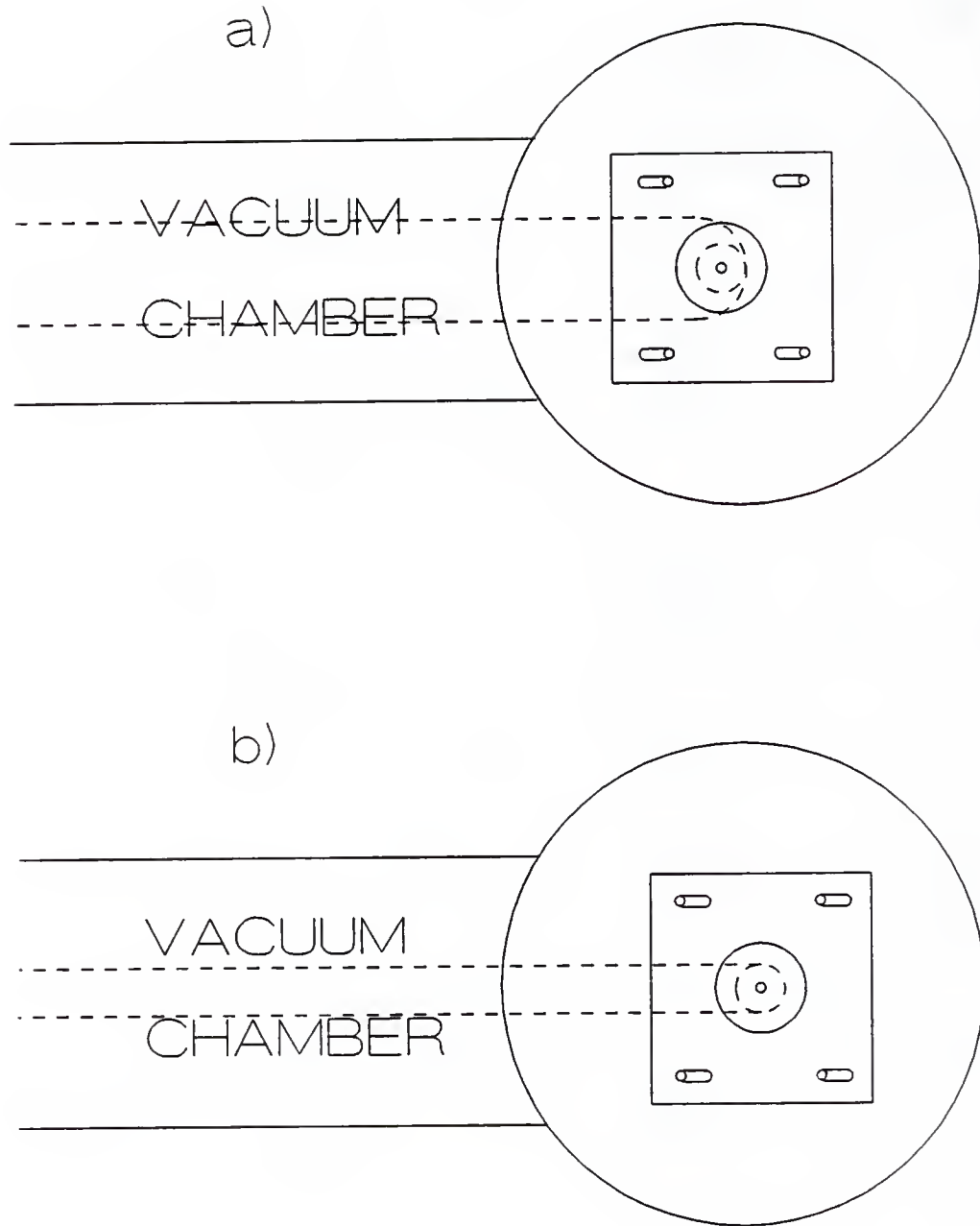
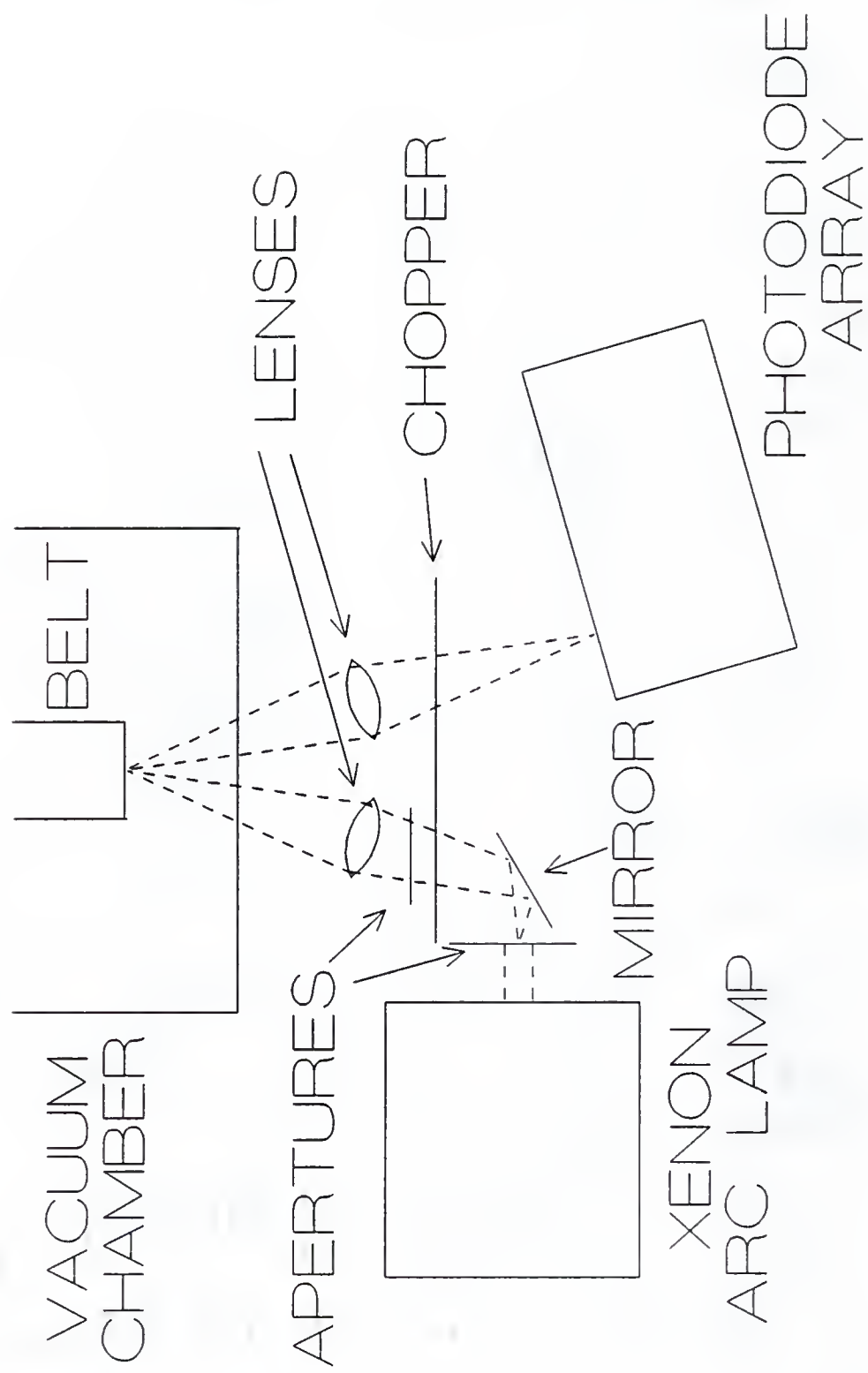


Figure 3-3. Schematic showing how the belt was tightened:
a) the belt loose and b) the belt tightened. Belt and spool
are shown as dashed lines.

wide so that the belt would remain on the spool. The rear spool was made of aluminum and also had a $11/16$ " wide groove so that the belt would remain in place. The portion of the spool which the belt passed over was $1/2$ " in diameter and the entire diameter was $3/4$ ". The belt itself was made of a 0.003" thick brass sheet cut $5/8$ " wide and $23\ 1/2$ " long. This strip of brass was then spot welded with a $1/4$ " overlap to form the belt.

The spectroscopic portion of the system is shown in Figure 3-4. The entire output of an Oriel Corp. (Stamford, CT) Model 8500 75-W xenon arc lamp was used for excitation. The output from the arc lamp was directed onto the belt by passing it through an adjustable aperture, reflecting it off a mirror, and then passing it through another adjustable aperture and a 6" focal length quartz lens. Another 6" focal length quartz lens was used for collecting the emission and focusing it into an Instruments SA, Inc. (Metuchen, NJ) Model UFS-200 flat field spectrograph. This spectrograph allowed the Princeton Instruments, Inc. (Princeton, NJ) Model IRY-700 photodiode array to see the 200-800 nm range. Along with the photodiode array, a Princeton Instruments, Inc. Model 120 OSMA Detector Controller and a PCs Limited (Austin, TX) Model AT113 personal computer were used for collecting data. An Ithaco, Inc. (Ithaca, NY) Model 382A optical chopper with a three-hole chopping wheel operated at 700 Hz was used for

Figure 3-4. Schematic diagram of the spectroscopic portion of the system. Dashed lines indicate light rays.



modulating the light. For the measurements at 77 K, a SPEX Fluorolog double monochromator fluorimeter was used.

Reagents

Pyrene, 1,2-benzofluorene, 2,3-benzofluorene, and triphenylene were obtained from Aldrich (Milwaukee, WI) and phenanthrene, fluorene, and chrysene were obtained from Eastman Kodak (Rochester, NY). All were labeled as 98% pure or better and were used as received. Hexane (UV Grade) was obtained from Burdick & Jackson (Muskegon, MI). It was labeled as 99.9% pure and also was used as received. Stock solutions of approximately 100 $\mu\text{g/mL}$ for each PAH was made and dilutions were made from the stock solutions as needed.

Procedure

When doing transfers from the gas chromatograph, the capillary was fed through the transfer line and an approximately 1 cm section of capillary was left protruding from the end of the stainless steel tubing. The liquid nitrogen trap was then filled and the roughing pump started. After approximately two minutes, the turbo pump was started. The transfer line was then heated and the helium refrigerator turned on.

It was necessary to wait until the system was under vacuum and the transfer line was heated to adjust the height of the capillary tip above the surface of the belt, since

the capillary would draw up into the stainless steel tubing upon heating the transfer line. The capillary was adjusted to a height of approximately 0.5 mm above the belt. It has been recommended to have the tip of the capillary approximately 100-200 μm above the deposition surface [55]. The tip of the capillary was farther from the surface than recommended because the column would become plugged by hexane freezing in the tip of the capillary unless it was atleast that high above the surface.

One microliter of the standards were then injected into the gas chromatograph. The injector was operated in the splitless mode for 2 min, then the split was opened for the rest of the run. The oven temperature was maintained at 130° C for 2 minutes, the temperature was then ramped at 30° C/min to 300° C and was held there for 10 min. The entire run was approximately 18 min. The injector and detector were maintained at 320° C.

Each spectrum was averaged for 2.5 s. Since large files were produced and they required a significant amount of memory, it was necessary to wait until just before the peaks eluted before beginning to collect data. Since the amount of hexane being introduced through the molecular beam valve was too low (see Chapter 4), only the lowest concentration injected and the origin were used to estimate the limits of detection. The average noise was determined by zooming in on a 30 diode section of the background

spectra where the emission peaks used for the calibration curves appeared. The photodiode array program automatically calculates the mean and standard deviation of those 30 diodes. The standard deviation was then multiplied by three, which was taken as the intensity at the limit of detection.

CHAPTER 4 RESULTS AND DISCUSSION

Phosphorescence Background

One of the major problems encountered in this project has been that of phosphorescence background, a spectrum of which is shown in Figure 4-1. This background is seen whenever a liquid is injected onto the belt, whether it is a pure solvent or a standard. Hexane, heptane, methanol, and acetonitrile all have been injected and each give the same background; however, it is not seen when nothing is injected. It is not scatter, since the phosphorescence can actually be seen on the belt with the naked eye as a blue glow. Also, it appears whether the solvent is injected manually with a syringe or by first injecting it onto the gas chromatograph. The background is also seen continuously when the molecular beam valve is used to introduce the hexane. Along with the background, the vacuum pressure is now in the 10^{-5} torr range for the chamber alone, which is approximately 2 orders of magnitude higher than previously obtained.

In order to remove or reduce the phosphorescence background, a number of experimental procedures have been performed (see Table 4-1). First, spectra were taken with

Figure 4-1. Phosphorescence spectrum of the background when hexane was injected.

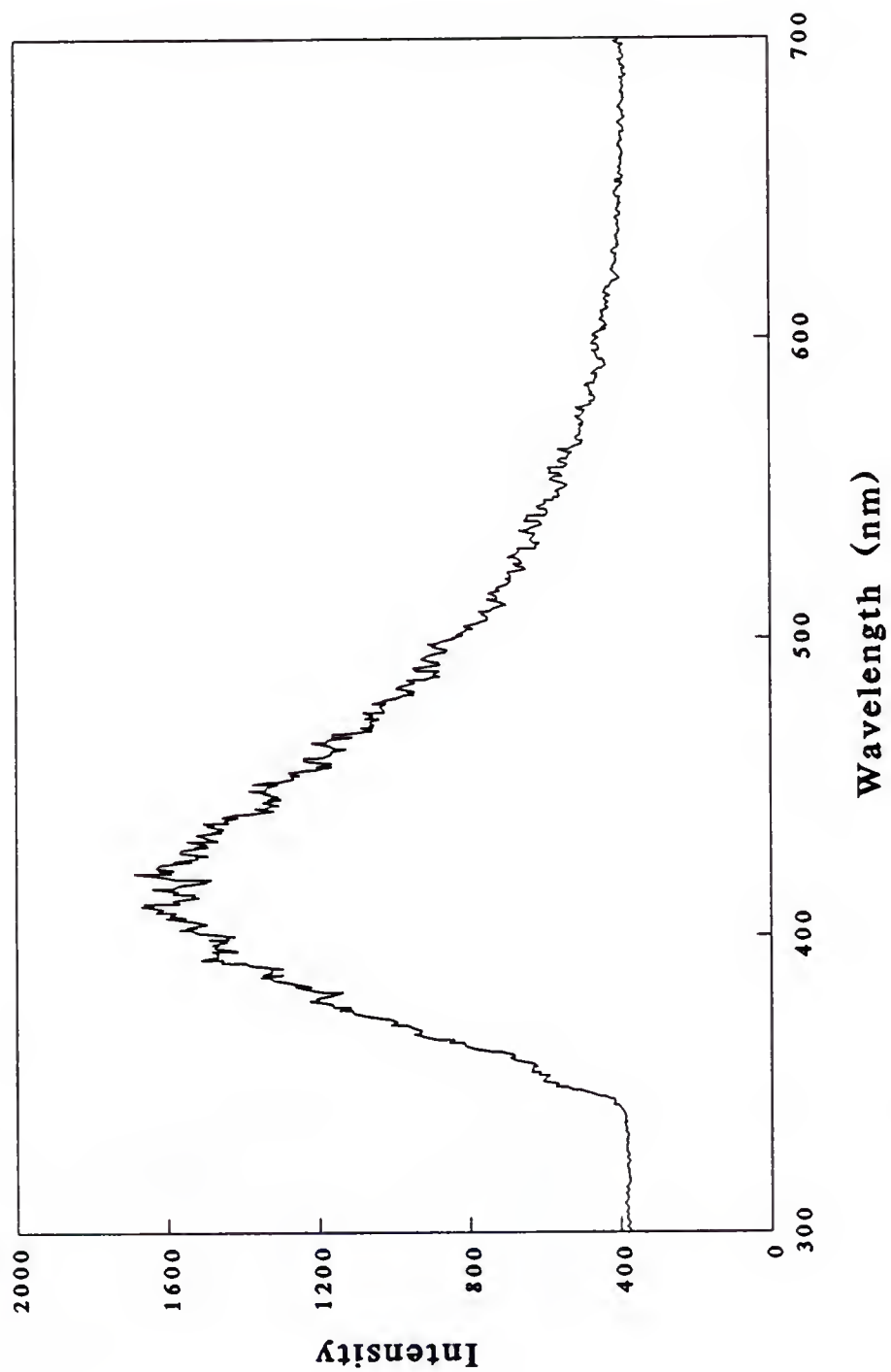


Table 4-1. List of experimental procedures to delineate and to minimize the phosphorescence background problem.

<u>Source</u>	<u>Experiment</u>	<u>Replicates</u>	<u>Results</u>
1. belt (no solvent)	spectrum at 15 K	many	NSB*
2. belt (with solvent)	same	many	background present
3. hexane	spectrum at 77 K on SPEX	once	NSB
4. pump oil in hexane	spectrum at 77 K on SPEX	once	PSB
5. leaks	leaks were found and corrected	-	no change from #2
6. belt (with hexane)	cleaned chamber with acetone (see text)	several	no change from #2
7. belt (with hexane)	same as #6, but also cleaned cryostat and turbo with Freon	once	no change from #2
8. belt (with hexane)	added molecular sieve and nitrogen traps	-	no change from #2
9. belt (with hexane)	wrapped chamber with heating tape while under vacuum	several	no change from #2
10. ion gauge	put on cold cathode and hot filament ion gauges simultaneously	once	no change from #2
11. ion gauge	put on hot filament ion gauge alone	-	pressure dropped to 2×10^{-7} torr

CONCLUSION: Since the pressure has dropped, most likely background is gone; therefore, phosphorescence background probably due to contamination in the ion gauge, most likely pump oil.

*NSB: not source of background; PSB: possible source of background.

the belt cooled, but no solvent or sample injected onto the belt. As stated previously, the phosphorescence background is not observed when there is no solvent or sample present.

Since the phosphorescence background is only seen when a solvent is injected, the first thought was that the solvents were contaminated. Figure 4-2 shows spectra of phenanthrene in hexane, hexane, and an empty tube (blank) taken at 77 K using the SPEX fluorimeter. As one can see, the signal is larger for the empty tube alone than when hexane is present, indicating that the signal must be due to scatter.

Another possible source of phosphorescence is pump oil from the roughing pump used to back-up the turbomolecular pump. Therefore, a spectrum of pump oil was taken using the SPEX fluorimeter, which is shown in Figure 4-3. One drop of pump oil was diluted in 20 mL of hexane. As one can see, the hexane gives essentially no signal, as is expected; however, the pump oil phosphoresces very strongly.

A large vacuum leak was discovered in the vacuum chamber near where the cold spool is located. It was hoped that when the leak was corrected, the background would go away. However, the background still remained after the leak was sealed. All of the leaks which were located using a helium leak detector were corrected. Therefore, the background was not a result of leaks in the system.

Figure 4-2. Spectra of 126 $\mu\text{g/mL}$ phenanthrene in n-hexane, hexane, and an empty tube (blank). Spectra were taken at 77 K using the SPEX fluorimeter. Excitation wavelength was 250 nm.

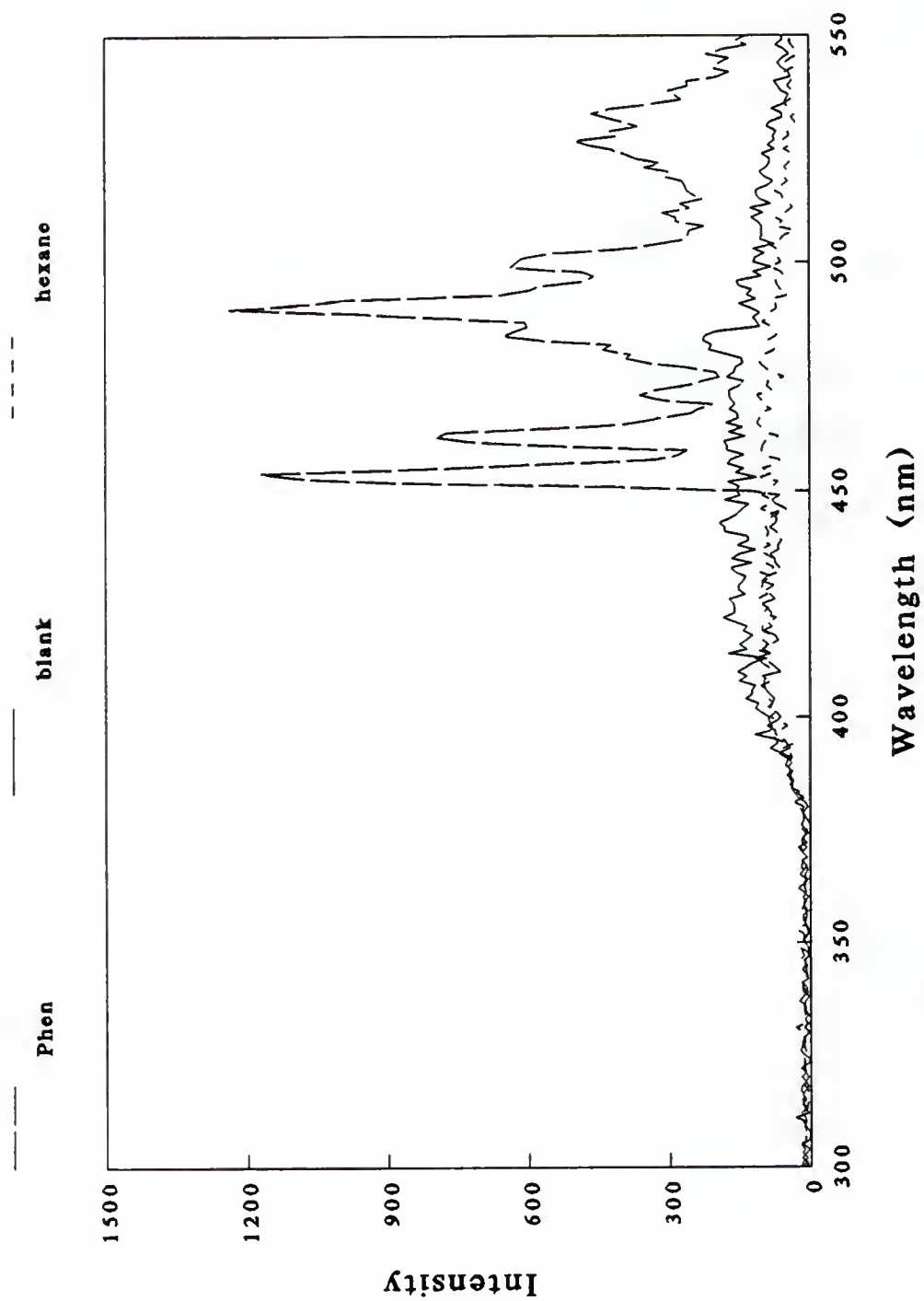
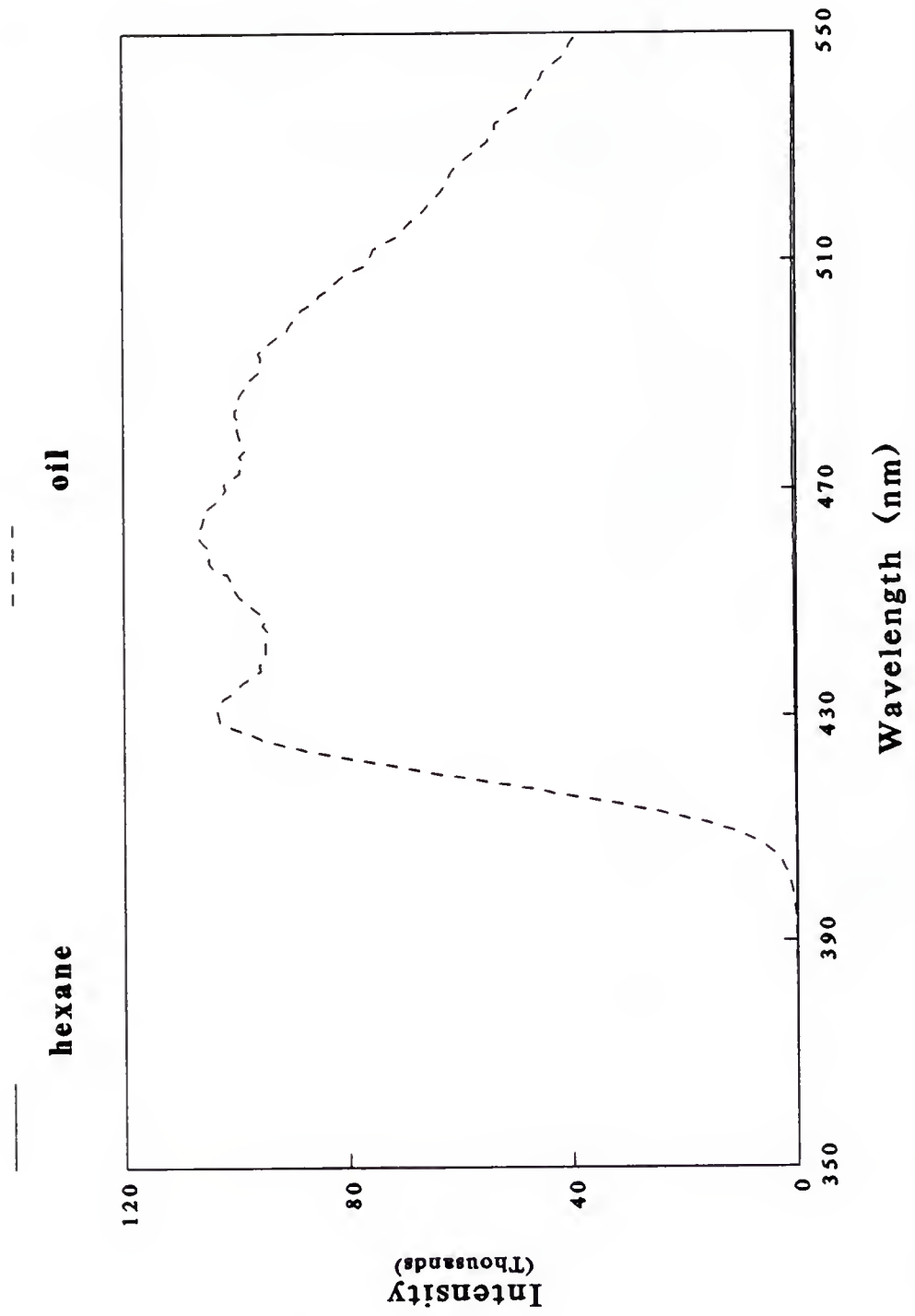


Figure 4-3. Spectra of hexane and pump oil diluted in hexane. Spectra taken at 77 K using the SPEX fluorimeter. Excitation wavelength was 317 nm.



The system has also been completely dismantled and thoroughly cleaned. All parts of the system which are bakable were placed in an oven at 200° C for 24 hr. The vacuum gauges were cleaned as thoroughly as possible with acetone. After reassembling the system, the vacuum pressure and the background remained the same. The cleaning process was then repeated with the exception that this time the turbomolecular pump and the cryostat were cleaned with Freon. The background still remained unchanged.

A molecular sieve trap and a liquid nitrogen trap were placed in line between the turbomolecular pump and the roughing pump to prevent backstreaming of pump oil when the turbomolecular pump was off. Also, the chamber was heated using heating tape while under vacuum. Neither of these things had any effect on the vacuum pressure or on the phosphorescence background. Since no other possibilities to correct the problem remained, it was decided to go ahead and collect the initial data in order to prove the efficacy of the approach.

After the data had been collected, the turbomolecular pump was connected directly to the ion gauge in an attempt to isolate the problem. The vacuum pressure was still approximately 10^{-5} torr. Another high vacuum gauge had been previously used on the system, but with the ion gauge also connected to the vacuum chamber. With a different ion gauge, the pressure now reached 2×10^{-7} torr. Therefore,

the problem may have been contamination in the ion gauge, since it read the same as the old gauge when both were on the system and no leaks were detected around the ion gauge with the helium leak detector. Since then, the chamber has been completely reassembled and a pressure of 2×10^{-7} torr has been achieved.

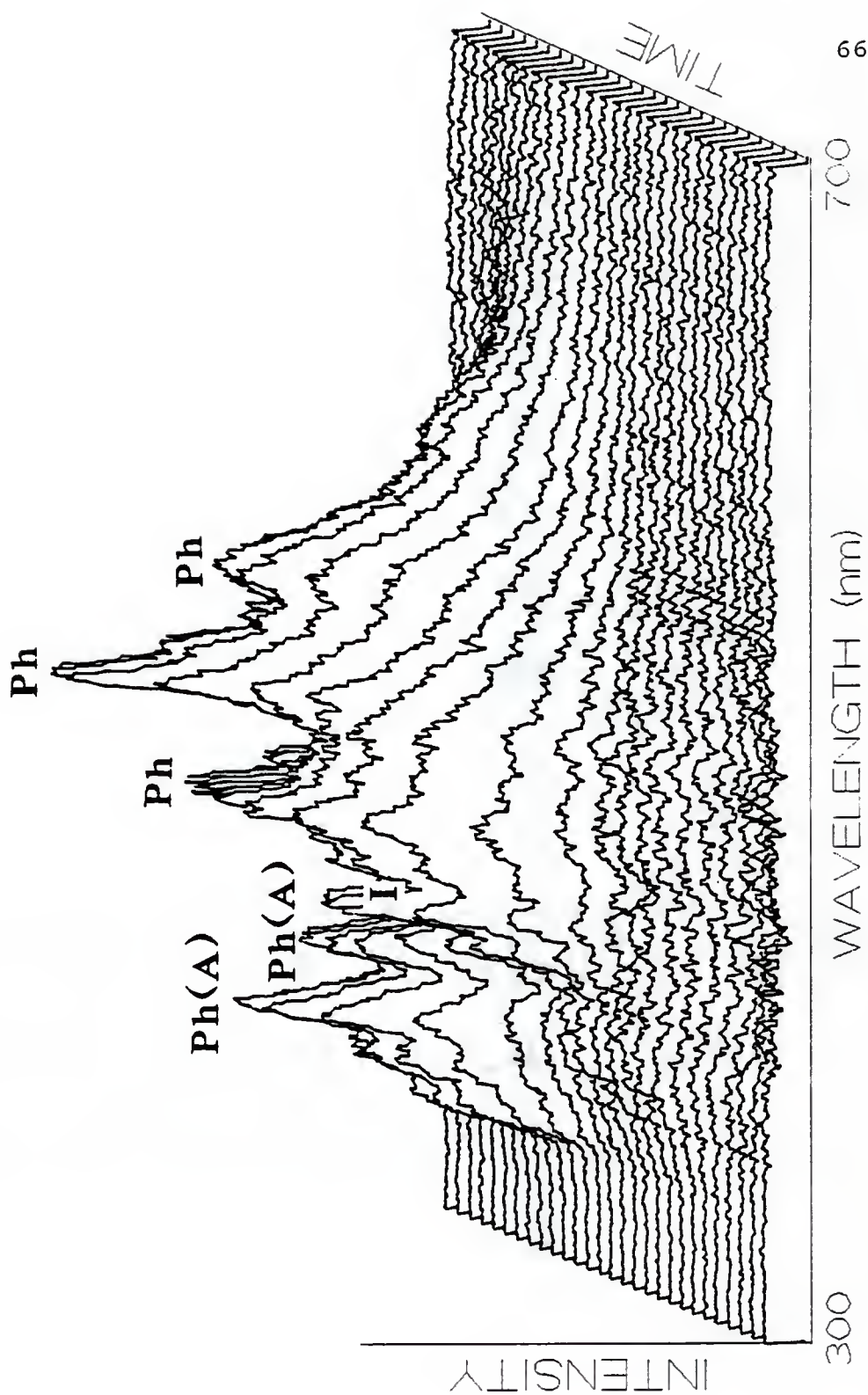
Since there were no leaks present and the solvent had been checked for phosphorescence background on another system at 77 K, the background was most likely a result of contamination in the system, probably from pump oil. One way to determine whether or not pump oil caused the background is to first correct the problem and then to introduce pump oil manually with a syringe and to see if the background returns. This experiment might be unwise since the system could simply become contaminated again with pump oil.

Chromatography

Chromatograms

Although the phosphorescence background degraded the effectiveness of the system, data were still collected which showed the potential of the GC/LTMLS system. All chromatograms shown have been background subtracted. Figure 4-4 shows a 3-D chromatogram of 78 $\mu\text{g/mL}$ phenanthrene. One can see that an impurity comes off at 8.39 min with a spectral maximum at 423 nm (I) just ahead of the

Figure 4-4. 3-D chromatogram of 78 $\mu\text{g/mL}$ phenanthrene; impurity peak (I): 8.39 min; phenanthrene peak (Ph): 8.59 min; phenanthrene aggregation: Ph(A); time scale is from 7.80 to 8.93 min.



phenanthrene peak. One can also see several peaks in the spectra when phenanthrene elutes which are not seen in either the 10 $\mu\text{g/mL}$ phenanthrene chromatogram (Figure 4-5) or in the manual injection of 131 $\mu\text{g/mL}$ of phenanthrene (Figure 4-6). These peaks can be seen more easily in Figure 4-7, which is a spectrum of 78 $\mu\text{g/mL}$ of phenanthrene at its chromatographic peak maximum.

In Figure 4-6, one can see a peak corresponding to the impurity (I) and the peaks for phenanthrene which is seen at both concentrations of phenanthrene in the chromatograms (Ph). However, the peak due to aggregation (Ph(A)) in the chromatogram of 78 $\mu\text{g/mL}$ is not seen in the manual injection. One explanation of this anomaly is that there may not have been a sufficient amount of hexane introduced through the beam valve for the higher concentration of phenanthrene. If the ratio of hexane to phenanthrene were too low, the phenanthrene molecules would not be isolated from one another enough to prevent interaction of them which could lead to spectral peaks arising from those interactions.

A similar effect to the one which was observed for phenanthrene was also observed for pyrene. A 3-D chromatogram of 94 $\mu\text{g/mL}$ pyrene is shown in Figure 4-8, a spectrum of pyrene at its chromatographic peak maximum is shown in Figure 4-9, and a spectrum of 123 $\mu\text{g/mL}$ pyrene is shown in Figure 4-10. Once again, there are peaks which are

Figure 4-5. 3-D chromatogram of 10 $\mu\text{g/mL}$ phenanthrene; conditions are the same as in Figure 4-4.

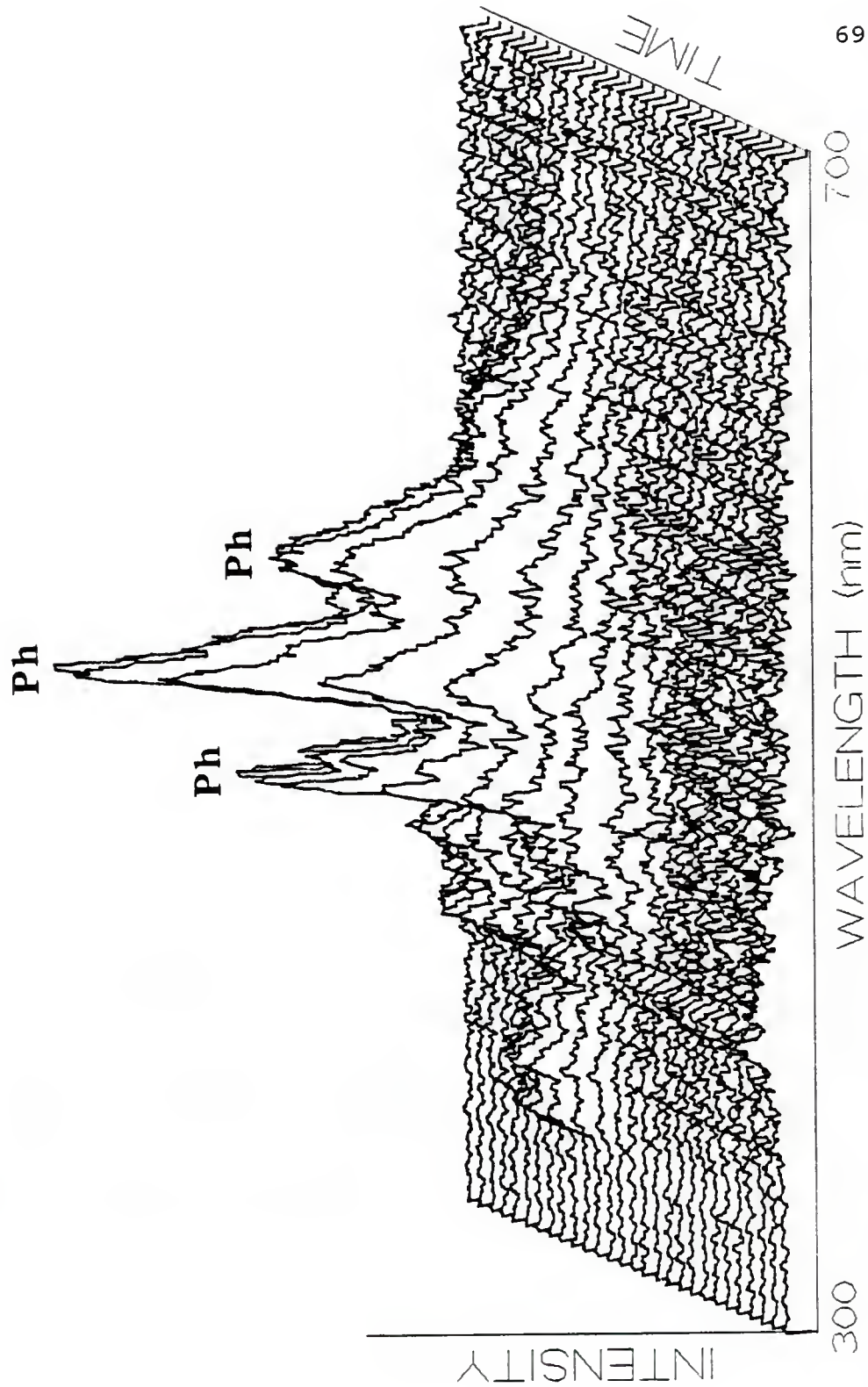


Figure 4-6. Spectrum of manual injection of 131 $\mu\text{g/mL}$ phenanthrene (Ph); impurity: I; where aggregation peaks appear in Figure 4-4: Ph(A).

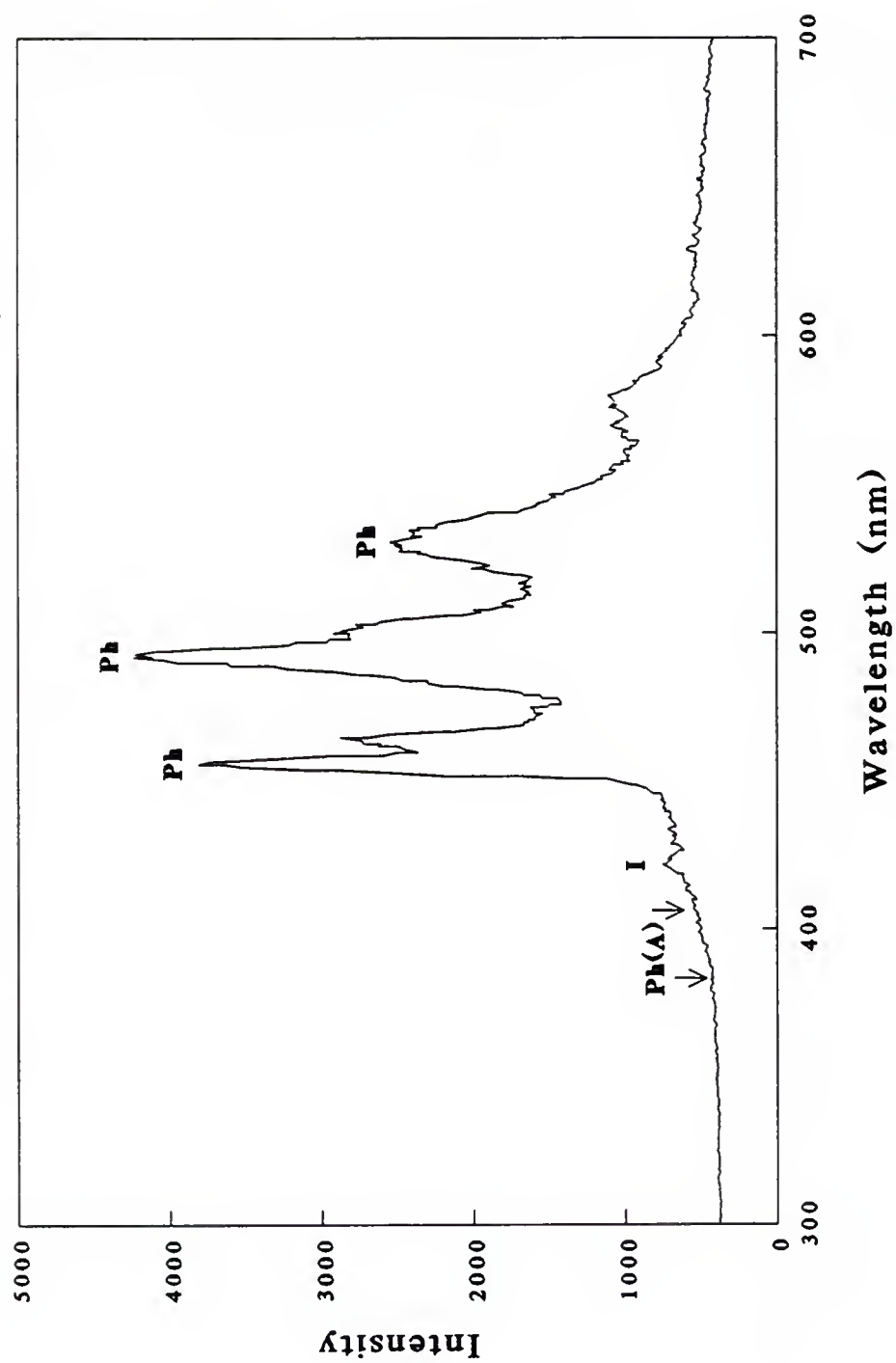


Figure 4-7. Spectrum of 78 $\mu\text{g/mL}$ of phenanthrene at its chromatographic peak maximum.

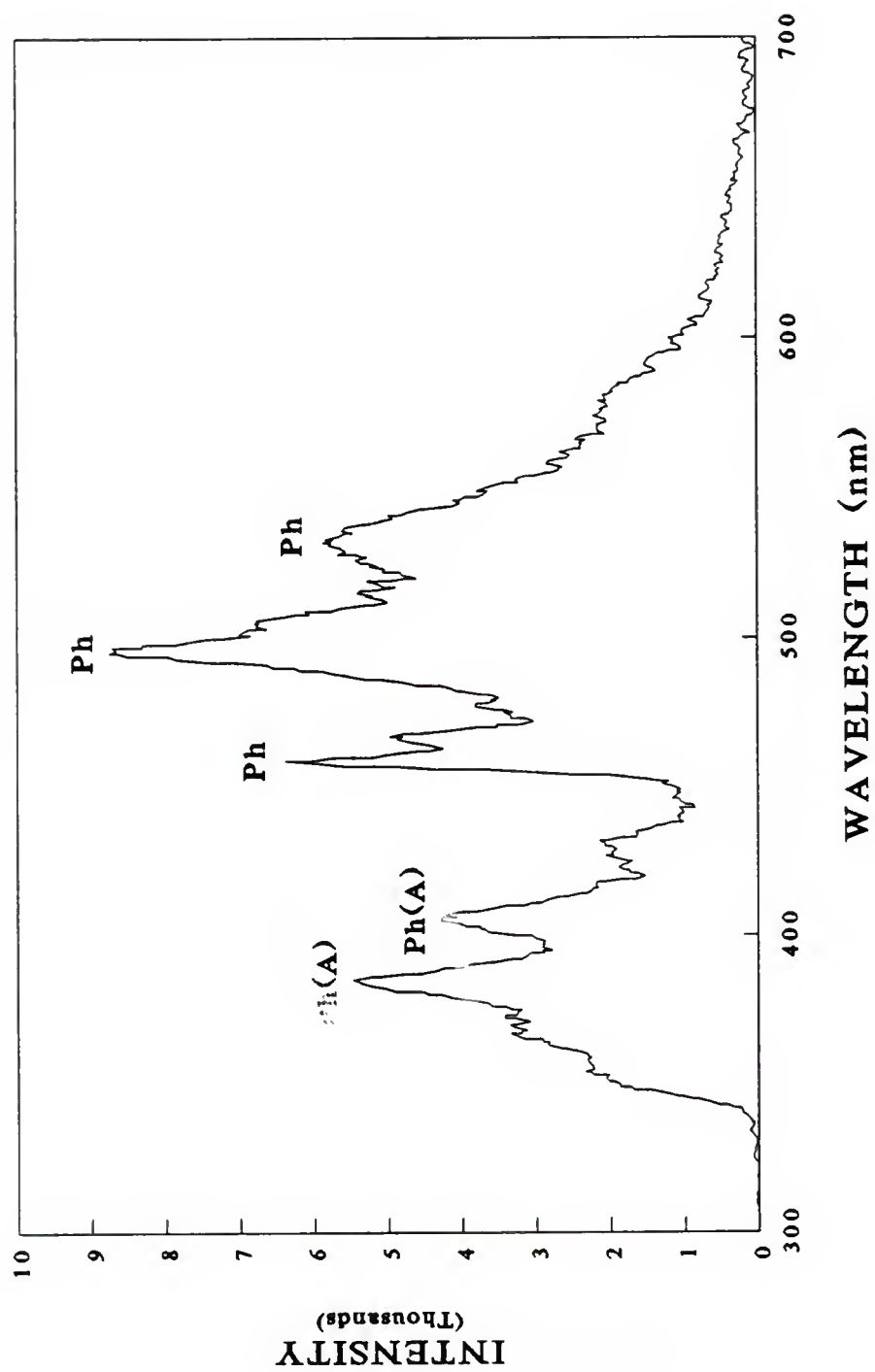


Figure 4-8. 3-D chromatogram of 94 $\mu\text{g/mL}$ pyrene; impurity peak (I): 10.76 min; pyrene peak (Py): 10.95 min; pyrene aggregation: Py(A); time scale is from 10.42 to 11.22 min.

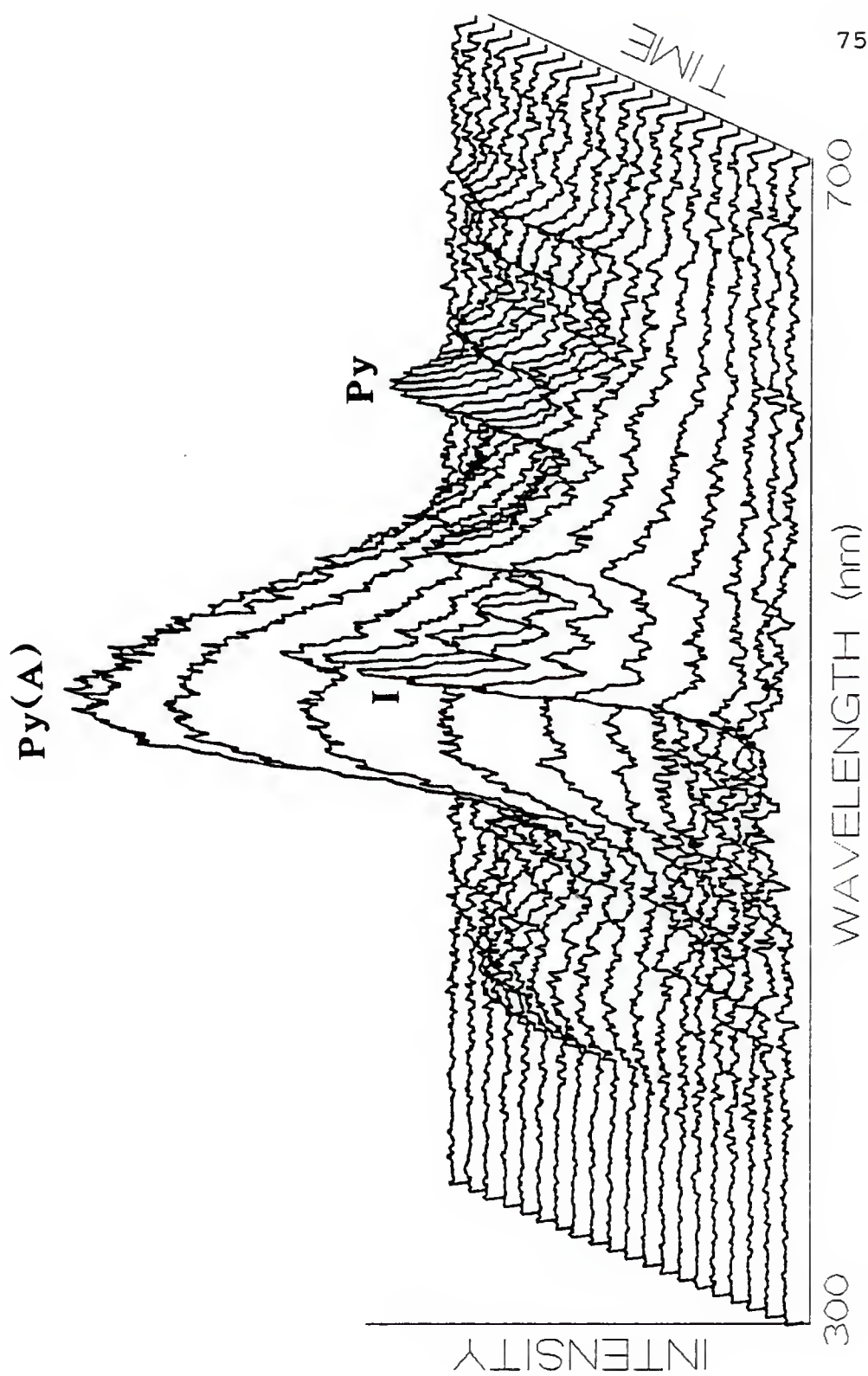


Figure 4-9. Spectrum of 94 $\mu\text{g/mL}$ of pyrene at its chromatographic peak maximum.

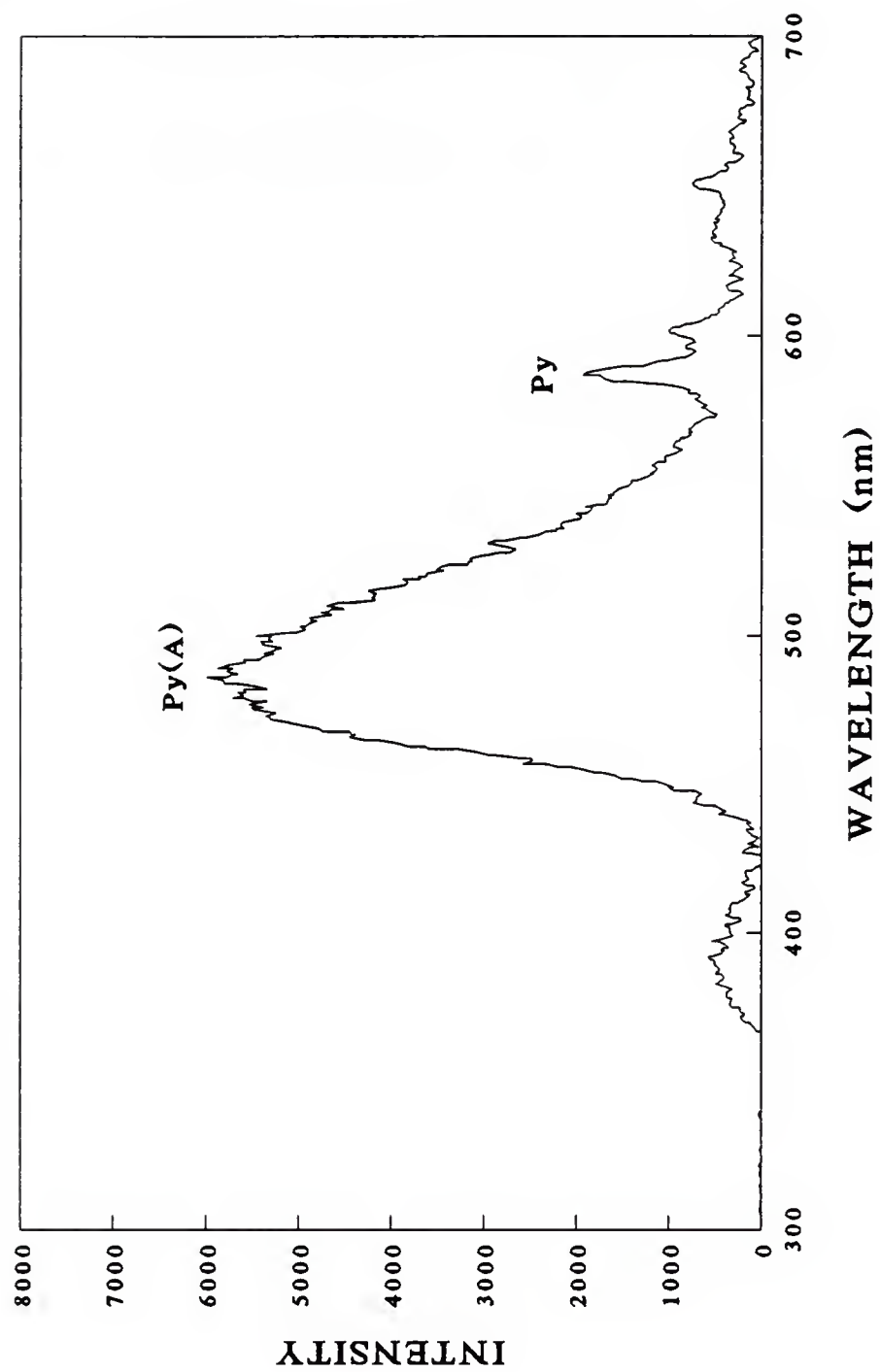
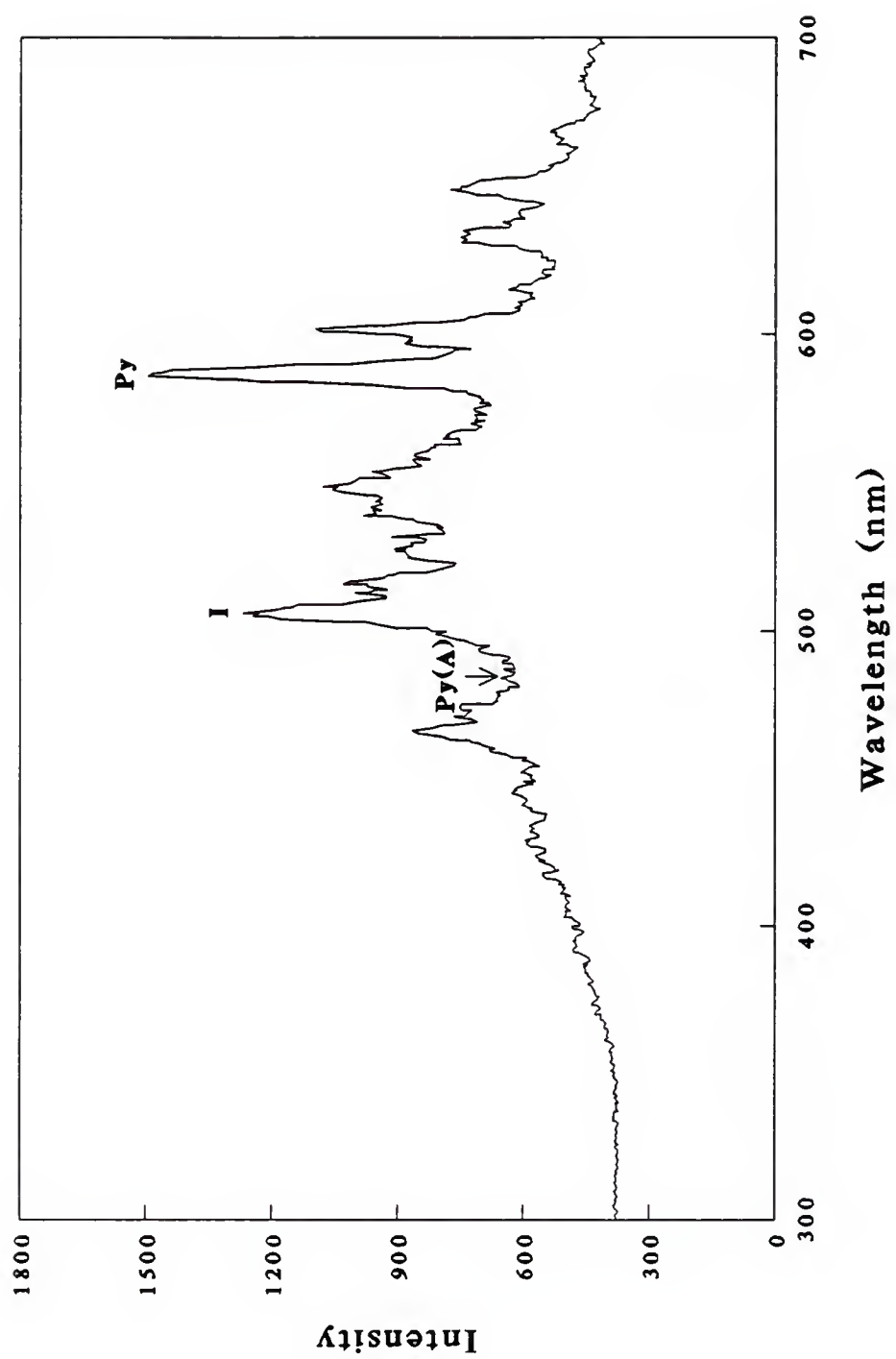


Figure 4-10. Spectrum of manual injection of 123 $\mu\text{g/mL}$ pyrene (Py); impurity: I; where aggregation peak appears in Figure 4-7: Py(A).



apparently due to impurities (I) (a spectrum of its peak maximum is shown in Figure 4-11), as well as ones that are a result of pyrene (Py) and ones that are a result of interactions among the pyrene molecules (Py(A)). Apparently, the interactions between like molecules are stronger for pyrene than they were for phenanthrene since the aggregation peak (Py(A)) is much larger than the Shpol'skii peaks for pyrene (Py).

Other PAHs investigated included fluorene (Figure 4-12 and 4-13), chrysene (Figure 4-14 and 4-15), and triphenylene (Figure 4-16 and 4-17). Although an impurity is seen for fluorene (I), no spectral peaks are present for these PAHs which are not present in their spectra of manual injections. Evidently, these PAHs are not as sensitive to the hexane/PAH ratio as pyrene and phenanthrene are. This is especially true for triphenylene, since its major peak is extremely narrow, even at 82 $\mu\text{g/mL}$ (approximately 6.2 nm wide at half-height). A 3-D chromatogram of a mixture of approximately 100 $\mu\text{g/mL}$ of pyrene, 1,2- and 2,3-benzofluorene, chrysene, and triphenylene is shown in Figure 4-18. Fluorene and phenanthrene are not shown since phenanthrene obscures pyrene and the benzofluorene isomers. The benzofluorene isomers were barely baseline resolved using the flame ionization detector, and with the added chromatographic broadening, are not resolved using the LTMLS system.

Figure 4-11. Spectrum of pyrene impurity at its chromatographic peak maximum.

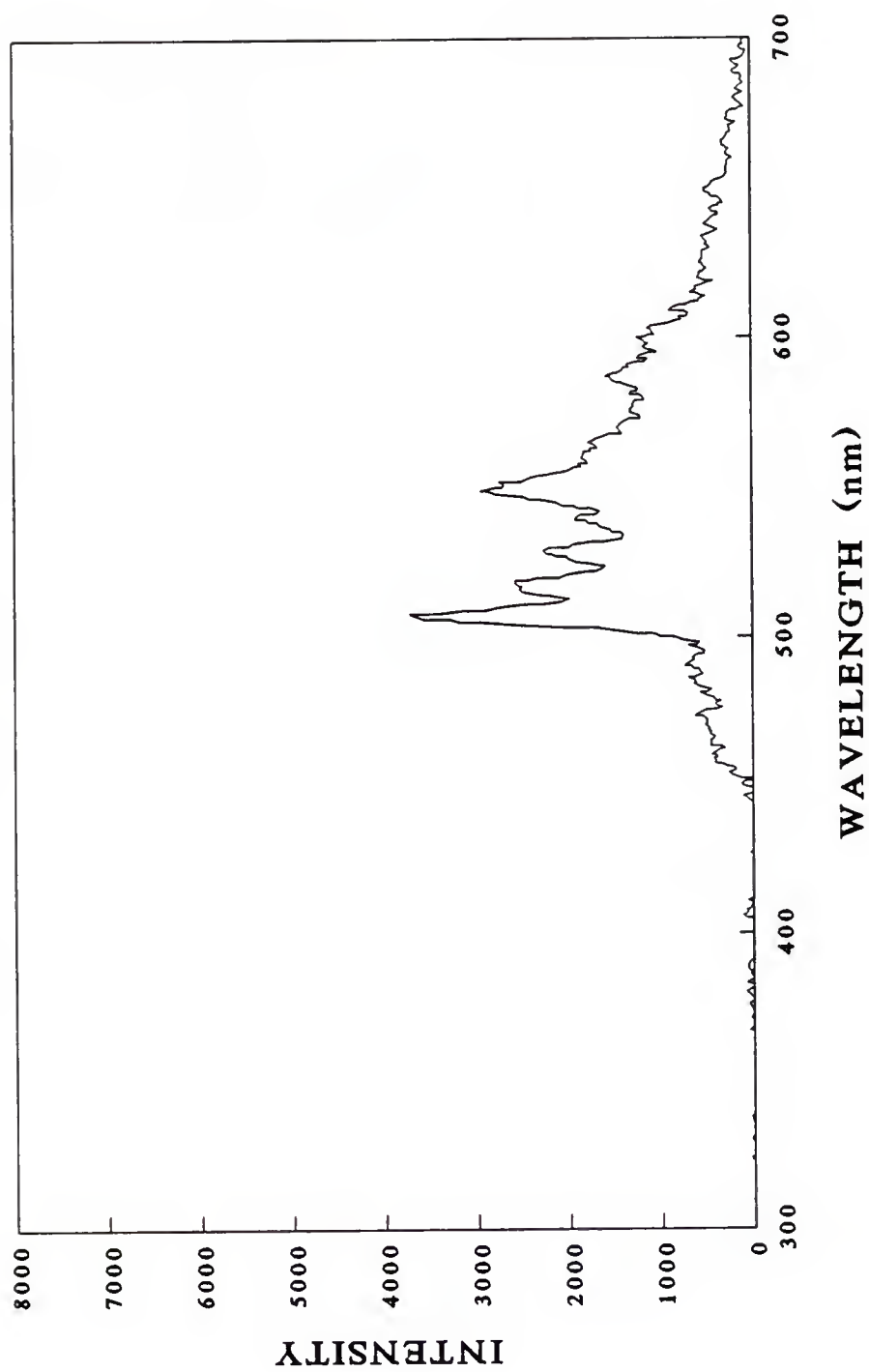


Figure 4-12. 3-D chromatogram of 87 $\mu\text{g/mL}$ fluorene; impurity peak (I): 7.09 min; fluorene peak (Fl): 7.51 min; time scale from 6.97 to 8.09 min.

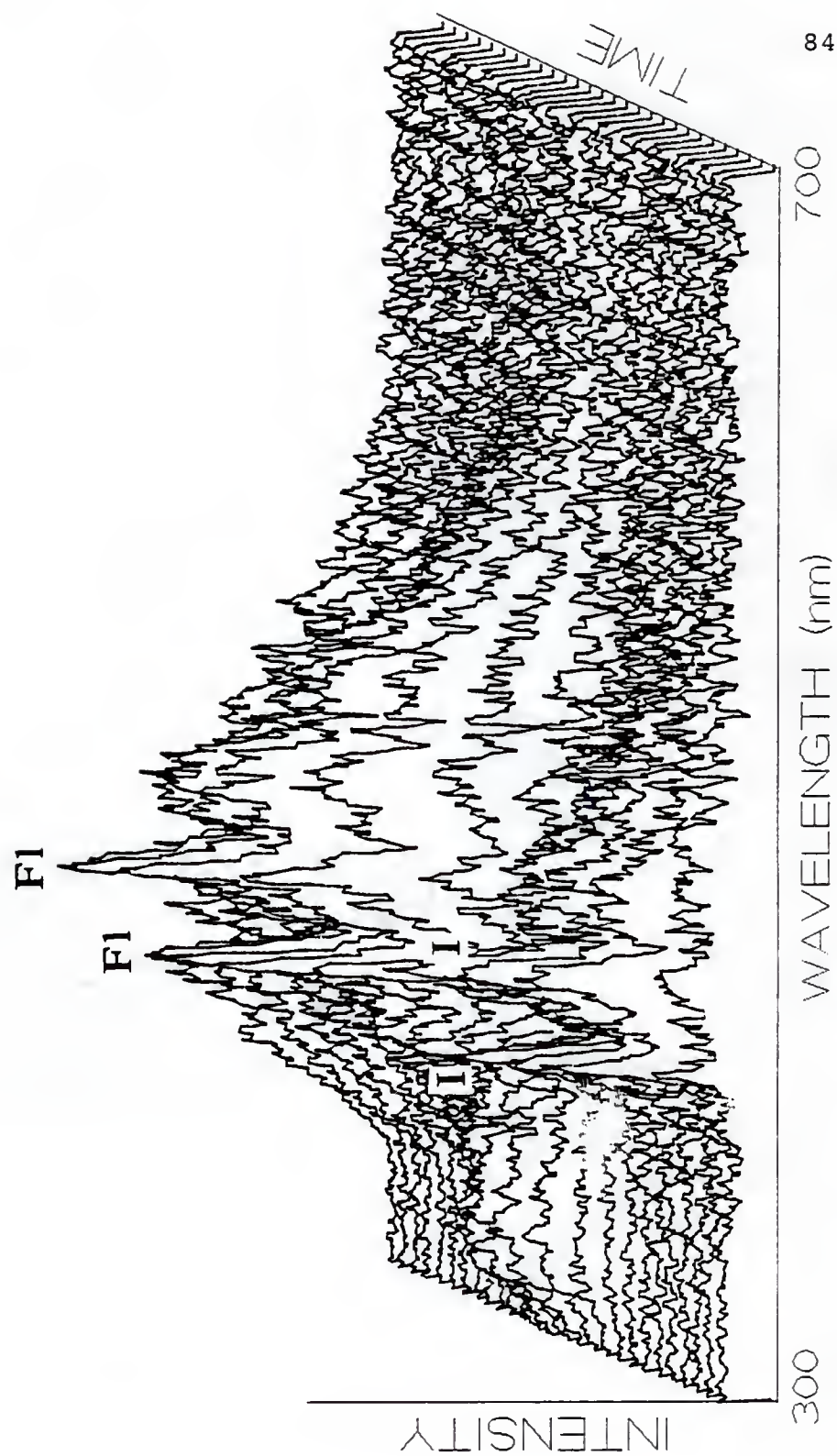


Figure 4-13. Spectrum of 87 $\mu\text{g/mL}$ of fluorene at its chromatographic peak maximum.

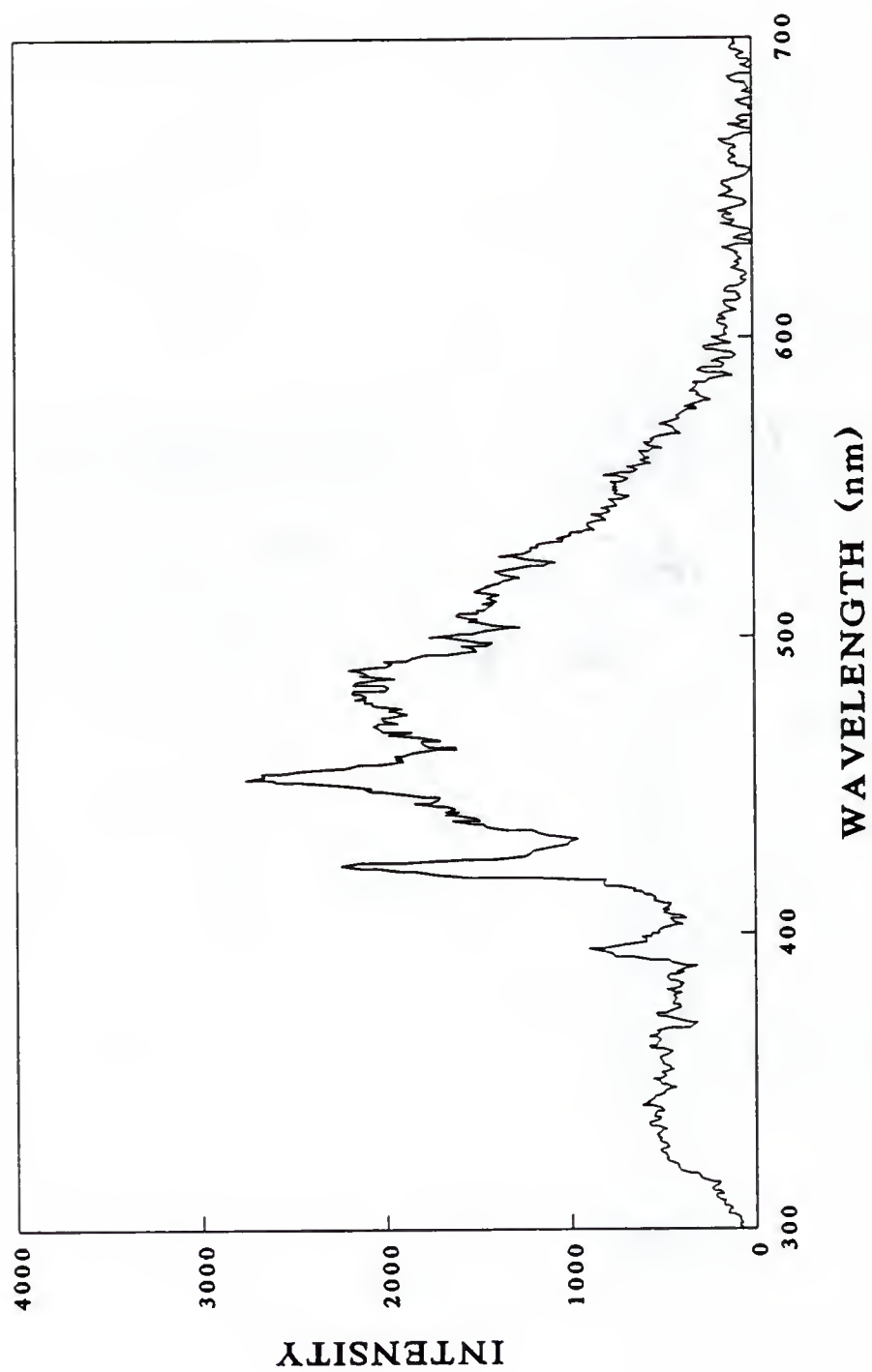


Figure 4-14. 3-D chromatogram of 82 $\mu\text{g/mL}$ chrysene; time scale is from 13.72 to 15.01 min.

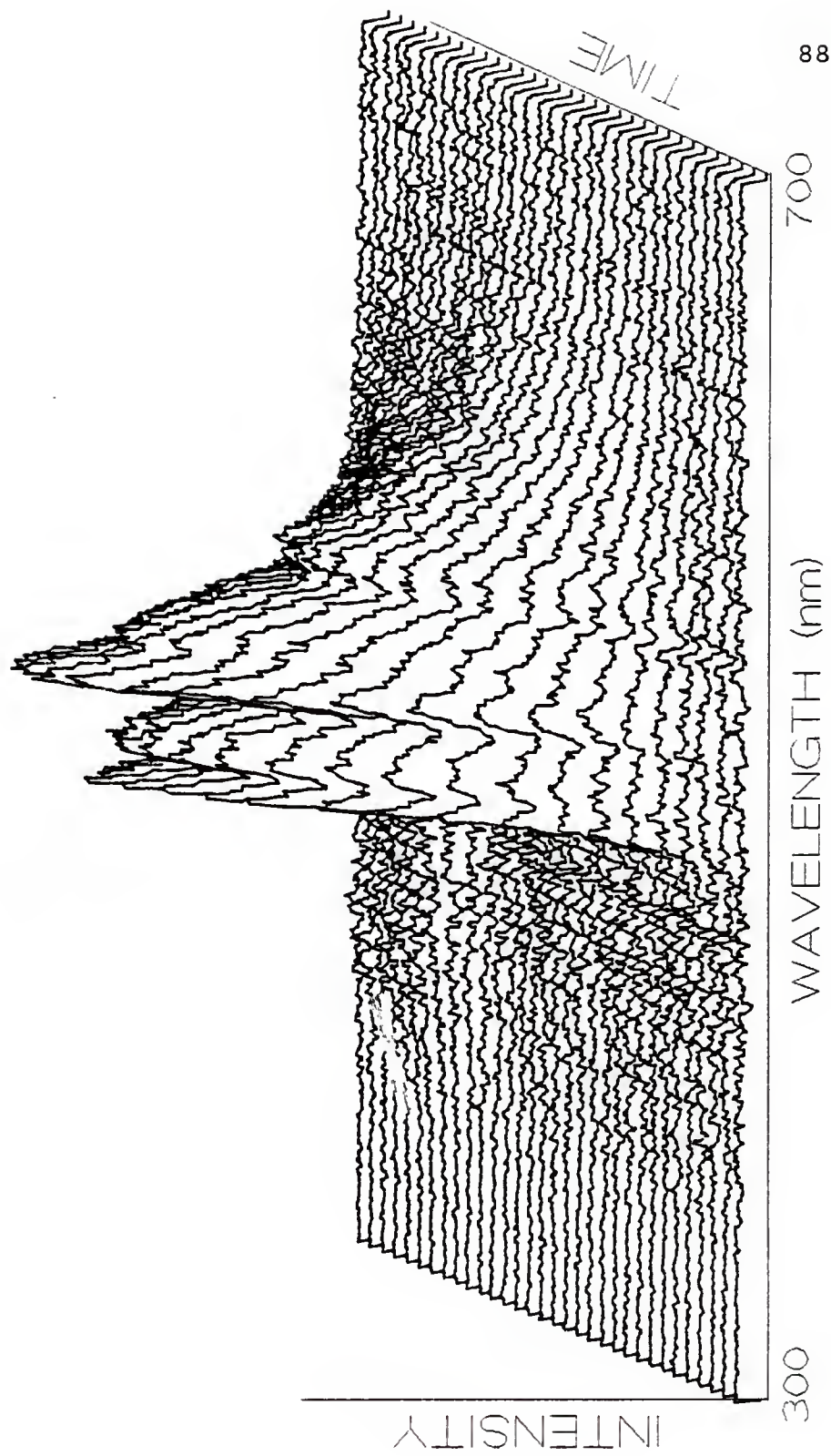


Figure 4-15. Spectrum of 82 $\mu\text{g/ml}$ of chrysene at its chromatographic peak maximum.

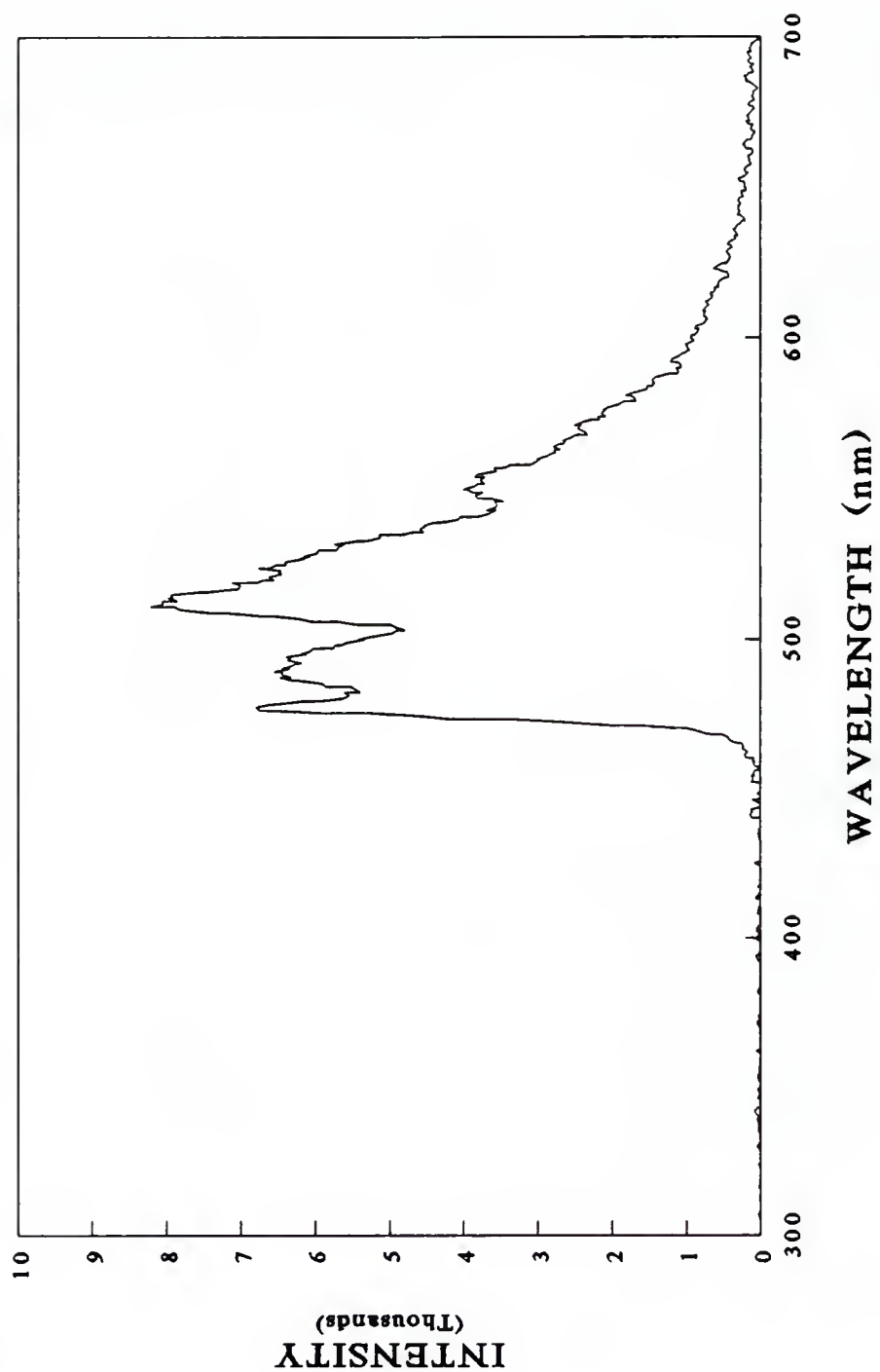


Figure 4-16. 3-D chromatogram of 82 $\mu\text{g/mL}$ triphenylene; time scale is from 15.17 to 17.93 min.

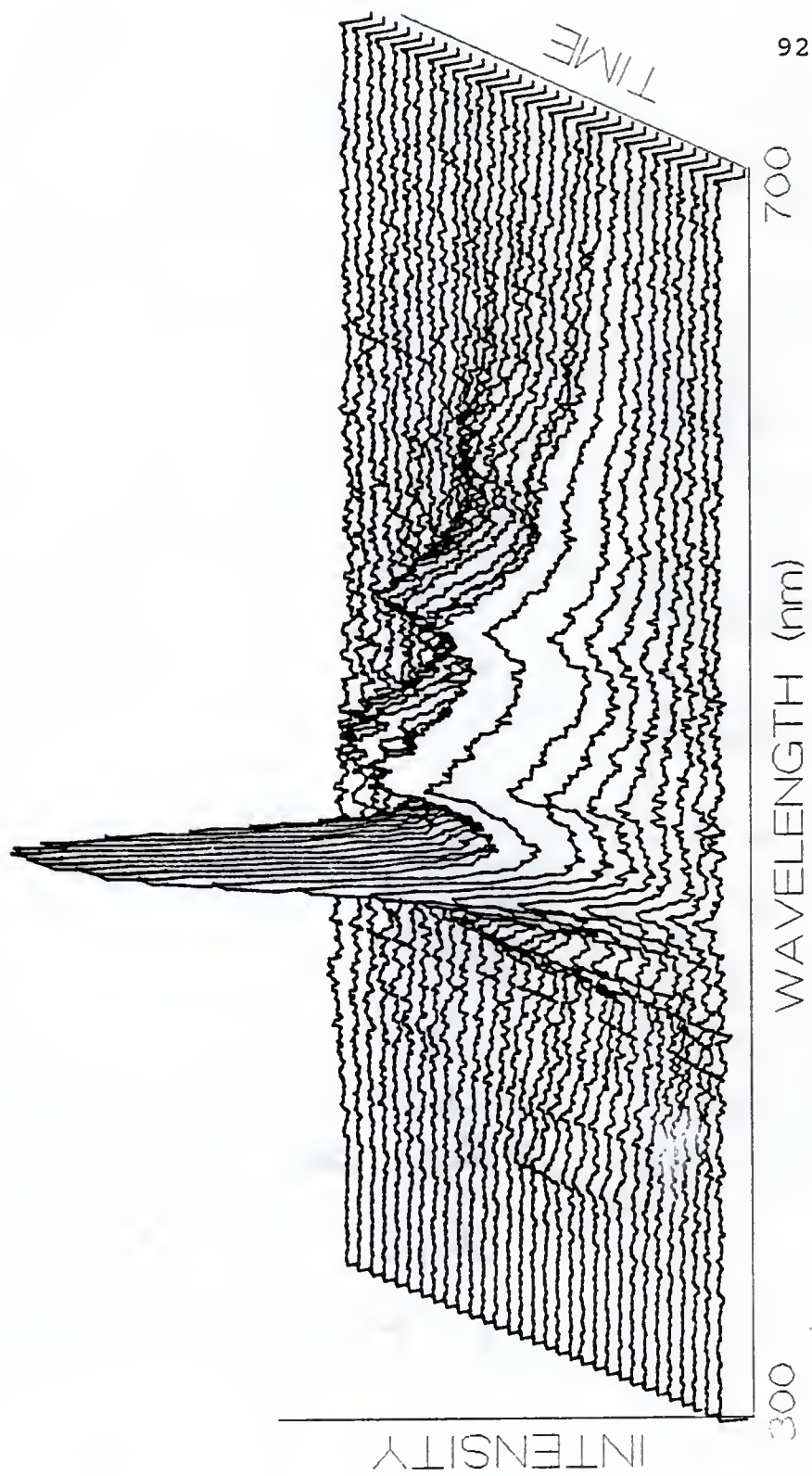


Figure 4-17. Spectrum of 82 $\mu\text{g/mL}$ of triphenylene at its chromatographic peak maximum.

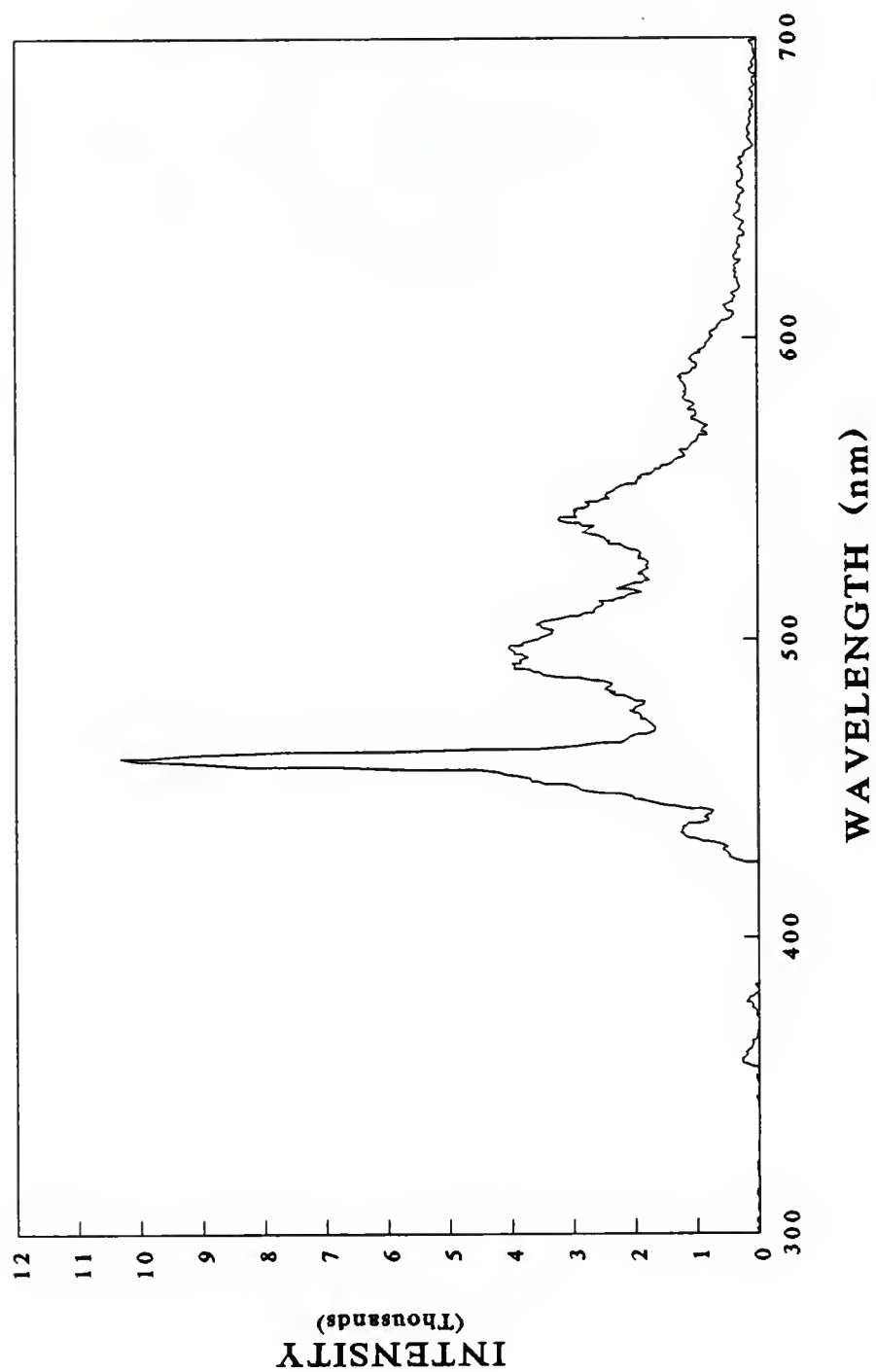
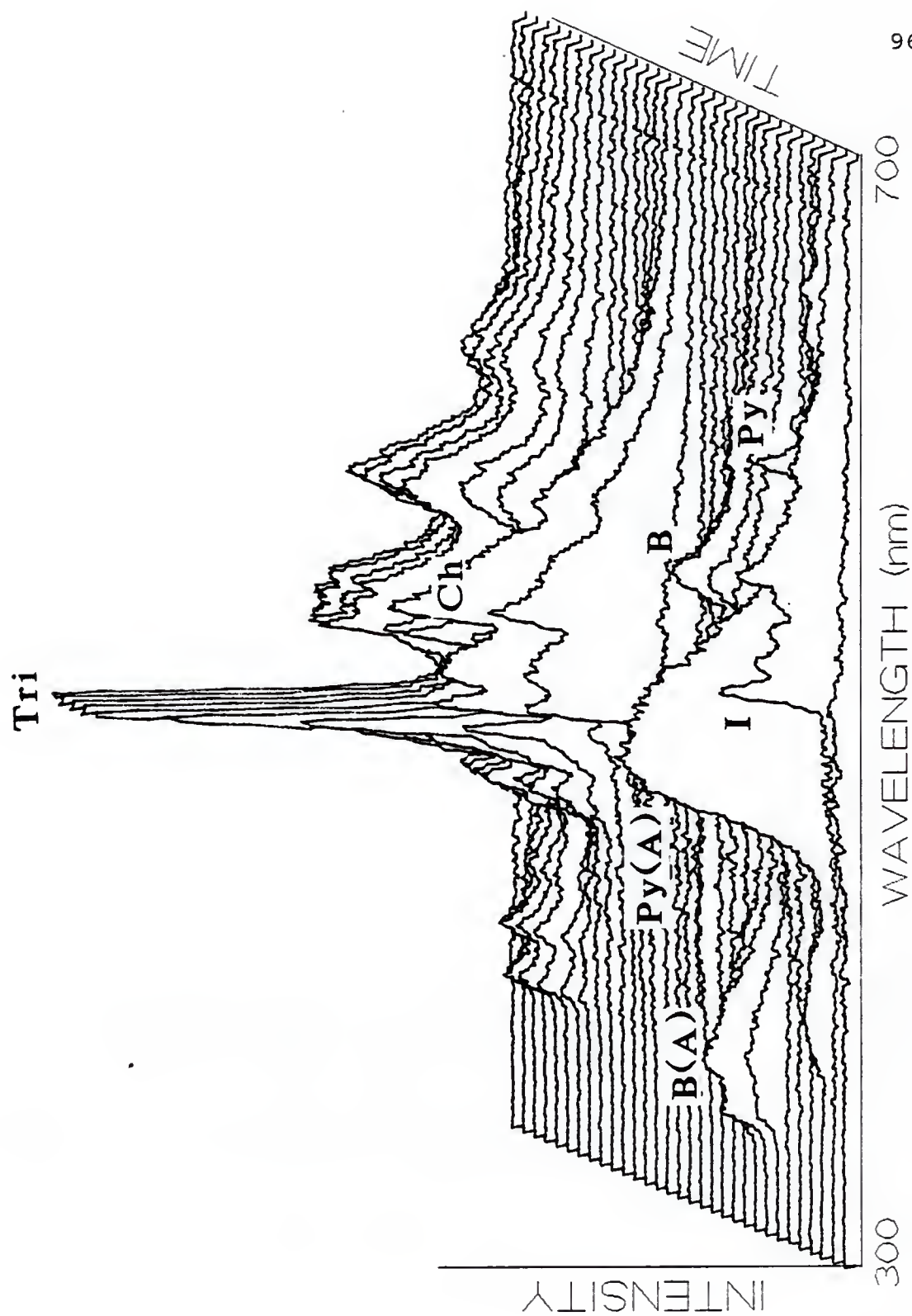


Figure 4-18. 3-D chromatogram mix of approximately 100 $\mu\text{g/mL}$ of pyrene (Py), 1,2- and 2,3-benzofluorene (B), chrysene (Ch), and triphenylene (Tri); impurity: I; pyrene aggregation: Py(A); benzofluorene aggregation: B(A); time scale is from 10.42 to 17.93 min.



However, this chromatogram shows the potential power of this technique, combining the separating power of gas chromatography with the spectral resolution of Shpol'skii spectroscopy. To further show the potential of this technique, chromatograms for each of the PAHs at one of their spectral peak maxima are shown in Figures 4-19 thru 4-23.

Retention Times, Peak Widths, and Limits of Detection

The retention times using both the flame ionization detector and the LTMLS system are shown in Table 4-2. For the LTMLS system, the dead volume (t_0) was estimated visually as the point at which the background began to rise since no spectra were taken when the solvent front would have been detected. The retention times for fluorene, phenanthrene, and pyrene determined using the LTMLS system are all near their retention times using the FID detector. This was surprising, since there should have been an increase in the dead volume due to the time necessary for the belt to rotate from the point of PAH deposition on the belt to where it was detected, which was calculated to be just under one minute. However, since the dead volume for the LTMLS system is also only slightly longer than that found using the FID detector, it was assumed that the dead volume decreased when the LTMLS system was used, possibly due to the low pressure. Although the retention times for

Figure 4-19. 2-D chromatogram of approximately 100 $\mu\text{g/mL}$ mix of fluorene (Fl), phenanthrene (Ph), pyrene (Py), benzofluorene isomers (B), chrysene (Ch), and triphenylene (Tri). Wavelength monitored: 421 nm. Time scale is from 6.00 min to 17.67 min.

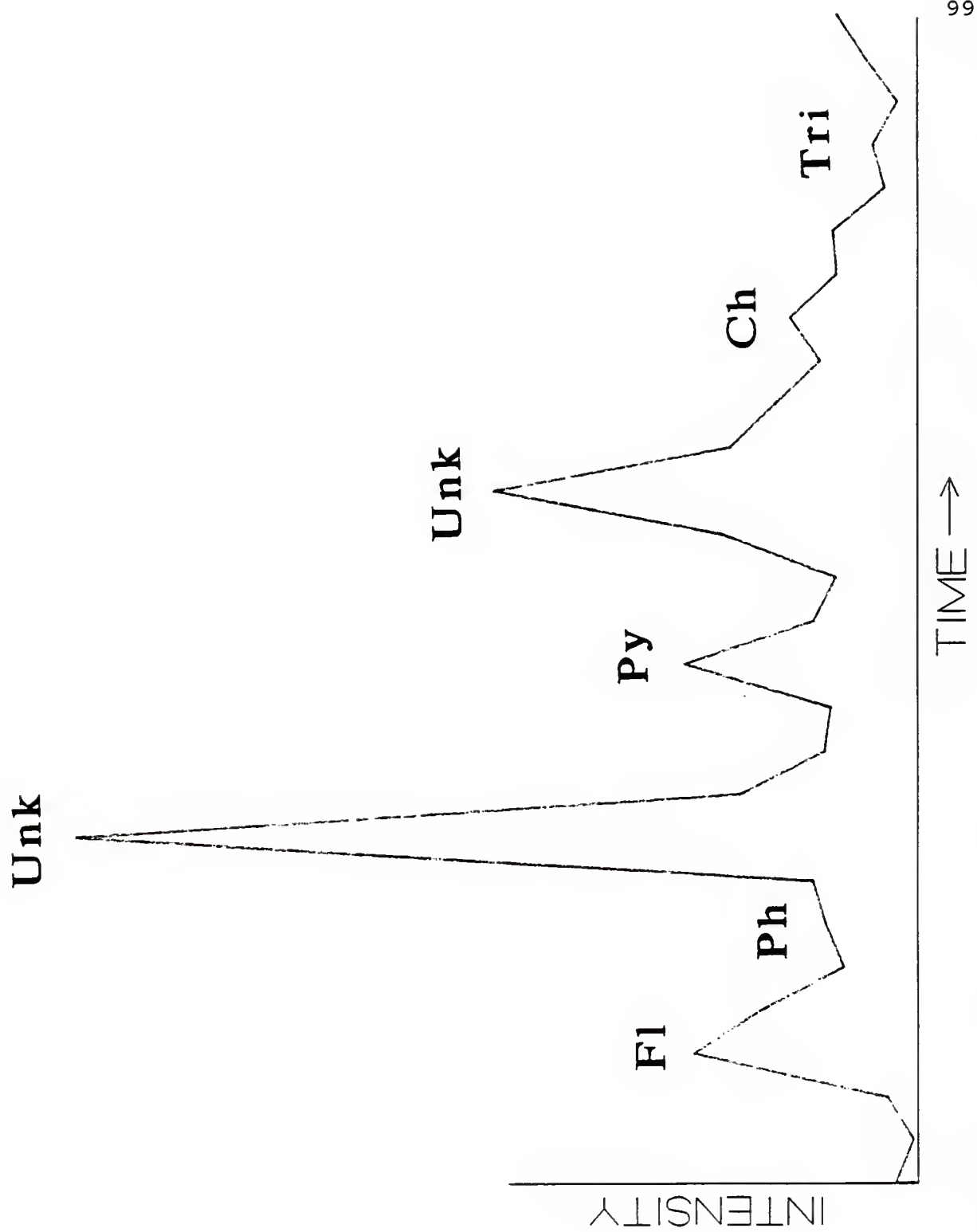


Figure 4-20. 2-D chromatogram of approximately 100 $\mu\text{g/mL}$ mix of fluorene (Fl), phenanthrene (Ph), pyrene (Py), benzofluorene isomers (B), chrysene (Ch), and triphenylene (Tri). Wavelength monitored: 495 nm. Time scale is from 6.00 min to 17.67 min.

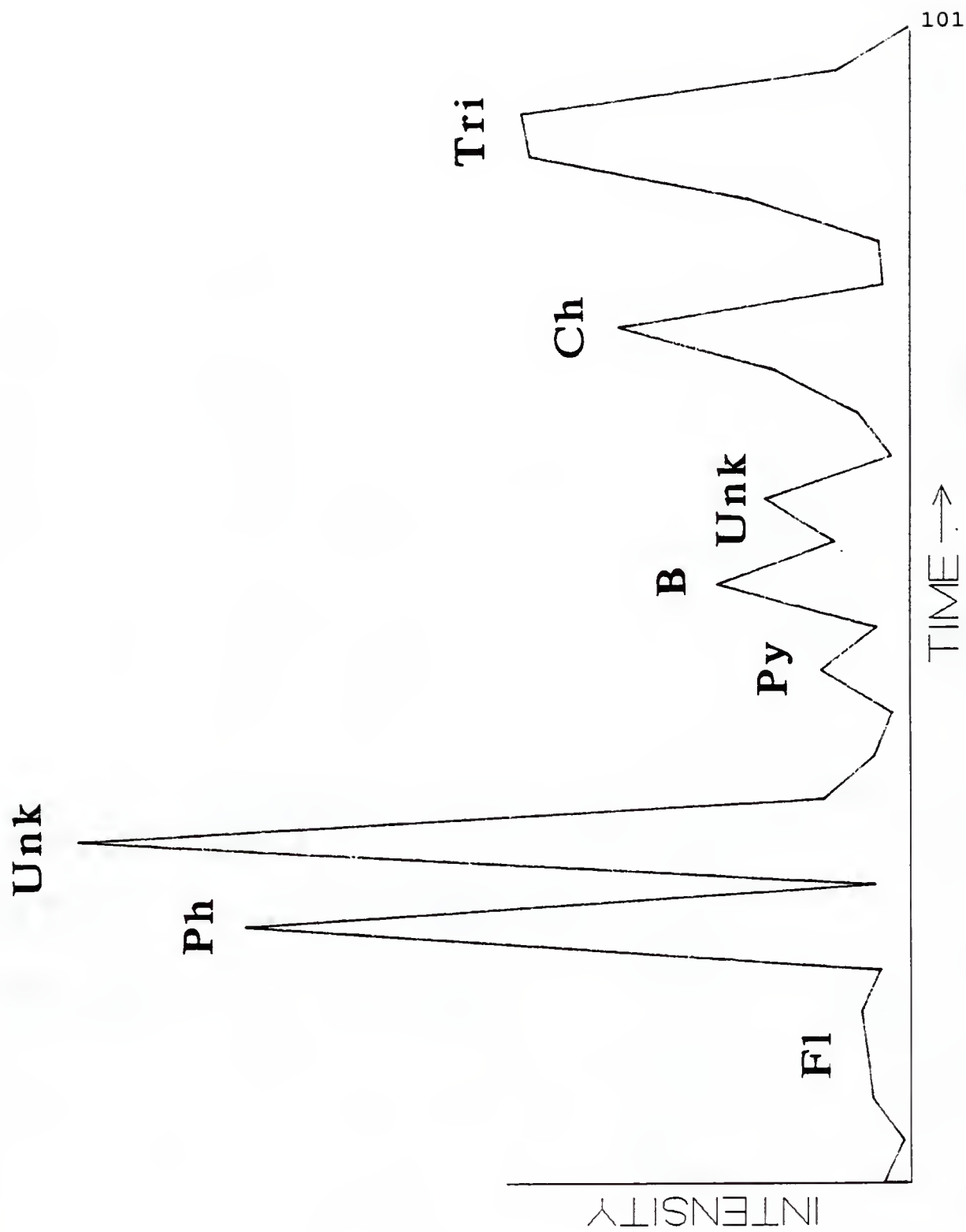


Figure 4-21. 2-D chromatogram of approximately 100 $\mu\text{g/mL}$ mix of fluorene (Fl), phenanthrene (Ph), pyrene (Py), benzofluorene isomers (B), chrysene (Ch), and triphenylene (Tri). Wavelength monitored: 587 nm. Time scale is from 6.00 min to 17.67 min.

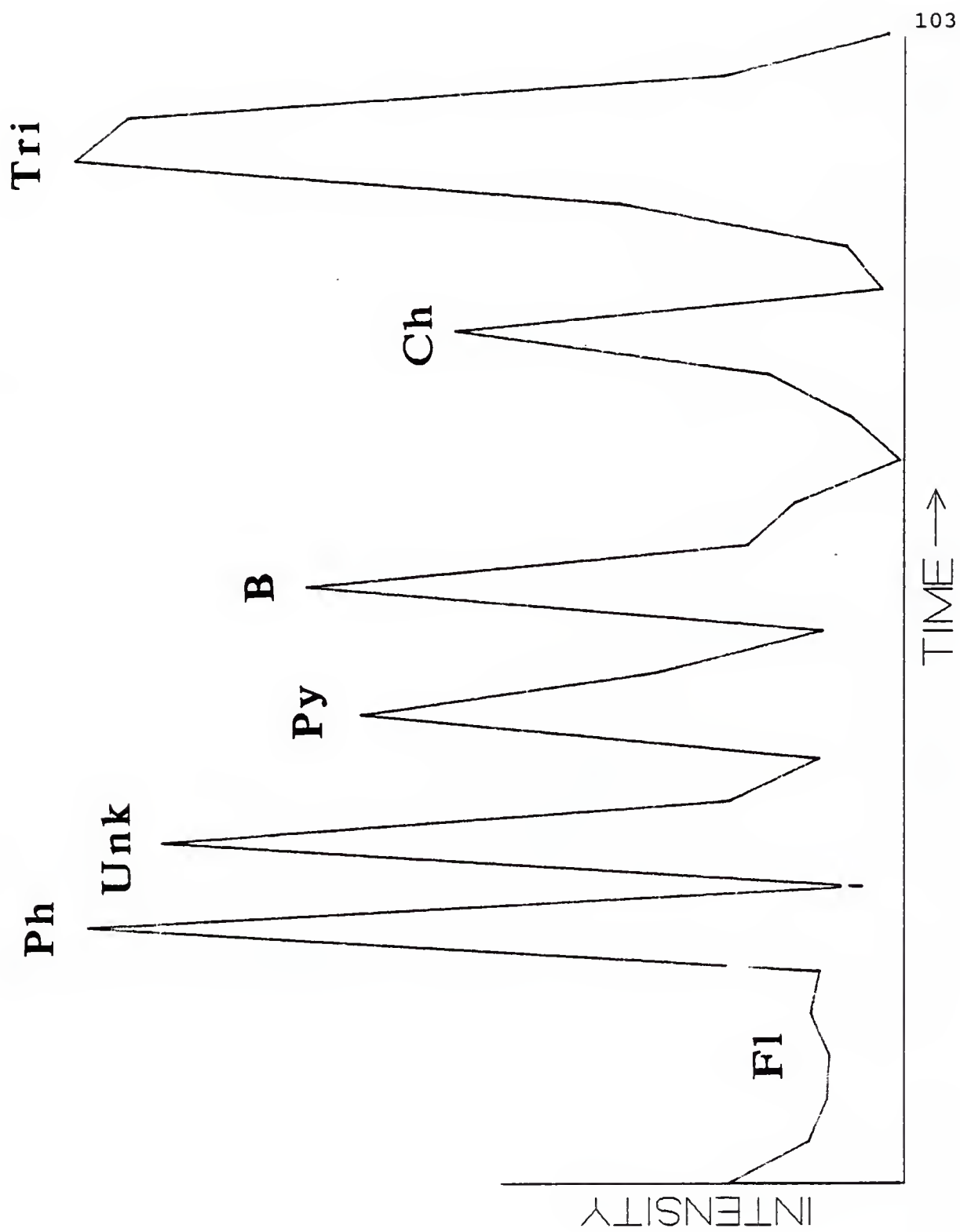


Figure 4-22. 2-D chromatogram of approximately 100 $\mu\text{g/mL}$ mix of fluorene (Fl), phenanthrene (Ph), pyrene (Py), benzofluorene isomers (B), chrysene (Ch), and triphenylene (Tri). Wavelength monitored: 513 nm. Time scale is from 6.00 min to 17.67 min.

Unk

Ph

Fl

Py

B Unk

Ch

Tri

INTENSITY

TIME →

105

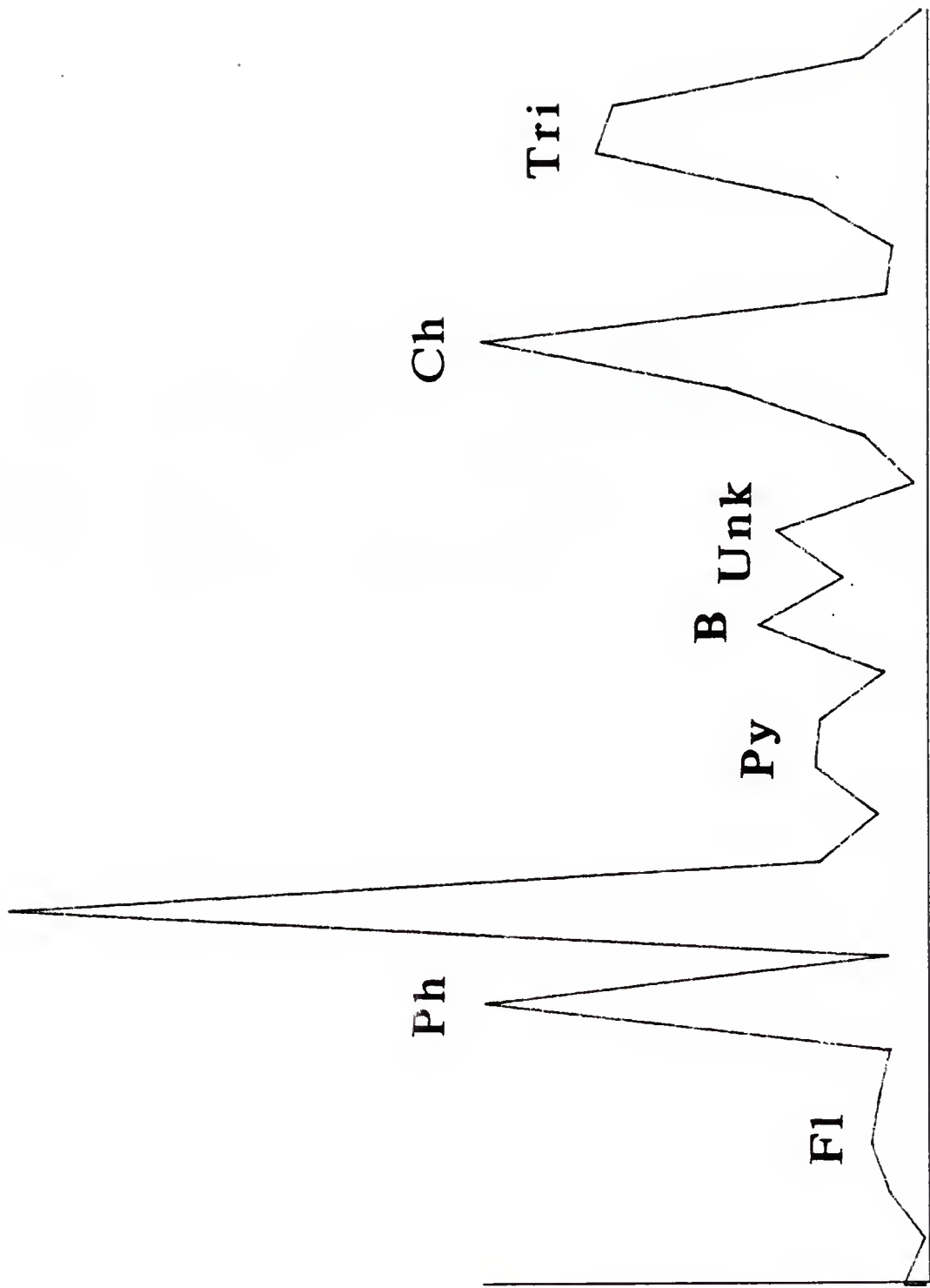


Figure 4-23. 2-D chromatogram of approximately 100 $\mu\text{g/mL}$ mix of fluorene (Fl), phenanthrene (Ph), pyrene (Py), benzofluorene isomers (B), chrysene (Ch), and triphenylene (Tri). Wavelength monitored: 459 nm. Time scale is from 6.00 min to 17.67 min.

Tri

Unk

Ph

Fl

Unk

Py

B

Ch

INTENSITY

TIME →

107

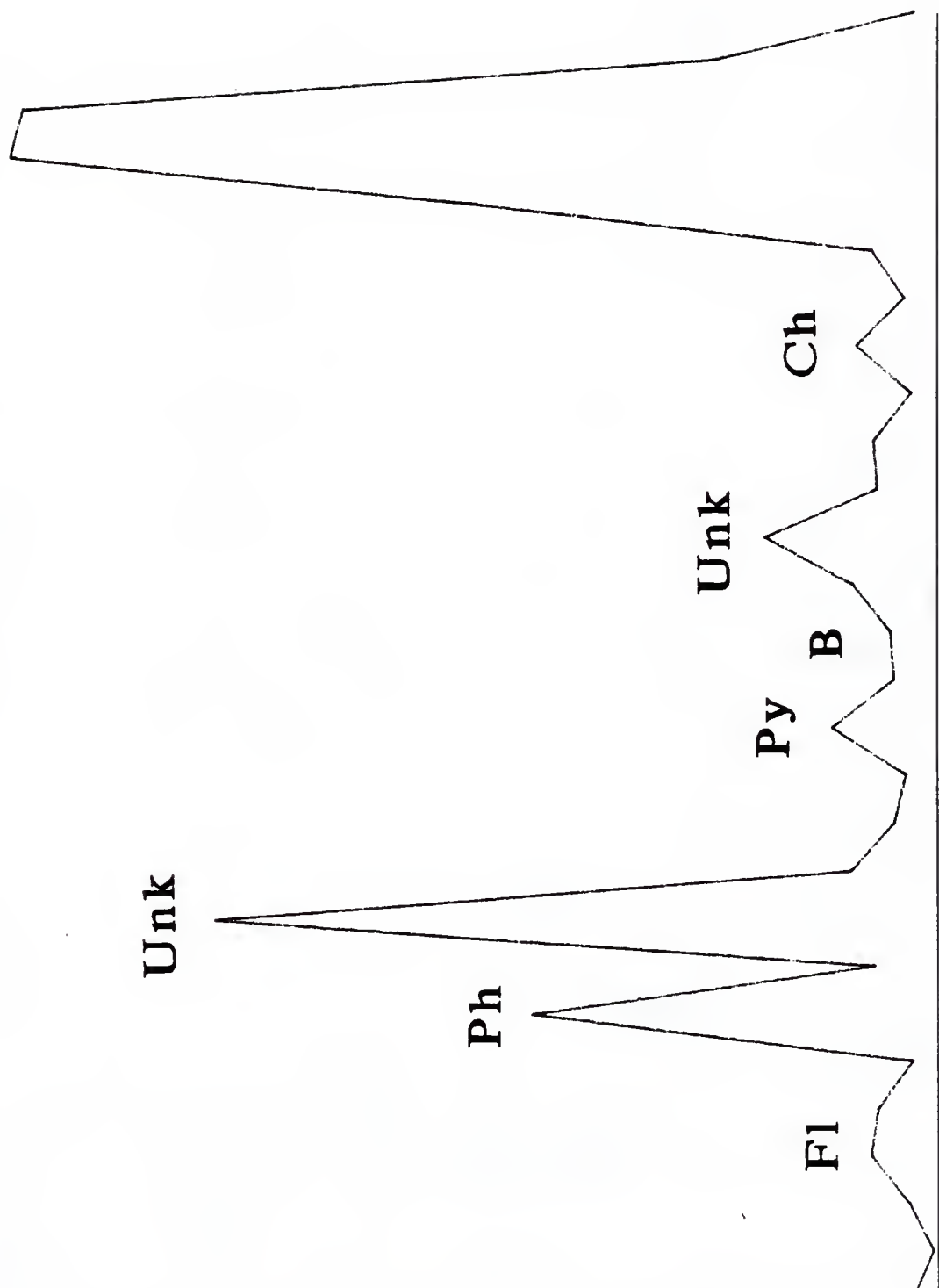


Table 4-2. Retention times and dead volume measured using the FID and the LTMLS system.*

<u>PAH</u>	<u>FID</u>	<u>LTMLS</u>
t_0	1.12 ± 0.01	$\sim 1.4^{**}$
fluorene	7.40 ± 0.02	7.51 ± 0.09
phenanthrene	8.51 ± 0.02	8.55 ± 0.02
pyrene	10.66 ± 0.03	10.89 ± 0.03
chrysene	13.85 ± 0.02	14.28 ± 0.05
triphenylene	13.78 ± 0.01	16.23 ± 0.23

*retention times in minutes \pm one standard deviation; for FID, $n=3$; for LTMLS, $n=6-12$.

**estimated.

the first three PAHs remained approximately the same, the retention time of chrysene increased by almost one half of a minute and the retention time of triphenylene increased by approximately two and one half minutes. This indicated that a second mode of retention may have been occurring somewhere in the separation, most likely in the transfer line. One possible cause of the increased retention time in the transfer line is a "cold spot", since the column was not heated to the very tip and the PAHs eluted at very high temperatures (300°C). Also the column had been overheated, causing the column to become charred. This could have produced active sites where the PAHs may have adsorbed.

Table 4-3 shows the chromatographic peak widths measured at 10% of peak maximum for the PAHs using the FID detector and the LTMLS system. All of the peaks were significantly broadened chromatographically when the LTMLS system was employed; however, for fluorene, phenanthrene, and pyrene, part of the chromatographic broadening may have been a result of the detector, since spectra were averaged for 2.5 s. Therefore, there were only approximately 10 points per peak, which could cause some distortion of the peaks (see Table 4-3). Chrysene and triphenylene, on the other hand, were severely broadened, which was a physical phenomena. This could be because of adsorption, which would concur with the retention time data, since those PAHs whose retention times for the two detectors differed significantly

Table 4-3. Peak widths measured using the FID and the LTMLS system.*

<u>PAH</u>	<u>FID</u>	<u>LTMLS</u>
fluorene	0.053 \pm 0.003	0.47 \pm 0.07
phenanthrene	0.057 \pm 0.003	0.41 \pm 0.04
pyrene	0.069 \pm 0.006	0.39 \pm 0.05
chrysene	0.11 \pm 0.01	0.85 \pm 0.08
triphenylene	0.11 \pm 0.01	1.55 \pm 0.19

*peak widths measured at 10% of peak maximum in minutes \pm one standard deviation; for FID, n=3; for LTMLS, n=6-12.

also were the ones which were being severely broadened when the LTMLS system was used.

The calibration curves were found to be nonlinear, which can be seen in Figures 4-24 thru 4-26. Most of them are probably linear just below the lower concentration measured and leveled off at the upper concentrations injected. Since the calibration curves were nonlinear, it was necessary to estimate the limits of detection (see Table 4-4) by assuming linearity between the lowest point measured and the ordinate. The limits of detection were estimated as described in the experimental section. The 3-D chromatograms of the PAHs for the lowest concentrations injected are shown in Figures 4-27 thru 4-31. The most probable causes of the nonlinear calibration curves were the background (and resulting background noise) and the low hexane-to-PAH ratio which was referred to when the chromatograms were discussed. Comparing them to the detection limits found previously (see Table 4-4), they are several orders of magnitude worse. The causes of these discrepancies have already been discussed: phosphorescence background, low hexane-to-PAH ratio, and chromatographic broadening. However, most of the detection limits are still estimated to be in the ng/mL range.

Figure 4-24. Calibration curve for phenanthrene.

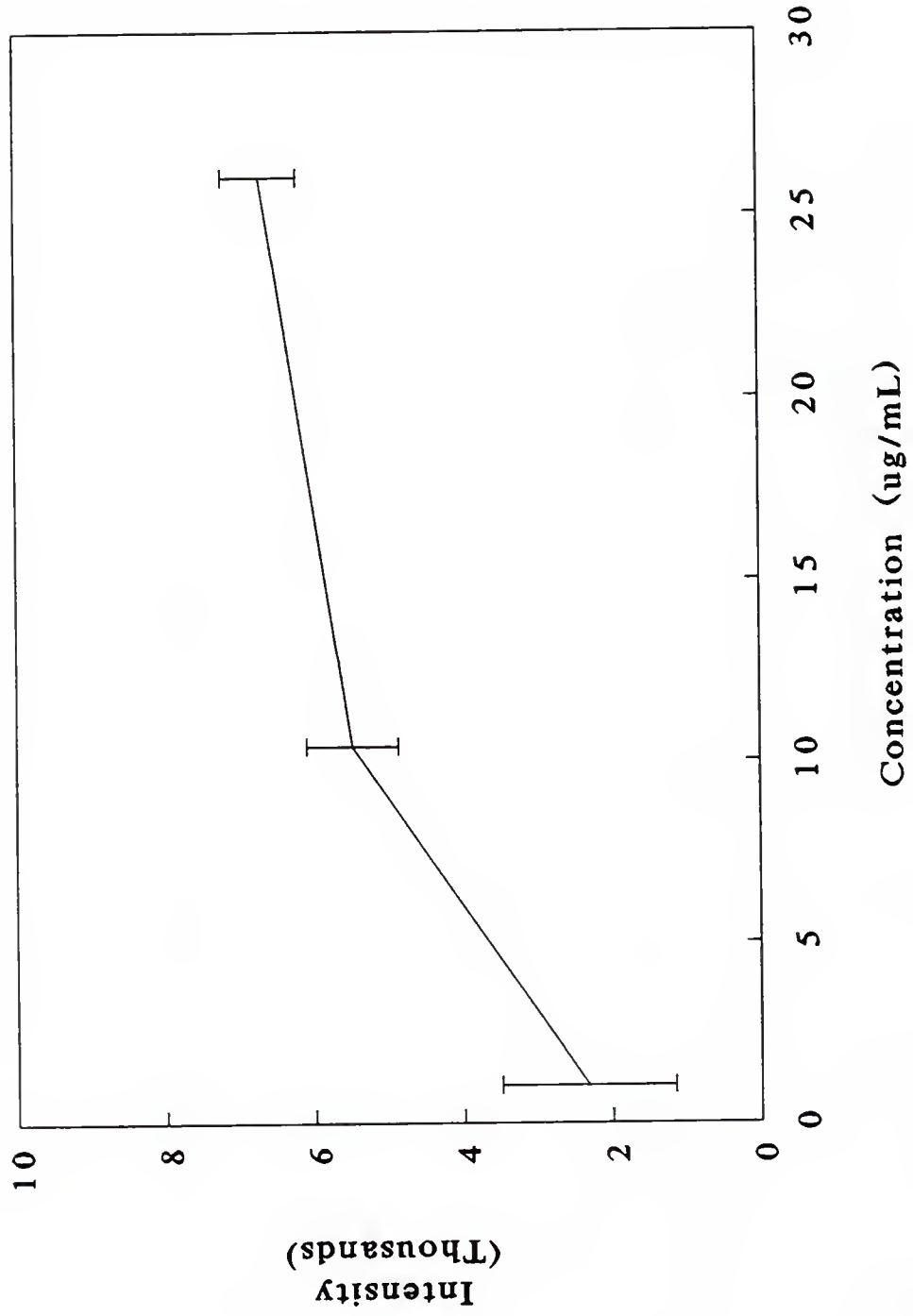


Figure 4-25. Calibration curve for chrysene.

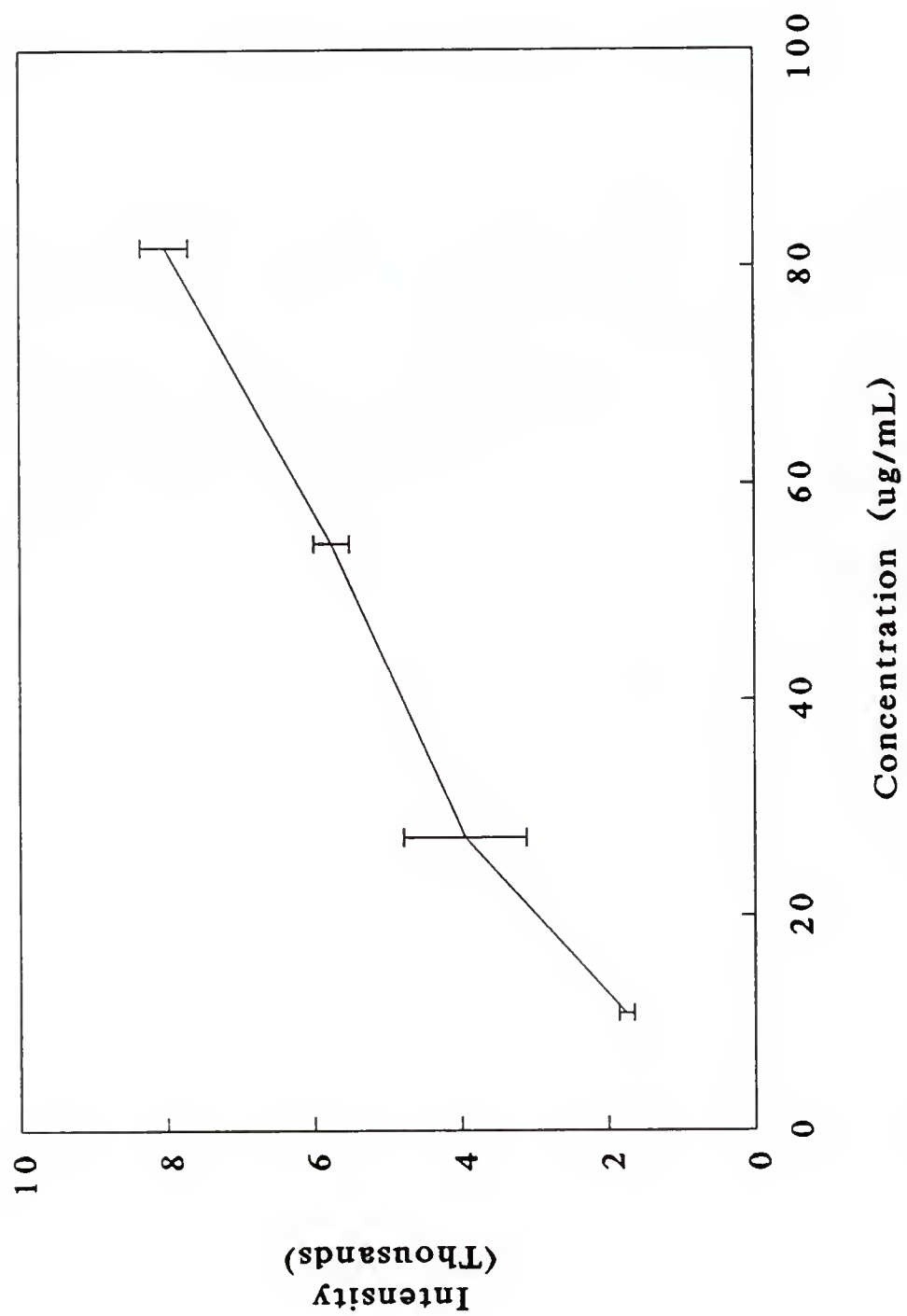


Figure 4-26. Calibration curve for triphenylene.

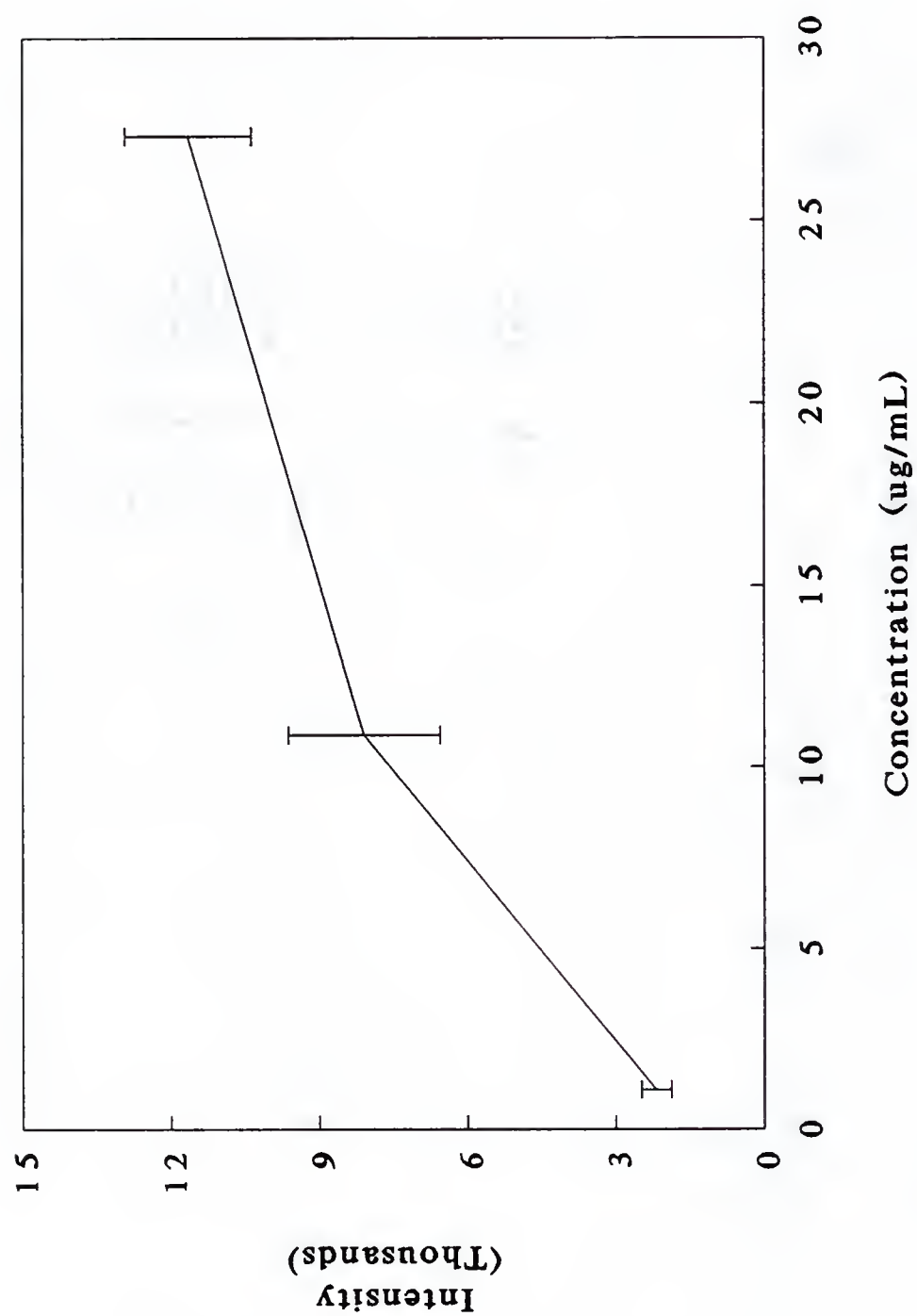


Table 4-4. Estimated limits of detection.

<u>PAH</u>	<u>GC/LTMLS</u>	LODs (ng/mL)	
		<u>LTMLS*</u>	<u>77 K**</u>
fluorene	500	-	20
phenanthrene	180	2	10
pyrene	710	-	8
chrysene	1400	-	9
triphenylene	55	0.4	0.4

*taken from reference 56

**taken from reference 27

Figure 4-27. 3-D chromatogram of 1.16 $\mu\text{g/mL}$ of fluorene.

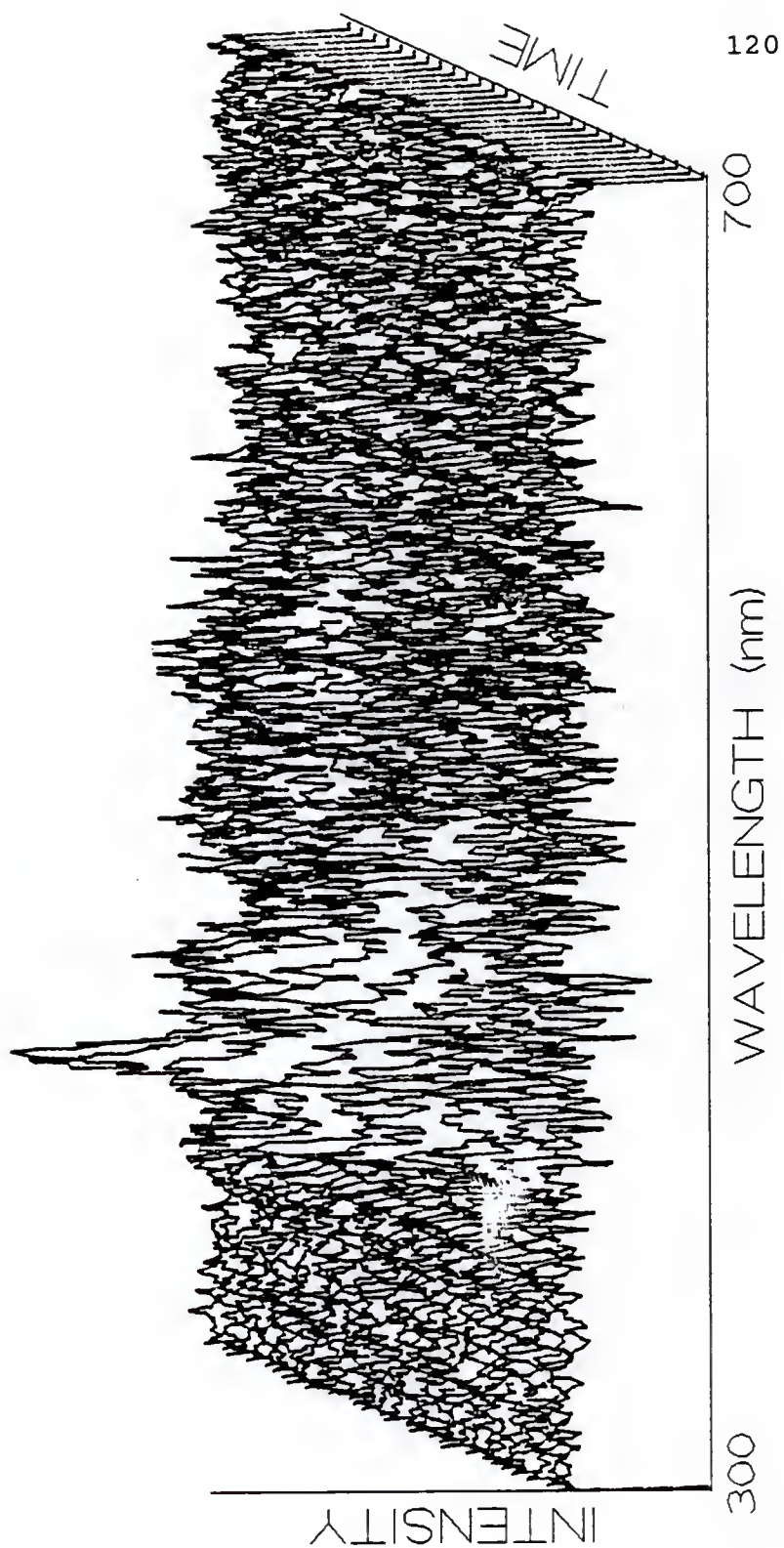


Figure 4-28. 3-D chromatogram of 1.04 $\mu\text{g/mL}$ of phenanthrene.

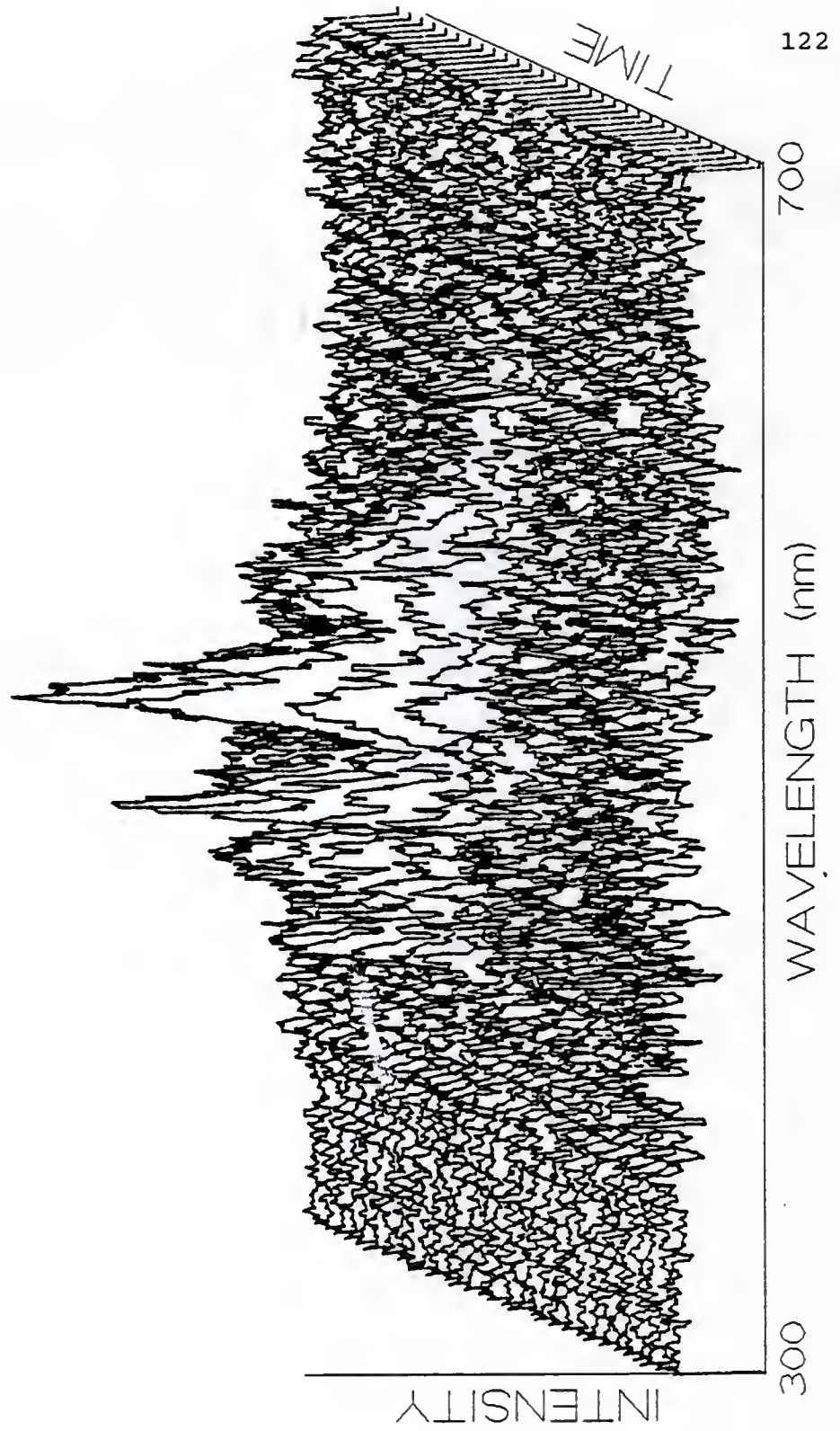


Figure 4-29. 3-D chromatogram of 12.6 $\mu\text{g/mL}$ of pyrene.

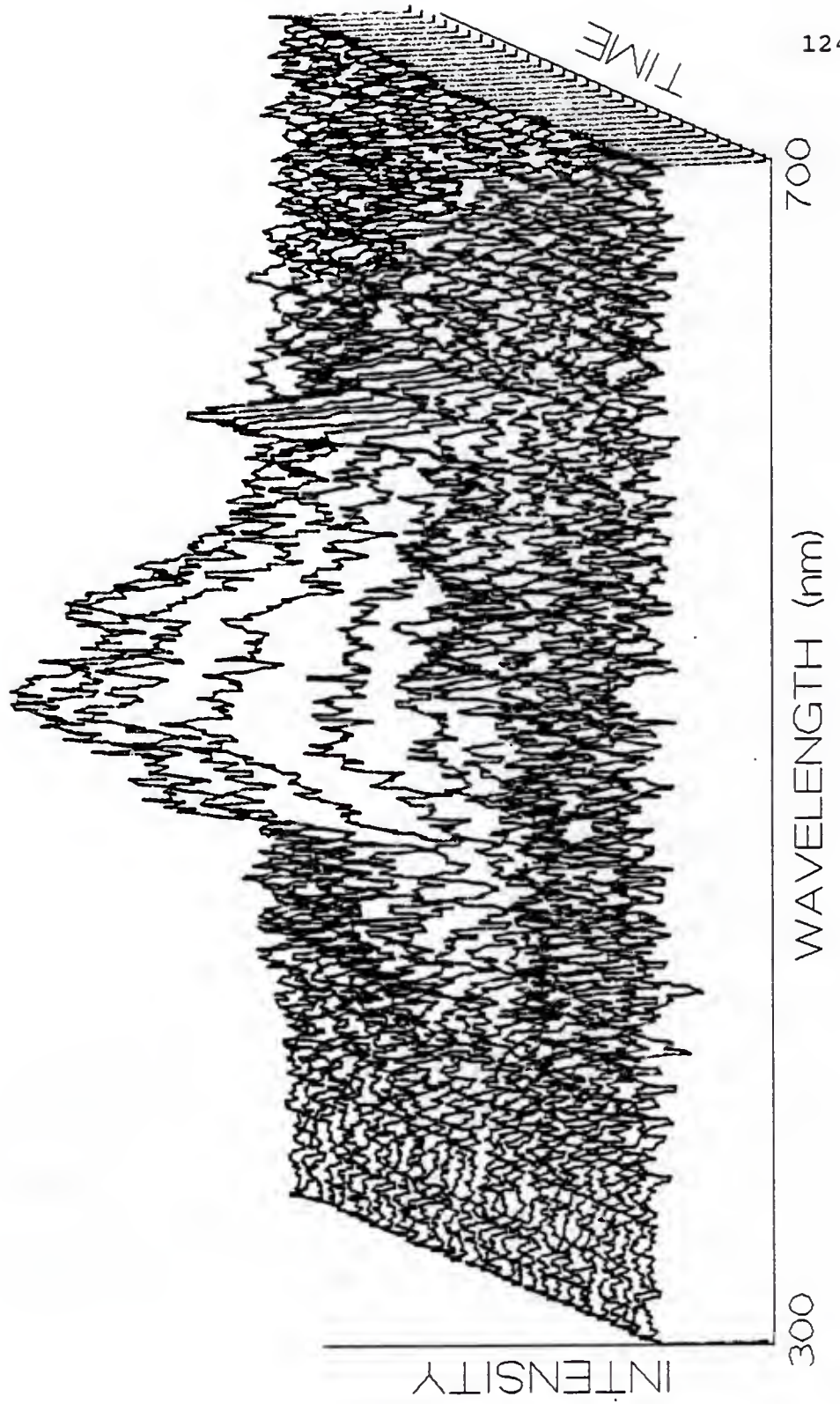


Figure 4-30. 3-D chromatogram of 10.9 $\mu\text{g/mL}$ of chrysene.

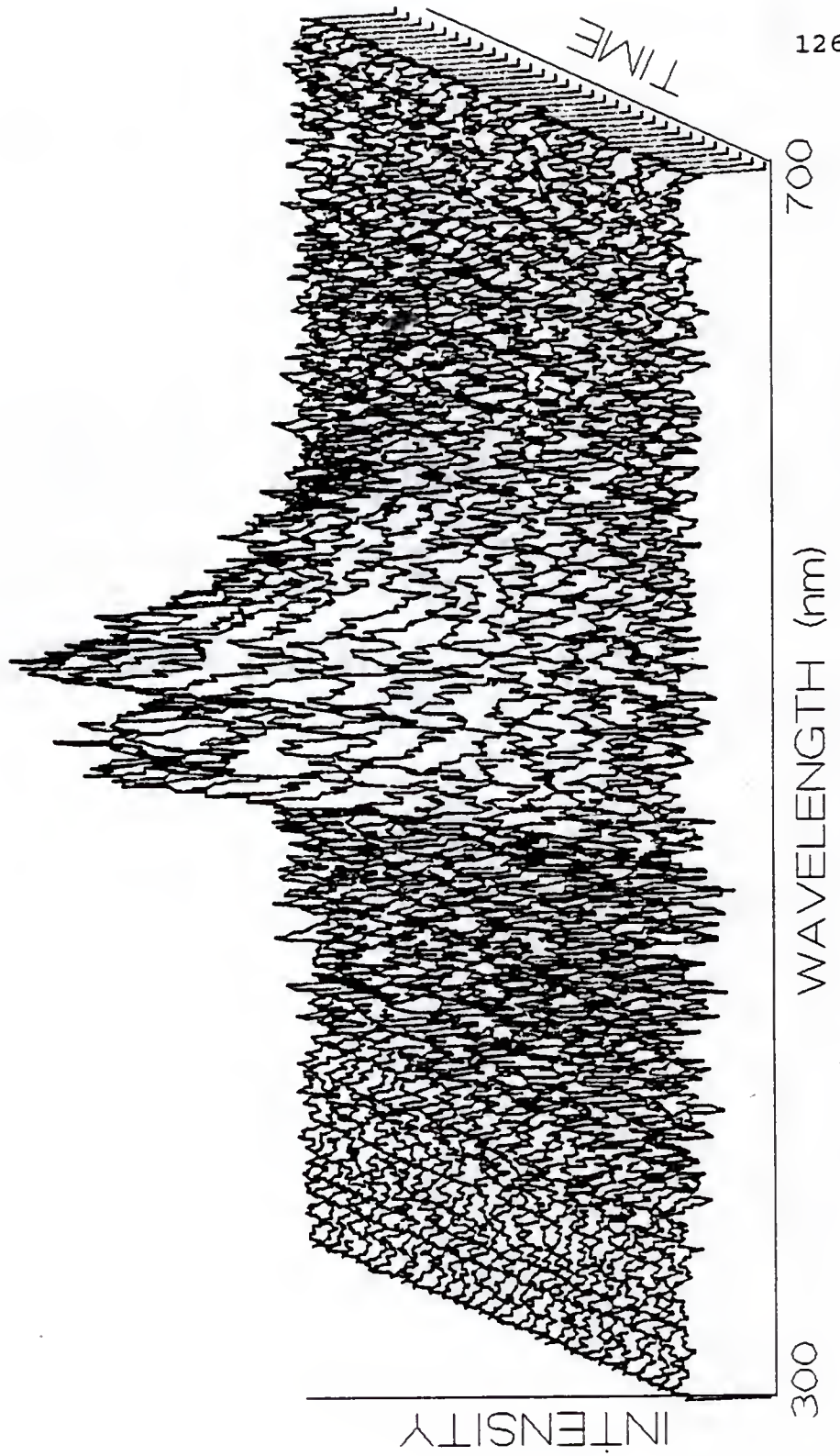
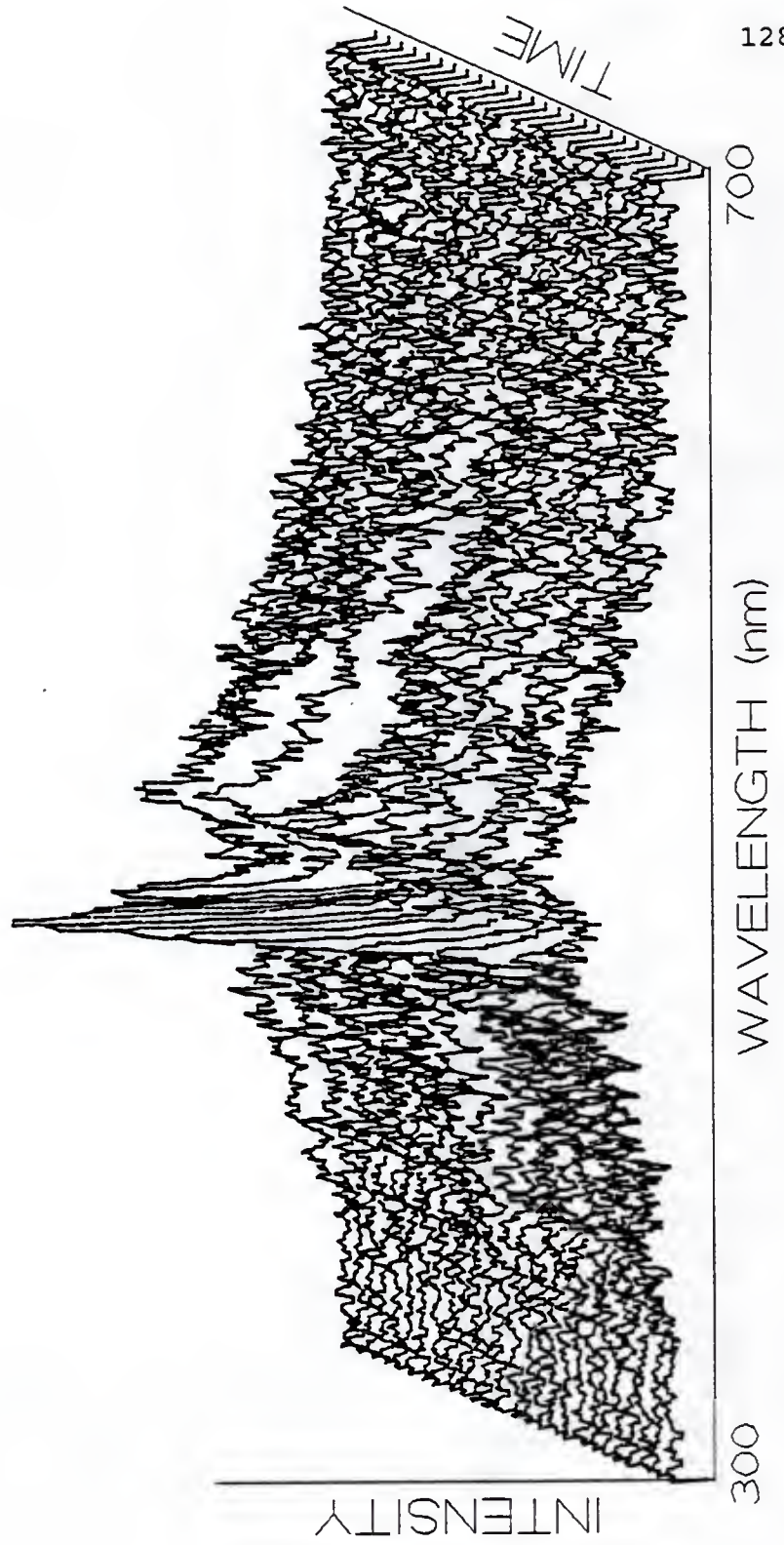


Figure 4-31. 3-D chromatogram of 1.09 $\mu\text{g/mL}$ of triphenylene.



CHAPTER 5 CONCLUSIONS AND FUTURE WORK

In this study, high phosphorescence background led to poorer limits of detection than had been hoped. The background was most likely the result of contamination, probably pump oil. It is thought that when the vacuum pressure is reduced to 10^{-7} torr that the background should be minimized.

It was apparent from the chromatograms that the amount of hexane introduced with the beam valve was insufficient to effectively isolate the PAH molecules from one another. However, although the background degraded the limits of detection, chromatograms were collected which showed the potential power of this technique. This was especially evident for the detection of trace impurities in some of the PAH standards (fluorene, phenanthrene, and pyrene).

The retention times of fluorene, phenanthrene, and pyrene were only slightly longer using the LTMLS system than those using the FID detector. Apparently, the dead volume decreased when the column was under vacuum since the dead volume using the LTMLS system was only slightly longer than when the FID system was used, even though it should have been just under one minute longer. However, the retention

time of chrysene was increased by almost one half of one minute and triphenylene was increased by approximately two and one half minutes. In view of this and the fact that they are also more severely broadened than the other PAHs, these two are apparently being retained by some other mechanism, such as adsorption.

Two major problems should be overcome to improve this system to its full potential. First, the phosphorescence background should be minimized, which is currently being worked on. By doing this, the PAHs will be detected at lower concentrations and the detection limits should be lowered several orders of magnitude. Second, the amount of hexane introduced should be increased once the vacuum pressure has been improved. Third, the peak shapes should be improved, especially for chrysene and triphenylene. This can be helped by not overheating the column and also using a column which does not retain the PAHs as strongly.

This system is not limited to Shpol'skii spectroscopy, and therefore, could also be used for site selection spectroscopy or infrared spectrometry. This would eliminate the problem of hexane introduction, since a gas such as argon is usually used as the matrix. Argon could simply be a part of the carrier gas, such as 3% in helium, eliminating the need for the molecular beam valve.

Also, one could try a different means of separation, such as liquid or supercritical fluid chromatography. It is

currently being attempted to interface the LTMLS system with a liquid chromatograph. Supercritical fluid chromatography would be interesting since often an organic modifier, such as hexane, is used to improve the separation. However, the most common supercritical fluid used is carbon dioxide, which would freeze at the cryogenic temperatures normally employed for this work. Still, site selection spectroscopy or infrared spectrometry could be used.

REFERENCE LIST

1. Shpol'skii, E. V.; Il'ina, A. A.; Klimova, L. A. *Dokl. Akad. Nauk. SSSR*, **87**, 935 (1952).
2. Dipple, A. in "Chemical Carcinogens, ACS Monograph 173," Charles E. Searle, Ed.; American Chemical Society: Washington, D.C. (1976), 245.
3. Lee, M. L.; Novotny, M. V.; Bartle, K. D. "Analytical Chemistry of Polycyclic Aromatic Compounds," Academic Press, Inc.: New York (1981).
4. Ewald, M.; Moinet, A.; Saliot, A.; Albrecht, P. *Anal. Chem.*, **55**, 958 (1983).
5. Yang, Y.; D'Silva, A. P.; Fassel, V. A.; Iles, M. *Anal. Chem.*, **52**, 1350 (1980).
6. Lee, M. L.; Novotny, M.; Bartle, K. D. *Anal. Chem.*, **48**, 1566 (1976).
7. Kolarovic, L.; Traitler, H. J. *Chromatogr.*, **237**, 263 (1982).
8. Wynder, E. L.; Hoffmann, D. "Tobacco and Tobacco Smoke, Studies in Experimental Carcinogenesis," Academic Press: New York (1967).
9. Shubik, P. *Proc. Natl. Acad. Sci. USA*, **69**, 1052 (1972).
10. Tsang, W.-S.; Griffin, G. W. "Metabolic Activation of Polynuclear Aromatic Hydrocarbons," Pergamon Press: New York (1979).
11. Klopman, G.; Namboodiri, K.; Kalos, A. N. in "Molecular Basis of Cancer, Part A: Macromolecular Structure, Carcinogens, and Oncogenes," Robert Rein, Ed.; Alan R. Liss, Inc.: New York (1985), 287.
12. Jerina, D. M.; Lehr, R. E. in "Microsomes and Drug Oxidations," V. Ullrich, I. Roots, A. G. Hildebrandt, R. W. Estabrook, and A. H. Conney, Eds.; Pergamon Press: Oxford (1977), 709.

13. Abramovich, M.; Zegar, I. S.; Prakash, A. S.; Harbey, R. G.; LeBreton, P. R. in "Molecular Basis of Cancer, Part A: Macromolecular Structure, Carcinogens, and Oncogenes," Robert Rein, Ed.; Alan R. Liss, Inc.: New York (1985), 217.
14. Richard, A. M.; Rabinowitz, J. R.; Waters, M. D. *Mut. Res.*, **221**, 181 (1989).
15. Cottini, G. B.; Mazzone, G. B. *Am. J. Cancer*, **37**, 186 (1939).
16. Payne, S. *Brit. J. Cancer*, **12**, 65 (1958).
17. Schoeny, R.; Cody, T.; Warshawsky, D.; Radike, M. *Mut. Res.*, **197**, 289 (1988).
18. Higashi, K. *Mut. Res.*, **197**, 273 (1988).
19. Joe, F. L.; Salemm, J.; Fazio, T. *J. Assoc. Off. Anal. Chem.*, **67**, 1076 (1984).
20. Liberti, A.; Ciccioli, P.; Cecinato, A.; Brancaleoni, E.; Di Palo, C. *J. High Res. Chromatogr. Chromatogr. Comm.*, **7**, 389 (1984).
21. Hayes, J. M.; Small, G. J. *Anal. Chem.*, **55**, 565A (1983).
22. Goates, S. R.; Sin, C. H. *Appl. Spec. Rev.*, **25**, 81 (1989).
23. Wehry, E. L.; Mamantov, G. *Prog. Anal. Spec.*, **10**, 507 (1987).
24. Conrad, V. B.; Carter, W. J.; Wehry, E. L.; Mamantov, G. *Anal. Chem.*, **55**, 1340 (1983).
25. Reedy, G. T.; Ettinger, D. G.; Schneider, J. F.; Bourne, S. *Anal. Chem.*, **57**, 1602 (1985).
26. Brown, J. C.; Duncanson, J. A.; Small, G. J. *Anal. Chem.*, **52**, 1711 (1980).
27. Inman, E. L.; Jurgensen, A.; Winefordner, J. D. *Analyst*, **107**, 538 (1982).
28. Colmsjo, A. L. *Anal. Chim. Acta*, **197**, 65 (1987).
29. Colmsjo, A. L. *Anal. Chim. Acta*, **197**, 71 (1987).

30. Renkes, G. D.; Walters, S. N.; Woo, C. S.; Iles, M. K.; D'Silva, A. P.; Fassel, V. A. *Anal. Chem.*, **55**, 2229 (1983).
31. Perry, M. B.; Wehry, E. L.; Mamantov, G. *Anal. Chem.*, **55**, 1893 (1983).
32. Colmsjo, A.; Stenberg, U. *Anal. Chem.*, **51**, 145 (1979).
33. Garrigues, P.; Parlanti, E.; Radke, M.; Bellocq, J.; Willsch, H.; Ewald, M. J. *Chromatogr.*, **395**, 217 (1987).
34. Jones, B. T.; Winefordner, J. D. *Anal. Chem.*, **60**, 412 (1988).
35. Jones, B. T.; Glick, M. R.; Mignardi, M. A.; Winefordner, J. D. *Appl. Spec.*, **42**, 850 (1988).
36. Chang, R. "Basic Principles of Spectroscopy," McGraw-Hill Book Co.: New York (1971).
37. Levine, I. N. "Molecular Spectroscopy," John Wiley & Sons: New York (1975).
38. Rebane, K. K. *J. Luminesc.*, **31/32**, 744 (1984).
39. Hanson, D. M.; Patel, J. S.; Winkler, I. C.; Morrobel-Sosa, A. in "Spectroscopy and Excitation Dynamics of Condensed Molecular Systems," V. M. Agranovich and R. M. Hochstrasser, Eds.; North-Holland Publishing Co.: Amsterdam (1983), 621.
40. Breene, R. G. "The Shift and Shape of Spectral Lines," Pergamon Press: New York (1961).
41. McColgin, W. C.; Marchetti, A. P.; Eberly, J. H. *J. Am. Chem. Soc.*, **100**, 5622 (1978).
42. Ingle, J. D.; Crouch, S. R. "Spectrochemical Analysis," Prentice Hall, Inc.: Englewood Cliffs, NJ (1988).
43. Thorne, A. P. "Spectrophysics," 2nd Ed., Chapman and Hall: New York (1988).
44. King, G. W. "Spectroscopy and Molecular Structure," Holt, Rinehart and Winston, Inc.: New York (1964).
45. Meyer, B. "Low Temperature Spectroscopy," American Elsevier Publishing Co., Inc.: New York (1971).
46. Jones, B. T. A Self-Cleaning, Continuous Cooling Belt for Low Temperature Molecular Luminescence

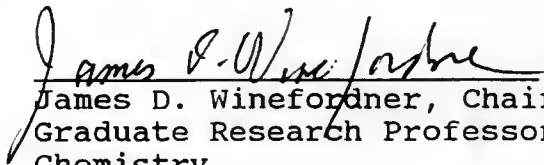
Spectrometry, Ph. D. Thesis, University of Florida, USA, 1988.

47. Personov, R. I. *Spectrochim. Acta*, **38B**, 1533 (1983).
48. Cunningham, K.; Morris, J. M.; Funfschilling, J.; Williams, D. F. *Chem. Phys. Lett.*, **32**, 581 (1975).
49. Personov, R.I. in "Spectroscopy and Excitation Dynamics of Condensed Molecular Systems," V. M. Agranovich and R. M. Hochstrasser, Eds.; North-Holland Publishing Co.: Amsterdam (1983), 555.
50. Al'shits, E. I.; Personov, R. I.; Kharlamov, B. M. *Chem. Phys. Lett.*, **40**, 116 (1976).
51. Shpol'skii, E. V. *Sov. Phys. Usp.*, **5**, 522 (1962).
52. Pfister, C. *Chem. Phys.*, **2**, 171 (1973).
53. Lai, E. P.; Inman, E. L.; Winefordner, J. D. *Talanta*, **29**, 601 (1982).
54. Merle, A. M.; Lamotte, M.; Risemberg, S.; Hauw, C.; Gaultier, J.; Grivet, J. *Ph. Chem. Phys.*, **22**, 207 (1977).
55. Brown, R. S.; Wilkins, C. L. *Anal. Chem.*, **60**, 1483 (1988).
56. Jones, B. T.; Mullins, N. J.; Winefordner, J. D. *Anal. Chem.*, **61**, 1182 (1989).

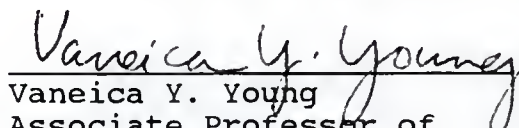
BIOGRAPHICAL SKETCH

John F. Clos was born in Cullman, Alabama, on June 20, 1964. He received his elementary school education at Sacred Heart Elementary School. In 1982, he received his high school diploma from Cullman High School. He then attended the University of Alabama at Birmingham, from which he received his Bachelor of Science degree in chemistry in 1986. While there, he worked as a co-op student for the Department of Hypertension Research on campus. During the summer of 1986, he participated in the summer research program at Proctor & Gamble in Cincinnati, Ohio. In 1989, he received his Master of Science degree in analytical chemistry from the University of Florida under Dr. John G. Dorsey. Currently, he is attending the University of Florida, from which he plans to receive his Doctor of Philosophy degree in analytical chemistry.


I certify that I have read this study and that in my opinion it conforms to acceptable standards of scholarly presentation and is fully adequate, in scope and quality, as a dissertation for the degree of Doctor of Philosophy.


James D. Winefordner, Chairman
Graduate Research Professor of
Chemistry

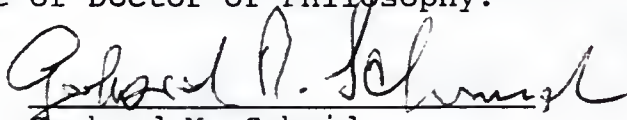
I certify that I have read this study and that in my opinion it conforms to acceptable standards of scholarly presentation and is fully adequate, in scope and quality, as a dissertation for the degree of Doctor of Philosophy.


Vaneica Y. Young
Associate Professor of
Chemistry


I certify that I have read this study and that in my opinion it conforms to acceptable standards of scholarly presentation and is fully adequate, in scope and quality, as a dissertation for the degree of Doctor of Philosophy.


Richard Yost
Professor of Chemistry

I certify that I have read this study and that in my opinion it conforms to acceptable standards of scholarly presentation and is fully adequate, in scope and quality, as a dissertation for the degree of Doctor of Philosophy.


Gerhard M. Schmid
Associate Professor of
Chemistry

I certify that I have read this study and that in my opinion it conforms to acceptable standards of scholarly presentation and is fully adequate, in scope and quality, as a dissertation for the degree of Doctor of Philosophy.


Ralph Dawson
Associate Professor of
Pharmacology

This dissertation was submitted to the Graduate Faculty of the Department of Chemistry in the College of Liberal Arts and Sciences and to the Graduate School and was accepted as partial fulfillment of the requirements for the degree of Doctor of Philosophy.

August 1991

Dean, Graduate School

UNIVERSITY OF FLORIDA



3 1262 08285 417 4